

DEVELOPMENT OF NANOPARTICLE PLATFORM FOR THERAPEUTIC
SIRNA AND DRUG DELIVERY TO BREAST CANCER

By

Worapol Ngamcherdtrakul

A DISSERTATION

Presented to the Department of Biomedical Engineering
and the Oregon Health & Science University
School of Medicine
in partial fulfillment of
the requirements for the degree of

Doctor of Philosophy

June 2015

School of Medicine
Oregon Health & Science University

CERTIFICATE OF APPROVAL

This is to certify that the PhD dissertation of
Worapol Ngamcherdtrakul
has been approved

Mentor: Wassana Yantasee, PhD, MBA
Associate Professor, OHSU

Chair: Joe Gray, PhD
Professor, OHSU

Member: Andras Gruber, MD
Associate Professor, OHSU

Member: Rosalie Sears, PhD
Professor, OHSU

Member: Oleh Taratula, PhD
Assistant Professor, OSU

Table of Contents

List of Abbreviations	v
List of Figures	viii
List of Tables	x
Acknowledgements	xi
Abstract	xiii
Chapter 1: Introduction and Background.....	1
1.1 Introduction.....	1
1.2 Overview of breast cancer.....	3
1.3 Biology of HER2 ⁺ breast cancer and HER2	7
1.4 Current treatment for HER2 ⁺ breast cancer	10
1.4.1 Trastuzumab	11
1.4.2 Other HER2-targeted agents	15
1.4.3 Other targeted pathways beyond HER2	18
1.4.4 Alternative strategies to targeted therapy	19
1.5 Non-coding oligonucleotides as therapeutics in cancer.....	20
1.6 Clinical translation of siRNA therapeutics.....	27
1.7 Nanoparticles for siRNA delivery: common rationale and concepts	29
1.8 Different classes of nanoparticles for systemic delivery of siRNAs	33
1.8.1 Lipid-based nanoparticles	33
1.8.2 Polymer-based nanoparticles	34
1.8.3 Inorganic nanoparticles	38
1.9 Translation of systemic siRNA delivery to cancer treatment in clinics	41
1.10 Scope of the dissertation	44
Chapter 2: Material Design, Synthesis and Characterization	47
Introduction	47

2.1 Materials and Methods	47
2.1.1 Reagents and siRNAs.....	47
2.1.2 Synthesis of nanoconstructs	48
2.1.3 Characterization of nanoconstructs.....	49
2.1.4 Buffering capacity measurement.....	50
2.1.5 Serum enzymatic siRNA protection assay	50
2.2 Results and discussion.....	51
2.2.1 Material design and composition.....	51
2.2.2 Nanoconstruct development and optimization	56
2.2.3 Nanoconstruct characterization.....	57
2.2.4 Composition analysis of nanoconstructs	60
2.2.5 Engineering endo-lysosomal vesicle escape: Buffering capacity of nanoconstructs.....	61
2.2.6 Different molecular weights of PEG molecules	63
2.2.7 Protection of siRNAs against blood enzymatic degradation.....	65
2.2.8 Significance of a PEG layer	66
2.3 Conclusions.....	69

Chapter 3: In vitro and in vivo efficacy evaluation of siRNA-nanoconstructs	70
Introduction	70
3.1 Materials and Methods	71
3.1.1 Material	71
3.1.2 Cell lines and media recipes	72
3.1.3 Luciferase knockdown efficacy	72
3.1.4 Cellular uptake analysis by flow cytometry	73
3.1.5 In vitro efficacy: HER2 protein knockdown and cell viability.....	74
3.1.6 Immunofluorescence staining and microscopy	75
3.1.7 Animal studies: a mouse tumor model and in vivo efficacy studies.....	76
3.1.8 Statistical analysis.....	76
3.2 Results and discussion.....	77

3.2.1 In vitro gene knockdown by siRNA-nanoconstructs	77
3.2.2 Targeted cellular uptake of the siRNA-nanoconstructs	78
3.2.3 HER2 knockdown efficacy and therapeutic effects	84
3.2.4 Impact of T-siHER2-NP ^{10C} on trastuzumab-resistant cells.....	92
3.2.5 In vivo HER2 silencing efficacy and tumor growth inhibition in an orthotopic mouse tumor model.....	93
3.3 Conclusions.....	98

Chapter 4: In vitro and in vivo safety evaluation of siRNA-nanoconstructs
..... **100**

Introduction	100
4.1 Materials and Methods	100
4.1.1 Material	100
4.1.2 Assessment of cytotoxicity and ROS generation in cell lines	100
4.1.3 Blood compatibility of nanoconstructs: hemolysis, thrombogenesis and platelet aggregation	101
4.1.4 Immune response: peripheral blood mononuclear cell (PBMC) cytokine release assay.....	103
4.1.5 Serum biochemistry profiles: kidney and liver functions	104
4.2 Results and discussion.....	104
4.2.1 Cytotoxicity.....	104
4.2.2 Reactive Oxygen Species	107
4.2.3 Blood compatibility	108
4.2.4 Immune response	111
4.2.5 Serum biochemistry profiles after long-term treatment with nanoconstructs.....	113
4.2.6 Body weights of mice after administration of multiple doses of siRNA- nanoconstructs.....	116
4.3 Conclusions.....	117

**Chapter 5: Optimization for large-scale synthesis of nanoconstructs:
reproducibility and scalability** **118**

Introduction	118
5.1 Materials and Methods	118
5.1.1 Large-scale synthesis of nanoconstructs	118
5.1.2 Characterization of nanoconstructs.....	119
5.1.3 Efficacy evaluation of nanoconstructs.....	119
5.2 Results and discussion.....	120
5.2.1 Optimizing synthesis condition for scale-up synthesis	120
5.2.2 Reproducibility and scalability of mesoporous silica nanoparticle synthesis	124
5.2.3 Reproducibility and scalability of nanoconstruct synthesis (polymer coatings)	127
5.3 Conclusions.....	128
Chapter 6: Other potential cargos (different oligonucleotides and chemotherapeutics)	130
Introduction	130
6.1 Materials and Methods	132
6.1.1 Material	132
6.1.2 Loading additional cargos on the nanoconstruct.....	132
6.1.3 Quantification of drug loading on the nanoconstruct	132
6.1.4 Efficacy evaluation	132
6.2 Results and discussion.....	133
6.2.1 Delivery of other oligonucleotides	133
6.2.2 Co-delivery of paclitaxel and siHER2 to HER2+ breast cancer.....	134
6.3 Conclusions.....	136
Chapter 7: Summary, conclusions, and future directions.	138
7.1 Summary.....	138
7.2 Conclusions and Future directions	145
References	148

List of Abbreviations

AGO	Argonaute
APAP	Acetaminophen
AST	Aspartate transaminase
BUN	Blood urea nitrogen
C	Cross-linked
CRE	Creatinine
CRP	Collage-related peptide
CTAB	Cetyltrimethylammonium bromide
CTAC	Cetyltrimethylammonium chloride
Da	Dalton(s)
DCIS	Ductal carcinoma in situ
DMF	Dimethylformamide
DNA	Deoxyribonucleic acid
DSP	Dithiobis(succinimidyl propionate)
dsRNA	Double-stranded RNA
ECD	Extracellular domain
EDTA	Ethylenediaminetetraacetic acid
EGFR	Epidermal growth factor receptor
EPR	Enhanced permeability and retention
ER	Estrogen receptor
Fc	Fragment crystallizable region (of antibody)
FDA	Food and Drug Administration
FT-IR	Fourier transform infrared spectroscopy
h	Hour(s)
H&E	Hematoxylin and eosin
HCl	Hydrochloric acid
HER2	Human epidermal growth factor receptor type 2
HSP	Heat shock protein
IDC	Invasive ductal carcinoma
IFN	Interferon
IGF1R	Insulin-like growth factor 1 receptor
IHC	Immunohistochemistry
IL	Interleukin
ILC	Invasive lobular carcinoma
kDa	Kilodalton(s)
kg	Kilogram(s)
LAL	Limulus Amebocyte Lysate

LCIS	Lobular carcinoma in situ
LDH	Lactate dehydrogenase
LPS	Lipopolysaccharides
LUC	Luciferase
mal	Maleimide
MAPK	Mitogen-activated protein kinase
mg	Milligram(s)
miRNA	Micro RNA
mL	Milliliter(s)
mM	Millimolar
MRI	Magnetic resonance imaging
mRNA	Messenger RNA
MSNP	Mesoporous silica nanoparticle
mTOR	Mechanistic target of rapamycin
NaOH	Sodium hydroxide
NCI	National Cancer Institute
NCL	Nanotechnology Characterization Lab
NDA	New drug application
NHS	N-Hydroxysuccinimide
nM	Nanomolar
NP	Nanoparticle
NP/siRNA	Nanoconstruct-to-siRNA mass ratio
nt	Nucleotide(s)
OH	Hydroxyl
PBMC	Peripheral blood mononuclear cell
PBS	Phosphate buffered saline
PEG	Polyethyleneglycol
PEI	Polyethyleneimine
PET	Positron emission topography
PIK3CA	Phosphatidylinositol-4,5-bisphosphate 3-kinase
PI3K	Phosphoinositide 3-kinase
PLK1	Polo-like kinase 1
PPP	Platelet-poor plasma
PR	Progesterone receptor
PRP	Platelet-rich plasma
PTEN	Phosphatase and tensin homolog
R	Rituximab
RES	Reticuloendothelial system
RISC	RNA-induced silencing complex
RNA	Ribonucleic acid

ROS	Reactive oxygen species
RPPA	Reverse-phase protein arrays
RTK	Receptor tyrosine kinase
scFv	Single-chain variable fragment
SCR	Scrambled
SDS	Sodium dodecyl sulfate
siRNA	Small-interfering RNA
SPION	Super paramagnetic iron oxide nanoparticle
T	Trastuzumab
TBIL	Total bilirubin
TCGA	The Cancer Genome Atlas
T-DM1	Ado-trastuzumab emtansine
TEA	Triethanolamine
TEM	Transmission electron microscope
TEOS	Tetraethyl orthosilicate
TGA	Thermogravimetric analysis
TLR	Toll-like receptor
TNF	Tissue necrosis factor
VEGF	Vascular endothelial growth factor

List of Figures

Figure 1.1: Anatomical features of different types of breast cancer.....	4
Figure 1.2: Classification of breast cancer subtypes	6
Figure 1.3: Crystal structure of four members of epidermal growth factor receptor family.....	9
Figure 1.4: Treatment algorithm for women diagnosed with metastatic HER2 ⁺ breast cancer.....	11
Figure 1.5: Potential mechanisms of action for trastuzumab.....	12
Figure 1.6: Molecular approaches to HER2-targeted therapies.....	15
Figure 1.7: Trend of research in oligonucleotides.....	21
Figure 1.8: Schematics illustrating siRNA mechanism inside the cells	23
Figure 1.9: Barriers of siRNA delivery upon systemic administration	32
Figure 1.10: Lipid-based nanoparticles for siRNA delivery	34
Figure 1.11: Polymeric structure for siRNA delivery	36
Figure 1.12: Strategies to load siRNAs on the siRNA-polymeric construct.....	37
Figure 2.1: Schematic illustration of the nanoconstruct.....	51
Figure 2.2: TEM images of different mesoporous silica nanoparticles.....	57
Figure 2.3: FT-IR spectra of MSNP before and after surfactant removal by acidic reflux.....	58
Figure 2.4: Hydrodynamic size of nanoconstructs	60
Figure 2.5: Thermogravimetric analysis.....	61
Figure 2.6: Buffering capacity of nanoconstructs.....	63
Figure 2.7: Size profile of siRNA-nanoconstructs with different molecular weights of PEG.....	65
Figure 2.8: SiRNA protection from serum degradation	66
Figure 2.9: Importance of PEG in protecting siRNA from serum enzymatic degradation and preventing aggregation upon siRNA binding	68
Figure 3.1: Luciferase silencing efficacy of nanoparticles.....	79
Figure 3.2: Cellular uptake of siRNA–nanoconstructs	81
Figure 3.3: Flow cytometry histograms demonstrating the uptake of fluorescent-labeled siRNA-nanoconstructs in breast cancer cells.....	82
Figure 3.4: HER2 knockdown by siHER2–nanoconstructs and therapeutic responses.....	87
Figure 3.5: HER2 protein reduction analyzed by Immunofluorescence imaging	88
Figure 3.6: HER2 mRNA reduction in JIMT1 and HCC1954	89
Figure 3.7: In vitro evaluation of siHER2-nanoconstructs on HER2 silencing and ability to overcome trastuzumab resistance.....	93

Figure 3.8: In vivo HER2 reduction and growth inhibition of orthotopic HCC1954 tumors	96
Figure 3.9: Drug resistance in HCC1954 in vivo	97
Figure 4.1: Cytotoxicity (cell viability).....	105
Figure 4.2: Cytotoxicity (LDH leakage)	106
Figure 4.3: ROS activity.....	108
Figure 4.4: Blood compatibility of siRNA-nanoconstructs	110
Figure 4.5: Cytokine induction in PBMCs	112
Figure 4.6: Images from the LAL gel-clot assay on the nanoconstructs (T-siHER2-NP ^{10C})	113
Figure 4.7: Histology of kidney and liver sections.....	115
Figure 4.8: Body weights of mice receiving multiple doses of T-siHER2-NP ^{10C} or saline	116
Figure 5.1: Hydrodynamic size distribution of T-siHER2-NP ^{10C} synthesized by a newly optimized method.	121
Figure 5.2: Stability of free siHER2 and siHER2 on T-NP (called T-siHER2-NP ^{10C}) in human serum	121
Figure 5.3: Impact of trastuzumab loading on efficacy of nanoconstructs	122
Figure 5.4: Effect of trastuzumab (T) loading on cellular uptake of siRNA-nanoconstructs	123
Figure 5.5: Mesoporous silica nanoparticle sol-gel synthesis	125
Figure 5.6: Size profile of mesoporous silica nanoparticles synthesized by 125-mL scale vs. 2.5-L scale	126
Figure 6.1: Delivery of other oligonucleotides to cells.....	134
Figure 6.2: Co-delivery of paclitaxel and siRNA to JIMT-1	135
Figure 6.3: Luciferase silencing efficacy of nanoconstructs.....	136

List of Tables

Table 1.1: Examples of polymeric construct for siRNA delivery	37
Table 1.2: Clinical Trials of nanoparticle-mediated siRNA delivery upon systemic administration for cancer treatment	43
Table 2.1: Hydrodynamic size and zeta potential of six different nanoconstructs	59
Table 2.2: Composition of T-siRNA-NP	61
Table 3.1: siRNA sequences	71
Table 3.2: Cell media recipes for all cell lines used	72
Table 4.1: Serum biochemistry profiles	114
Table 5.1: Size profile and the siRNA delivery efficacy of four larger batches (60-100 mg, Batches 1-4) of nanoconstructs T-NP ^{10C} vs. those of a small batch (10 mg, Batch S).....	128

Acknowledgements

I would like to express my sincere gratitude and appreciation to the following individuals who have made my graduate school experience fruitful and remarkable.

I am very grateful to the members of the dissertation advisory committee and the oral exam committee who have guided the direction of my dissertation project and provided insightful input regarding both research strategies and data presentation. My mentor, Dr. Wassana Yantasee, has introduced me to research on mesoporous silica nanoparticles and taught me significantly on properly conducting meaningful and good-quality research -- planning and thinking critically. She is also a very supportive, caring and understanding mentor. Above all, she always makes time for all of her trainees. I am thankful for the motivation, guidance and support she provided and could not have asked for a better mentor. I would like to thank Dr. Joe Gray for introducing our lab to the concept of siRNA-based cancer therapy for HER2⁺ breast cancer and proving to be an invaluable resource for our breast cancer research endeavors. I thank Dr. Andras Gruber for providing expertise in developing compounds towards clinical applications and allowing us to use his equipment for blood compatibility studies. I want to thank Dr. Rosalie Sears for providing expertise in breast cancer, helping our lab with establishing an orthotopic breast tumor model, and serving as an independent review for the manuscript. I also want to thank Dr. Oleh Taratula for bringing in his expertise in nanomedicine to the oral exam committee.

As this is a highly collaborative project, I would like to extend thanks to all previous and current members of the Yantasee lab and our collaborators. I would like to thank Dr. David Castro for assisting significantly in reviewing this dissertation and helping with toxicity studies (blood compatibility studies and histology analysis). I would like to acknowledge Dr. Joe Gray, Dr. Zhi Hu and Shenda Gu's contributions in screening for the most optimum siRNA sequence targeting HER2 and providing expertise in HER2⁺ breast cancer and biological techniques (e.g., Quantigene mRNA assay, immunofluorescence and flow cytometry). Dr. Shaun Goodyear, Jingga Morry, Brandon Beckman and Richard Lee were of great help with the animal studies. Appreciation also to Thanapon Sangvanich, Moataz Reda, Samuel Mihelic and Dr. Xinran Li for their assistance with material synthesis and characterization. I sincerely thank all of the lab members for the positive and friendly working environment.

Other specific experimental contributions are as follows,

TEM analysis and FT-IR analysis: Dr. Josephrajan Thainashmuthu (OHSU)

MDA-MB-231-H2N cell line: Dr. Robert Kerbel (University of Toronto)

BT474-R cell line: Shenda Gu (OHSU)

I'd like to thank Dr. Rachel Dresbeck and Julie Rogers at the Research Development & Communication Services, OHSU, for assistance in technical writing and editing the dissertation.

I thank Dr. Owen McCarty and Janet Itami who have helped me with all the questions and paperwork required for my graduate study. I appreciate the help of Virginia Howard, who has always been a go-to person for questions and graciously ordered all the supplies and chemicals necessary for my research in an always timely and reliable manner throughout the past five years. I also would like to acknowledge all of the faculty and administrative staff in the BME department at OHSU.

Importantly, I would like to acknowledge all of the funding sources that have made this project possible. This work was funded by the Prospect Creek Foundation (OHSU, PIs: Yantasee/Gray), NIH/NIGMS (Grant No. R01GM089918, OHSU, PI: Yantasee), NIH/NIDDK (Grant No. R41DK094571, OHSU, PI: Yantasee), OHSU's KCI pilot award (PIs: Yantasee/Hu) and OHSU's VPR fund (PI: Yantasee).

Lastly, I would like to extend sincere gratitude to all of my family members in Thailand who have always been on my side through happy and difficult times. Thank you my late mom, who is the strongest woman I know. She always guided me through life and supported me in every way until her last day. Thank you my dad for being a great leader for our family and a massive supporter for my education and life decisions. I am grateful to my brother and sisters, who have taken great care of my parents and always been there for me. I feel very lucky to be born to this family.

Abstract

Despite the advent of novel targeted therapies and early diagnosis, breast cancer remains the second cause of cancer death in women in the US since 1950. More effective treatments are still needed to improve its prognosis. Her2-positive (HER2⁺) breast cancer represents 15-25% of invasive breast cancer. Although HER2-targeted therapy has significantly improved the prognosis of this breast cancer subtype, resistance is common. The Cancer Genome Atlas project has identified genomic aberrations in breast cancer which can be used to guide the development of a wide range of therapeutic agents. However, most attractive therapeutic targets, that may be used to overcome cancer resistance to current treatment modalities, are considered 'undruggable' by conventional small molecule inhibitors or monoclonal antibodies. RNA interference (RNAi) using small interfering RNAs (siRNAs) is a promising alternative to inhibiting these otherwise intractable therapeutic targets. This strategy has proven effective in vitro. However, because the delivery of siRNAs to tumors in patients is still challenging, this technology has yet to be fully capitalized.

In this dissertation project, a novel nanoparticle construct has been engineered for efficient delivery of siRNAs to tumors. The construct consists of a 47-nm mesoporous silica nanoparticle core coated with cross-linked polyethyleneimine–polyethyleneglycol copolymer, electrostatically loaded with the siRNA against human epidermal growth factor receptor type 2 (HER2) oncogene, and coupled to the anti-HER2 monoclonal antibody (trastuzumab). The construct has been engineered to increase siRNA half-life in the blood, enhance tumor-specific cellular uptake, and maximize siRNA knockdown efficacy. The optimized anti-HER2 nanoconstructs produced apoptotic death in HER2⁺ breast cancer cells grown in vitro but not in HER2-negative (HER2⁻) cancer or nonmalignant epithelial cells. One dose of the siHER2-nanoconstructs reduced HER2 protein levels by 60% in trastuzumab-resistant HCC1954 xenografts. Administration of multiple intravenous doses over 3 weeks significantly inhibited tumor growth ($p < 0.004$). The siHER2-nanoconstructs have an excellent safety profile in terms of blood compatibility and low cytokine induction when exposed to human peripheral blood mononuclear cells. In addition, mice that received multiple doses of siHER2-nanoconstructs did not show signs of liver or kidney toxicity, as determined by serum biochemistry markers and histology. The construct can be produced with high batch-to-batch reproducibility and the production methods are suitable for large-scale production.

In conclusion, the developed nanoconstructs have great potential for clinical translation. This platform development coupled with genome analysis and RNAi functional screening could provide a more effective treatment in HER2⁺ refractory breast cancer. Further, the nanoconstructs have capacity to load multiple cargos simultaneously, including chemotherapeutic drugs and a cocktail of siRNAs. This affords a targeted combination therapy that may provide better synergistic outcomes. Application to other types of cancers can be done with ease by utilizing appropriate siRNAs or other therapeutic cargos and targeting components.

1. Chapter 1: Introduction and Background

1.1 Introduction

Cancer is caused by genetic aberrations in cells. These alterations can affect oncogenes, tumor-suppressor genes, and microRNA genes [1]. Due to functional redundancy, multistep genetic changes are typically required for the development and growth of malignant tumors. The accumulation of these changes allows cells to gain certain functional advantages over normal cells and transforms them into cancer cells. These so-called “hallmarks of cancer” [2] include sustaining proliferative signaling, evading growth suppressors, resisting cell death, enabling replicative immortality and angiogenesis, activating invasion and metastasis, and evading immune destruction. In general, cancer develops and sustains a complex redundant signaling network that regulates these different unique properties.

This dissertation focuses on HER2⁺ breast cancer, which is a breast cancer subtype that overexpresses HER2 (Human epidermal growth factor receptor type 2) proteins on the cancer cell membrane. This breast cancer subtype was once known for its aggressive growth and poor prognosis. However, it has recently responded well to new targeted therapies. This success has prompted many attempts to better understand the molecular blueprint underlying cancer pathogenesis and, in turn, design better therapeutic compounds.

Despite these advancements, HER2⁺ breast cancer still recurs and progresses, and the treatment advantage lengthens survival time but does not necessarily cure the disease at late stages. This is partly due to an inability to effectively inhibit certain intracellular genes with current conventional small molecule inhibitors or monoclonal antibodies. Therefore, there are still unmet needs for the treatment of this refractory cancer.

RNA interference (RNAi) with small interfering RNA (siRNA) is potentially a more effective therapeutic candidate for cancer treatment than conventional drugs because it can target virtually any gene with higher specificity. This therapeutic strategy is an ideal candidate for drug-resistant HER2⁺ breast cancer, where targeted therapies with conventional small molecules or antibodies are not sufficient. However, the application of RNAi is mainly limited to the research laboratory as a tool to understand the functional roles of each gene/protein in the cells under study. A significant hurdle blocking effective patient application of RNAi technology lies with the lack of an effective delivery system.

In light of this, this dissertation project focuses on developing mesoporous silica nanoparticles, MSNPs, as a platform for siRNA delivery to HER2⁺ breast cancer. More specifically, the nanoparticle is modified and loaded with different components in an attempt to render the nanoparticle functional for delivering siRNA. Further, the ability of these developed nanoparticles to load additional cargos beyond siRNAs will be also explored. Therefore, this system allows for the simultaneous delivery of different compounds to cancer cells, potentially eliciting synergistic or additive effects. Although this dissertation focuses on

mesoporous silica nanoparticles, these possible collateral outcomes could be utilized in other nanoparticle systems.

If successful, targeted delivery of siRNAs will be attainable and could revolutionize cancer treatment for patients. Subsequently, treatments could be designed to target virtually any genes responsible for cancer progression, abrogate tumor burden, and ultimately improve patient survival. Lastly, as cancer is a very heterogenous disease, and the treatment of different types of cancer requires the abrogation of different oncogenes, this siRNA-nanoparticle system offers greater flexibility for targeting different genes by employing different siRNAs, creating more personalized cancer treatments.

1.2 Overview of breast cancer

Cancer is a disease wherein the body's cells become abnormal and grow uncontrollably. In most cases, cancer leads to the formation of a mass called a tumor. Cancer is conventionally classified by the organ in which it originates. Breast cancer originates in breast tissue, either in **lobules**, which are milk-producing glands, or **ducts**, which connect the lobules to the nipples [3]. When breast cancer is confined within breast tissues, it is referred to as carcinoma in situ (i.e., **DCIS** – ductal carcinoma in situ or **LCIS** – lobular carcinoma in situ). By contrast, if the cancer cells start to spread to nearby tissues, it is referred to as invasive carcinoma (i.e., **IDC** – invasive ductal carcinoma, and **ILC** – invasive lobular carcinoma). These differences are depicted in **Figure 1.1**. However,

these classifications do not sufficiently address the heterogeneity of breast cancer, resulting in poor prognostic implications and clinical utility.

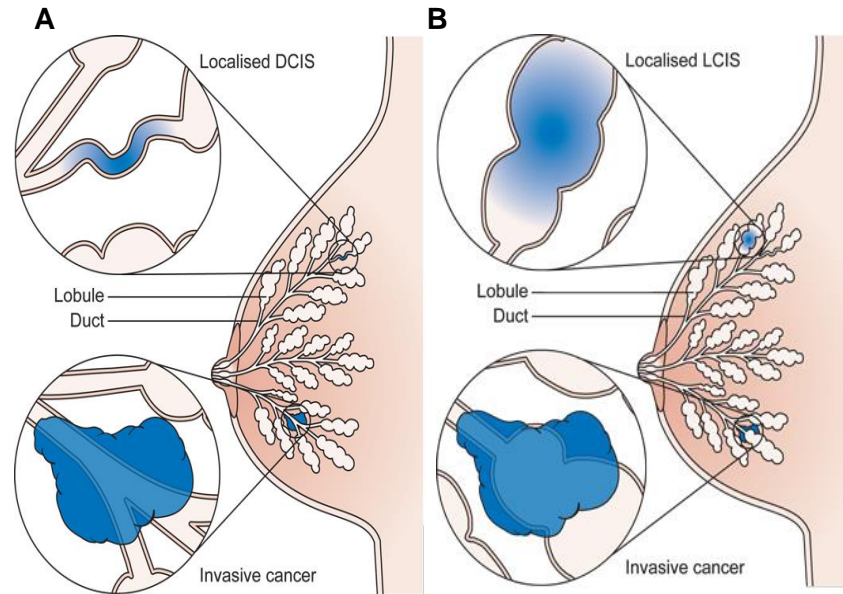


Figure 1.1: Anatomical features of different types of breast cancer (Cancer Research UK). (A) Breast cancer originated in ducts, (B) Breast cancer originated in lobules.

As the second most common cause of death in the US after heart disease, cancer remains one of the most fatal diseases. Breast cancer is the most frequently diagnosed cancer in women, and, after lung cancer, the second leading cause of cancer death in women in the US since 1950 [3, 4]. The current risk of American women developing breast cancer in their lifetime is one in eight. It is estimated that 234,190 new cases will be diagnosed in the US in 2015 [3]. Meanwhile, owing to the early detection and development of new treatments, five-year survival rates for breast cancer have improved substantially, from 84% in 1987-1989 to 91% in 2004-2010. Recurrence in breast cancer is common,

however, and the treatment for these recurrent cases and advanced metastatic cases is still rather ineffective. For metastatic breast cancer, the five-year survival rate is 25% [3].

A more refined molecular-based classification of breast cancer includes six subtypes: luminal A, luminal B, basal-like, HER2-enriched, normal breast-like, and claudin-low [5, 6]. These subtypes were derived from hierarchical clustering using an “intrinsic” gene list. In particular, Prat et al. reported hierarchical clustering of 320 human breast tumors and 17 normal breast samples using ~1900 genes [7], as illustrated in **Figure 1.2A** [5, 8]. The Cancer Genome Atlas (TCGA) has also found good correlation between these intrinsic (mRNA) subtypes and the breast cancer subtypes defined from information integrated across five different platforms (i.e., miRNAs, DNA methylation, copy number, mRNA expression, and reverse-phase protein arrays) [6]. However, due to limitations in translating research to clinical practice, this microarray-based diagnosis is not considered a routine practice. Diagnoses based on classical immunohistochemical markers still remain a mainstream practice in clinics. Standard practice examines only the hormone receptor (estrogen receptor “ER” and progesterone receptor “PR”) and HER2 status. For example, patients with hormone receptor-positive tumors are candidates for hormone therapy, and patients with HER2-positive tumors are candidates for HER2-targeted therapies. Although these HER2-positive tumors (as determined by IHC) largely overlap with the HER2-enriched subtype, all of the intrinsic subtypes can be identified within HER2-positive tumors (**Figure 1.2B**) [5]. Therefore, ER, PR, and HER2

status determined by IHC do not necessarily suggest the intrinsic subtype status, and these two classifications should be considered unique.

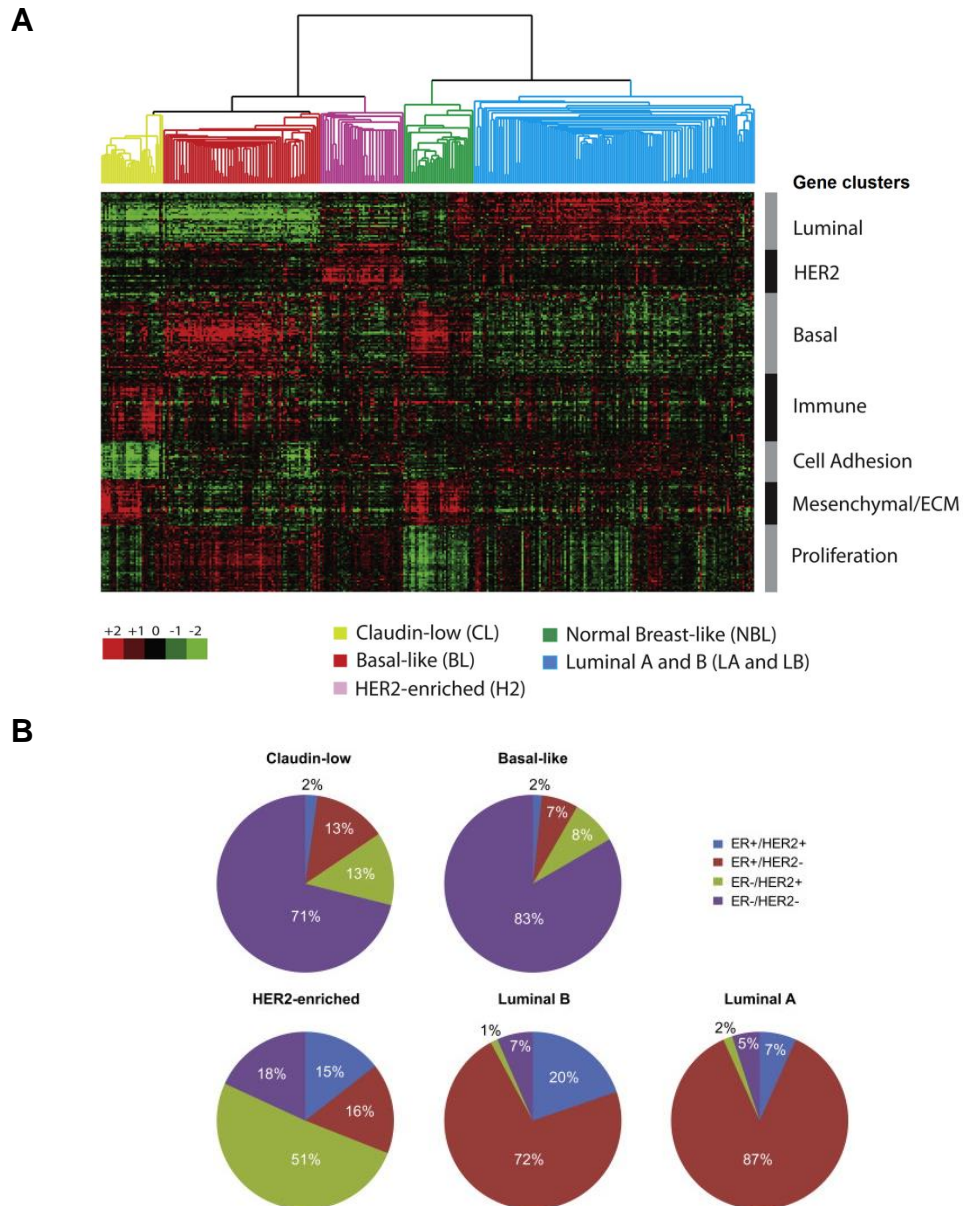


Figure 1.2: Classification of intrinsic (molecular) breast cancer subtypes. (A) Hierarchical clustering of ~1900 genes (by the abundance of transcript of each gene) with the sample-associated dendrogram colored according to specified intrinsic (mRNA) subtypes (Data are presented in matrix format: each row represents a single gene, and each column represents each tumor sample), (B) Distribution of ER and HER2 in different intrinsic (mRNA) subtypes of breast cancer. Reproduced with permission from Elsevier [5].

1.3 Biology of HER2⁺ breast cancer and HER2

HER2⁺ breast cancer is a subtype that presents HER2 overexpression on the tumor cell surface. This is caused by the amplification of HER2 oncogene and related genetic elements in the amplicon on chromosome 17 [9]. This subtype accounts for approximately 15-25% of invasive breast cancer [10, 11]. HER2 (ERBB2) belongs to a family of transmembrane receptor tyrosine kinases (RTKs), which also include HER1 (EGFR; epidermal growth factor receptor), HER3 (ERBB3), and HER4 (ERBB4). RTKs have key roles in regulating several cellular processes, such as proliferation, migration, metabolism, differentiation, and survival, particularly during embryogenesis [12, 13]. In normal cells, this signaling network is tightly regulated. However, when these genes mutate, amplify, or overexpress, they become oncogenes responsible for the onset, progression, and aggressiveness of many types of cancer (**Figure 1.3**) [13, 14].

Each receptor is composed of a cysteine-rich ligand-binding domain (extracellular domain; ECD), a hydrophobic transmembrane segment, and an intracellular tyrosine kinase portion with a regulatory carboxyl-terminal segment [15] (**Figure 1.3**). HER receptors exist as monomers but dimerize upon ligand binding, either as homodimers (e.g., HER2-HER2) or heterodimers (e.g., HER2-HER3). The activating ligands for each of the HER receptors are shown in **Figure 1.3**. Although HER2 does not have a known specific ligand, it is the preferred heterodimerization partner for other HER receptors. Each ligand with a bivalent structure will bind to HER1, HER3 or HER4 via its high-affinity, narrow-

specificity site. Meanwhile, the other low-affinity broad-specificity site of the ligand will recruit a homo- or heterodimerization partner. It has been shown that HER2 preferentially binds to the low-affinity sites of the ligands [15, 16]. Therefore, HER2 can participate in several signal transduction pathways as a heterodimer. Further, an alternatively spliced human HER2 isoform encoding a receptor lacking exon 16 (which immediately precedes the transmembrane domain containing two cysteine residues) was reported to evoke more aggressive tumorigenicity and metastasis [17, 18]. The structural change of this HER2 variant promotes the formation of stable HER2 homodimers (by intermolecular disulfide bridge) and, in turn, renders HER2 constitutively active. Excess dimerization (homo- and hetero-) of HER proteins results in a subsequent increase in cellular signaling [11, 19]. This HER2 aberration thus contributes to poor clinical outcome and resistance of this subtype of breast cancer.

As mentioned earlier, not all clinically HER2⁺ tumors are of the HER2-enriched (HER2E) mRNA subtype. In fact, only ~50% of HER2⁺ tumors fall into the HER2E mRNA subtype, while ~40% of other HER2⁺ tumors are of the luminal subtypes [6, 20]. HER2E-mRNA/HER2⁺ tumors showed coordinated overexpression of HER2, EGFR, phosphorylated HER2, and phosphorylated EGFR, suggesting more heterodimerization and cross-phosphorylation of the two HER receptors. In contrast, this was not observed in luminal-mRNA/HER2⁺ tumors, where a higher expression of luminal cluster of genes was present, including GATA3, BCL2 and ESR1.

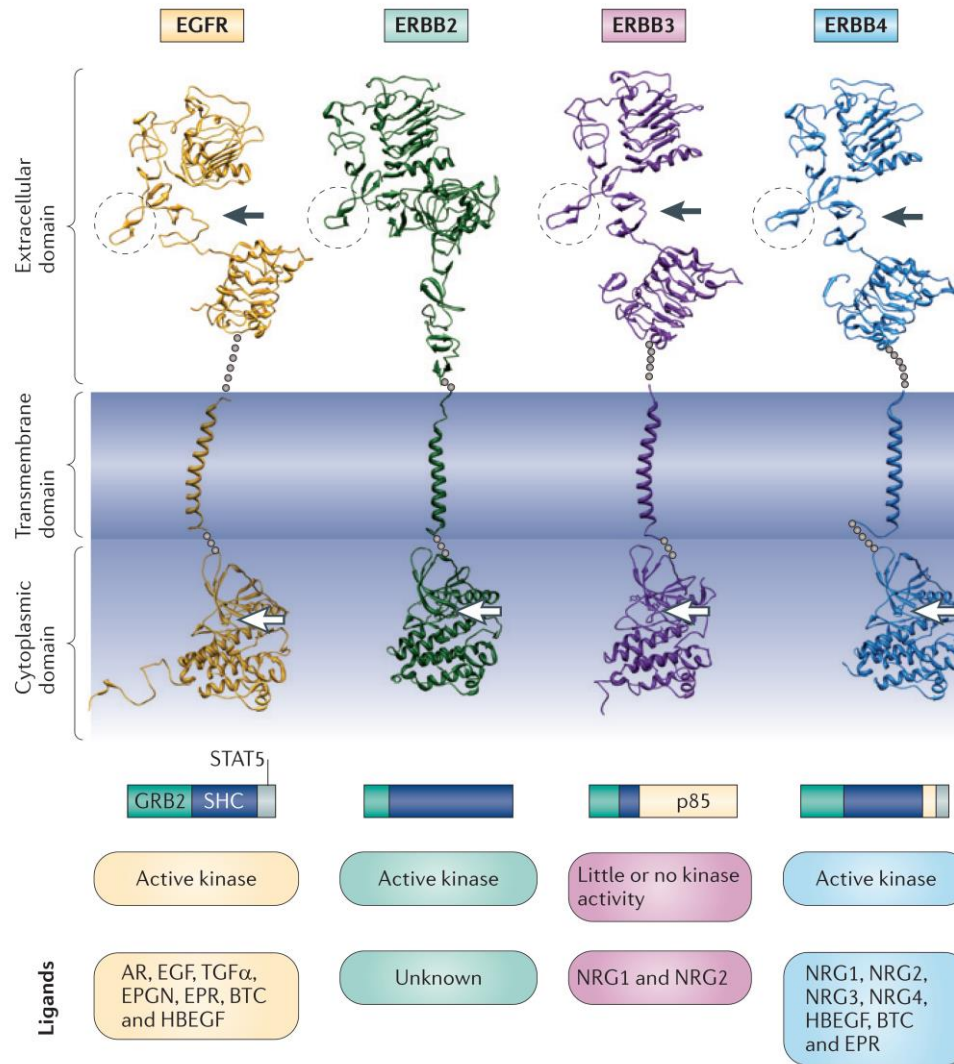


Figure 1.3: Crystal structure of four members of epidermal growth factor receptor family. The ligand-binding clefts are marked by black arrows and the dimerization loops by dashed circles. ERBB2 has no ligand-binding cleft. White arrows mark the ATP-binding sites. AR, amphiregulin; BTC, β -cellulin; EGF, epidermal growth factor; EPGN, epigen; EPR, epiregulin; HBEGF, heparin-binding EGF-like growth factor; NRG, neuregulin; TGF- α , transforming growth factor- α . Reproduced with permission from Nature Publishing Group [21].

1.4 Current treatment for HER2⁺ breast cancer

Current treatments for HER2⁺ breast cancer typically include a combination of chemotherapeutic drugs and HER2-targeted therapies. This treatment regimen was designed based on the extrapolation of previous clinical trials. If the tumor is resectable, adjuvant therapy is usually administered after surgery to limit any potential micro-metastatic disease [22]. A lack of relapse is commonly an end-point for such treatment. The following review will focus on HER2-targeted therapies, the most relevant to the scope of this dissertation.

Figure 1.4 shows the current treatment scheme for women diagnosed with metastatic breast cancer. It can be seen that, despite the development of new HER2-targeted compounds, trastuzumab remains part of a first-line treatment. Consequently, trastuzumab will be discussed in more detail next. Other HER2-targeted therapies in line will also be briefly described at the end.

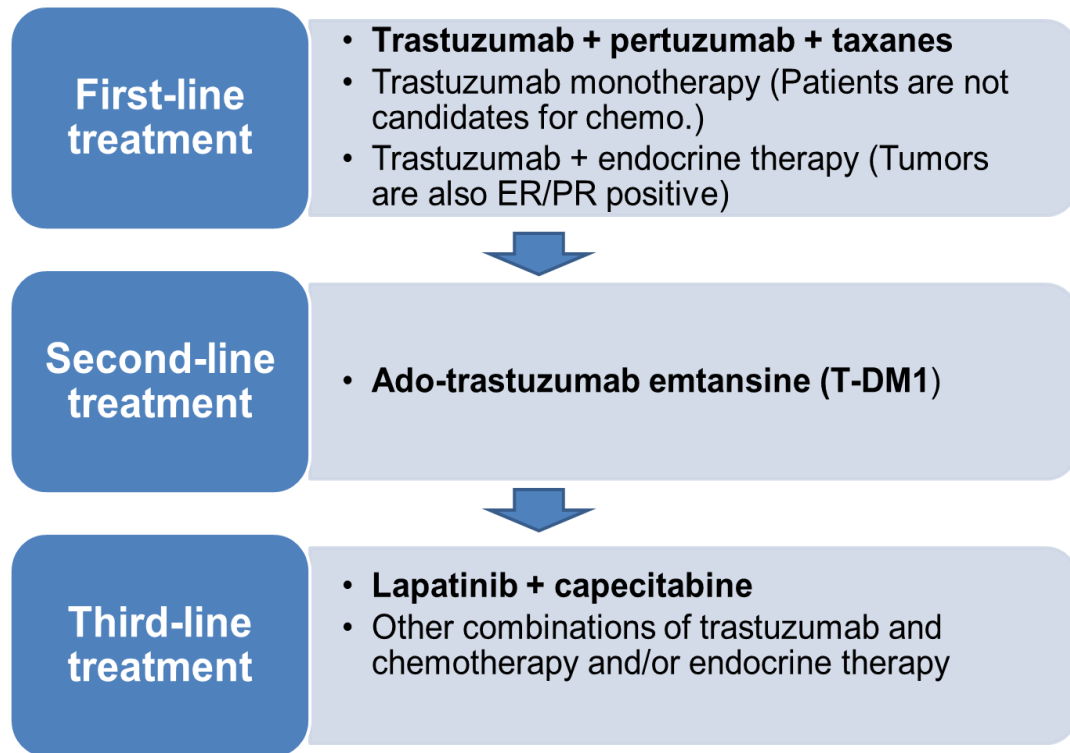


Figure 1.4: Treatment algorithm for women diagnosed with metastatic HER2⁺ breast cancer (2015) [23].

1.4.1 Trastuzumab

Trastuzumab is a humanized monoclonal antibody that targets the HER2 extracellular domain (ECD). It has been a gold standard for HER2⁺ breast cancer and has shown good clinical outcomes. It has significantly improved the prognosis of this aggressive subtype of breast cancer. However, trastuzumab is well-known for its cardiac side effects, most of which are treatable and reversible (unlike anthracycline-related cardiac toxicity, which is not reversible) [24]. The prevalence of these toxicities is most likely due to the inhibition of HER2 signaling in cardiac myocytes [25]. Of note, the exact mechanism of trastuzumab

action is not completely known; It is believed, nonetheless, that trastuzumab has more than one simultaneous mechanism of action. Several postulates are summarized in **Figure 1.5** and discussed below.

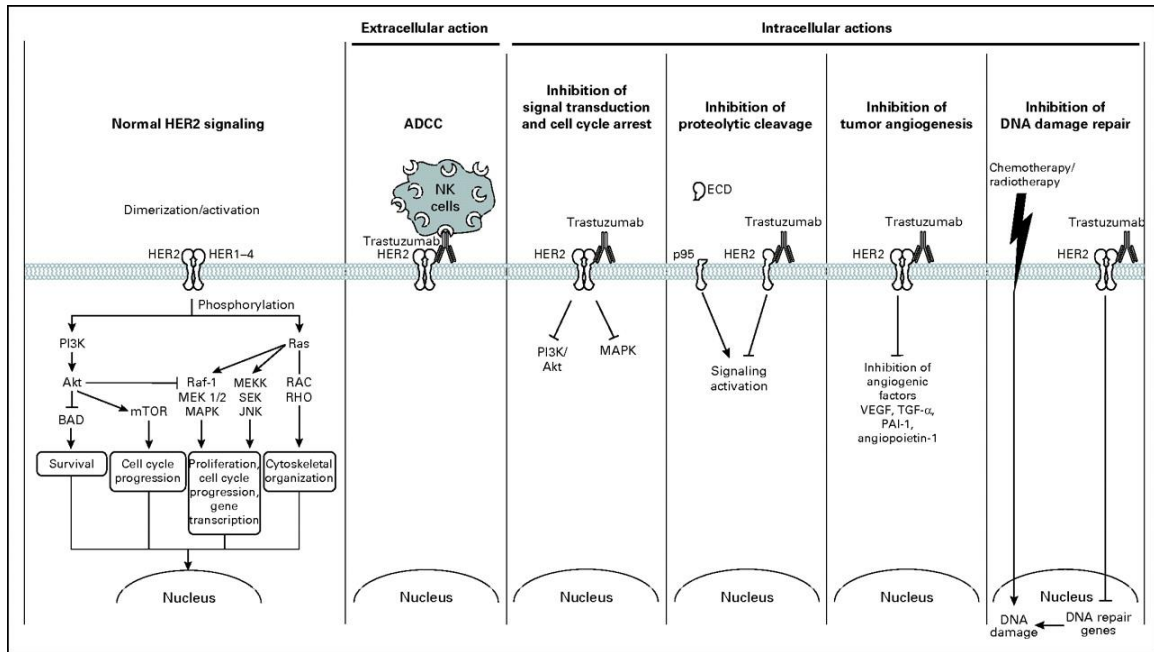


Figure 1.5: Potential mechanisms of action for trastuzumab. Mechanisms of action for trastuzumab can be extracellular or intracellular. Trastuzumab can recruit natural killer cells, harnessing the immune system to kill cancer cells. Intracellular actions include disruption of HER2 signaling, HER2 extracellular domain shedding, tumor angiogenesis, and DNA repair. Reproduced with permission from American Society of Clinical Oncology [13].

Inhibition of intracellular signal transduction is predicated on the inhibition of HER2 activation and phosphorylation by trastuzumab. Reports indicate that this affects HER2 downstream pathways, primarily MAPK (Mitogen-activated protein kinases) and PI3K-Akt (Phosphoinositide 3-kinase-Akt) [26-28]. Dysregulation of the PI3K pathway in cancer activates Akt and also delays p53-mediated apoptosis, resulting in disease progression [13]. Trastuzumab

modulates these signaling pathways to promote apoptosis and proliferation arrest in cancer. Accordingly, downstream activation of the PI3K pathway was shown to correlate with poorer trastuzumab response. For instance, tumors lacking PTEN (a negative regulator of the PI3K pathway) and/or containing mutations in PIK3CA (the catalytic subunit of PI3K) were more resistant to trastuzumab, compared to tumors with wild-type PI3K (rate of disease progression of 50% vs. 20%) [29].

Inhibition of HER2 ECD shedding is the process through which trastuzumab inhibits the formation of the truncated form of HER2, known as p95. p95 is a constitutively active RTK that leads to increased signal transduction. Trastuzumab was found to inhibit HER2 ECD cleavage from HER2⁺ cells. The maintenance of the intact form of HER2 on the cell surface could decrease constitutive receptor activation and, in turn, inhibit cell growth [28]. Unsurprisingly, decreases in serum HER2 ECD in patients (suggesting lower ECD shedding events) during trastuzumab treatment were shown to correlate with better treatment response and survival [30, 31].

Inhibition of tumor angiogenesis can also be induced with trastuzumab treatment. The treatment of HER2⁺ breast cancer cells with trastuzumab has previously resulted in dose-dependent reduction in vascular endothelial cell growth factor (VEGF), one of the most important inducers of tumor angiogenesis [32]. This angiogenic suppression was observed both in vitro and in vivo and is thought to be an important anti-tumor effect of trastuzumab [33].

Inhibition of DNA damage repair is another possible mechanism of action for trastuzumab. Upregulation of HER2/PI3K-Akt signaling was reported to take part in the repair of specific DNA lesions produced by chemotherapy [34]. It was also shown that trastuzumab delays the repair of DNA interstrand cross-links induced by chemotherapeutic agents.

ADCC (Antibody dependent cellular toxicity) is the process whereby immune effector cells are recruited to attack (lyse) target cells. In this case, the Fc (Fragment crystallizable region) portion of trastuzumab that is bound to cancer cells can be detected by Fcγ receptors on immune effector cells, principally natural-killer (NK) cells [13, 35]. This effect was reported in several breast cancer cell lines [36] and mouse models of breast cancer [37]. ADCC has also been reported in early breast cancer patients. In a pilot study with 11 early breast cancer patients who received neoadjuvant trastuzumab, all tumors showed a strong infiltration of lymphoid cells [38]. Also, patients in remission were reported to have a higher degree of leukocyte infiltration in their tumors and, therefore, a higher capability to mediate ADCC than patients whose tumors failed to respond to trastuzumab [39].

Trastuzumab is typically used in the early stages and metastatic cases of breast cancer as a monotherapy or in combination with paclitaxel and docetaxel. Although trastuzumab has revolutionized HER2⁺ breast cancer treatment and serves as an ideal example of a HER2-targeted therapy, resistance to trastuzumab is common. In fact, more than 70% of the HER2⁺ metastatic breast cancer patients fail to respond to single-agent trastuzumab [40], and most

patients who initially respond to trastuzumab will eventually develop resistance within one year, suggesting acquired resistance [41, 42]. There are a number of hypotheses about the mechanisms of trastuzumab resistance [14, 43]. These mechanisms include (1) steric effects hindering trastuzumab binding to HER2, (2) upregulation of HER2 downstream signaling pathways (e.g., PI3K pathway activation), (3) the ability of HER2 to signal through alternate pathways, and (4) the failure to trigger immune-mediated mechanisms to destroy tumor cells.

1.4.2 Other HER2-targeted agents

Due to the shortcomings of trastuzumab, other agents have been developed to either replace or to be combined with trastuzumab. **Figure 1.6** illustrates the molecular targets for agents that are currently used or being considered in HER2⁺ breast cancer treatment.

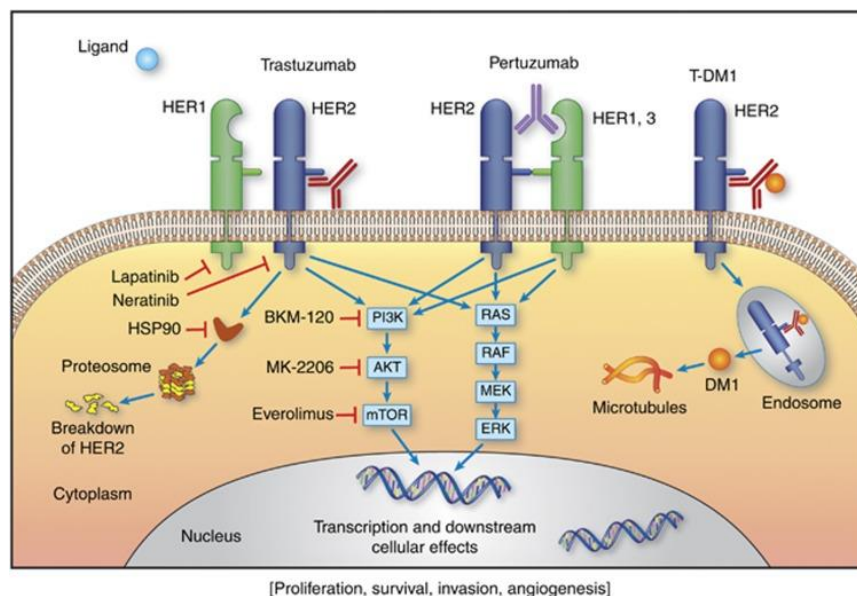


Figure 1.6: Molecular approaches to HER2-targeted therapies. Copyright © 2014, Rights Managed by Nature Publishing Group [44].

Pertuzumab is another HER2 monoclonal antibody that can bind to the HER2 extracellular domain, but at a different site than trastuzumab (**Figure 1.6**) [45]. Unlike trastuzumab, pertuzumab is active against HER2 heterodimers. The combination of pertuzumab and trastuzumab could provide a more complete blockade of the HER2 pathway and has shown better outcomes in patients. Specifically, the combination of pertuzumab, trastuzumab, and docetaxel was reported to improve progression-free survival over the combination of just trastuzumab and docetaxel (18.5 months vs. 12.4 months) with no increase in cardiac toxicity [46]. This combination is now a standard first-line treatment for patients with HER2⁺ metastatic breast cancer.

Ado-trastuzumab emtansine (T-DM1) is the most recently approved HER2-targeted therapy. Ado-trastuzumab is trastuzumab that has been conjugated with an average of 3.5 molecules of DM1 (emtansine, a derivative of maytansine) [47, 48]. Maytansine is a potent inhibitor of the polymerization of microtubules. However, maytansine therapy did not progress to clinical application due to non-selective toxicity and a poor therapeutic window. DM1 was developed as a derivative of maytansine to enable conjugation with the targeting antibody, trastuzumab. DM1 was also shown to have 3-10 times greater in vitro cytotoxicity than maytansine [12]. Conjugation with trastuzumab provides DM-1 with selectivity and targetability for HER2⁺ breast cancer. T-DM1 is currently used in a second-line setting.

T-DM1 was also shown to provide better response rates than the combination of trastuzumab and docetaxel in the first-line setting (progression

free survival of 14.2 months vs. 9.2 months) [49]. Its toxicity profile was also favorable, as the trastuzumab-associated cardiotoxicity was not exacerbated in T-DM1. However, a recent press release by Roche regarding the phase III MARIANNE study (NCT01120184, 2014) did not support this result [50]. The three arms in the Phase III MARIANNE study include T-DM1 alone, T-DM1 plus pertuzumab, and trastuzumab plus taxane chemotherapy. Neither of the T-DM1-containing treatment arms improved progression-free survival compared to trastuzumab plus chemotherapy. Therefore, the current treatment algorithm (**Figure 1.4**) will unlikely change in the near future.

Lapatinib disrupts the intracellular tyrosine kinase activity of both EGFR and HER2. The combination of trastuzumab and lapatinib, despite targeting the same pathway, results in a significant improvement in progression-free survival [51, 52]. In patients with prior trastuzumab-based therapies, a 4.5-month median overall survival advantage was reported with the combination of trastuzumab and lapatinib versus lapatinib alone (Phase III EGF104900 trial (2012)). However, the combination of lapatinib and taxane was shown to be inferior to that of trastuzumab and taxane in the first-line setting of HER2⁺ metastatic breast cancer (Phase III MA.31 trial (2012)) [53]. The median progression-free survival times were 8.8 months and 11.4 months, respectively. Further, in patients pretreated with trastuzumab and a taxane, T-DM1 (as a second-line therapy) outperformed the combination of capecitabine and lapatinib in the Phase III EMILIA trial (2012) [54]. The median progression-free survival times were 9.6

and 6.4 months, respectively. Consequently, lapatinib is now used in combination with capecitabine as a third-line therapy.

Neratinib was developed as an irreversible tyrosine kinase inhibitor and was shown to be more potent than lapatinib. The combination of neratinib and capecitabine showed efficacy in patients pretreated with lapatinib with a median progression-free survival rate of 35.9 weeks (~9 months) [55]. Neratinib was further evaluated in an extended adjuvant setting (ExteNET trial: NCT00878709 (2014)). Following trastuzumab, patients were randomized to one-year of neratinib or placebo. Results indicated that an extended adjuvant treatment with neratinib prolonged disease-free survival by 33% compared with placebo [56, 57]. Based on this finding, Puma Biotech planned to file for a new drug application in 2015.

1.4.3 Other targeted pathways beyond HER2

The alternative targeted pathways to HER2 include the PI3K, HSP90, VEGF, and IGF1R pathways [12, 58-60]. The PI3K pathway can be inhibited by PI3K inhibitors [61] or Akt and mTOR inhibitors. HSP90 is a molecular chaperone that stabilizes HER2 among other proteins. Inhibition of HSP90 increases HER2 degradation and fortifies the effect of trastuzumab treatment [62]. Multi-kinase and angiogenesis inhibitors are also being considered for HER2⁺ breast cancer because overexpression of HER2 is associated with VEGF and angiogenesis [63]. In fact, bevacizumab (angiogenesis inhibitor) was granted accelerated approval by the FDA for metastatic breast cancer in 2008 [64]. However, it was

later revoked in the US in 2010 after it failed to improve efficacy and also had a poor safety profile.

Current HER2-targeted agents only prolong survival in patients with advanced cancer – even after decades of development. Clearly, alternatives or additions are needed. Non-coding RNA molecules are discussed below as one class of alternative targeted therapy.

1.4.4 Alternative strategies to targeted therapy

Knocking down oncogenes/oncoproteins at the mRNA level may be a more effective approach because this process inhibits the synthesis of the active oncoproteins, while monoclonal antibodies and small molecule inhibitors merely block the activity of oncoproteins but do not halt the synthesis of the new active oncoproteins. Further, while monoclonal antibodies and small molecule inhibitors can target only certain accessible proteins (so-called “druggable targets”), RNA interference (RNAi) can be designed to modulate virtually any gene with known mRNA sequences. Large-scale genomic projects, such as The Cancer Genome Atlas project, have identified genomic aberrations and affected regulatory networks that enable aspects of cancer progression including proliferation, angiogenesis, invasion, drug resistance, and metastasis [2, 6]. These discovery efforts and associated large-scale functional studies [65-67] are guiding the development of a wide range of therapeutic agents designed to inhibit the genes and pathways on which cancers depend. Many of the identified attractive therapeutic targets are considered ‘undruggable.’ RNAi can provide a possible

alternative to these undruggable targets and, in turn, can revolutionize cancer treatment. The next section will review the efforts and progress of using RNA molecules (with the focus on RNAi approach with small interfering RNA (siRNA)) in targeting oncogenes in cancer.

1.5 Non-coding oligonucleotides as therapeutics in cancer

The functional roles of oligonucleotides (nucleic acids), beyond their use in encoding genes and proteins, were discovered in the 1990s. The identified non-coding oligonucleotides were shown to have a role in regulating gene expression and cell function in all organisms [68]. These non-coding oligonucleotides include siRNAs, miRNAs, antisense oligonucleotides, ribozymes, and aptamers. This section describes the different classes of such oligonucleotides and examples from clinical trials. **Figure 1.7** shows the research trend for each oligonucleotide and reveals that siRNAs have received rapidly increasing interests since 2005. miRNAs has also had a similar upward trend which is expected because the mechanisms of siRNAs and miRNAs are very similar. Although these oligonucleotides have promise in many disease applications, this review is limited to applications in cancer.

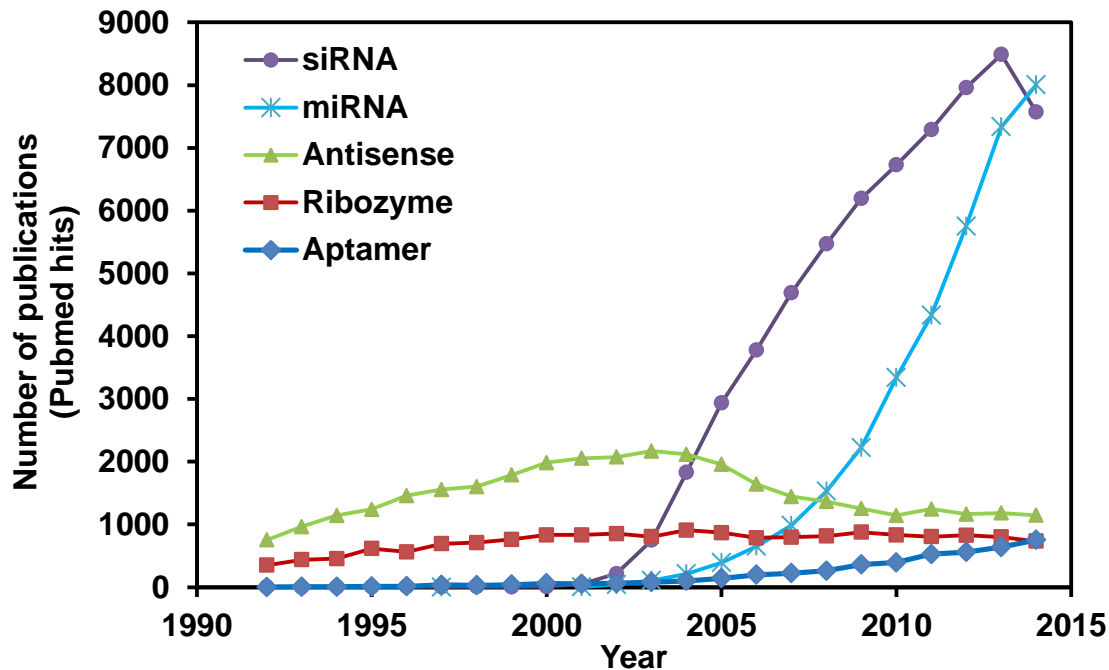


Figure 1.7: Trend of research in oligonucleotides. The number of publications each year (1992-2014) based on Pubmed queries with specified keywords.

siRNAs (small interfering RNAs) are small (20-24 nt) double-stranded RNAs, which are incorporated into a protein complex called RNA-induced silencing complex (RISC) upon cellular internalization (**Figure 1.8**) [69]. Each siRNA has two strands, a sense strand and an antisense strand. The sense strand will be degraded by an endonuclease of RISC, argonaute 2 (AGO2). The antisense strand will guide RISC towards complementary target mRNA and induce cleavage of the mRNA. Unlike antisense oligos which act stoichiometrically on target mRNA molecules, siRNA machinery (RISC) can be recycled upon degrading each mRNA [70]. In addition, siRNAs have only one mechanism of gene ablation, which is mRNA cleavage. This is deemed more effective and controllable than the multiple mechanisms offered by antisense

oligos (see next section). While siRNAs and miRNAs share the same RISC-mediated RNA cleavage, siRNAs are optimized and designed to target certain genes with high specificity. By contrast, miRNA mimics--which are small, chemically modified double-stranded RNAs that mimic endogenous miRNAs--follow the sequence of miRNAs that already exist in cells, are involved in cell functions, and in turn typically target multiple genes. This could be beneficial in some scenarios but also increases the likelihood of unwanted effects. Also, the role of miRNAs in non-targeted cells can be uncertain. Therefore, siRNAs are considered the most effective oligonucleotide at knocking down target genes. Despite their intracellular potency, delivery remains a major hurdle to translate siRNAs into clinical applications. Unlike antisense oligos, siRNAs cannot be delivered by themselves. Chemical modification and/or delivery materials are required to introduce siRNAs to targeted cells effectively. The subsequent section will review a detailed delivery strategy for siRNAs in cancer, with the main focus on solid tumors and breast cancer.

miRNAs (mature microRNAs) are involved in regulating post-transcriptional gene expression and thus serve as one of the mechanisms that regulate cellular events and homeostasis [71]. miRNAs have been extensively studied for their cancer diagnostic and therapeutic properties. As a diagnostic tool, tumor miRNA profiles can correlate with patient survival and treatment responses [72-74]. Further, miRNA expression can be upregulated or downregulated in cancer to promote cancer's survival advantages. As miRNAs can behave as oncogenes or tumor suppressors [75], one can strategize with

miRNA therapeutically by either suppressing oncogenic miRNAs or introducing tumor suppressor miRNAs (e.g., miRNA mimics).

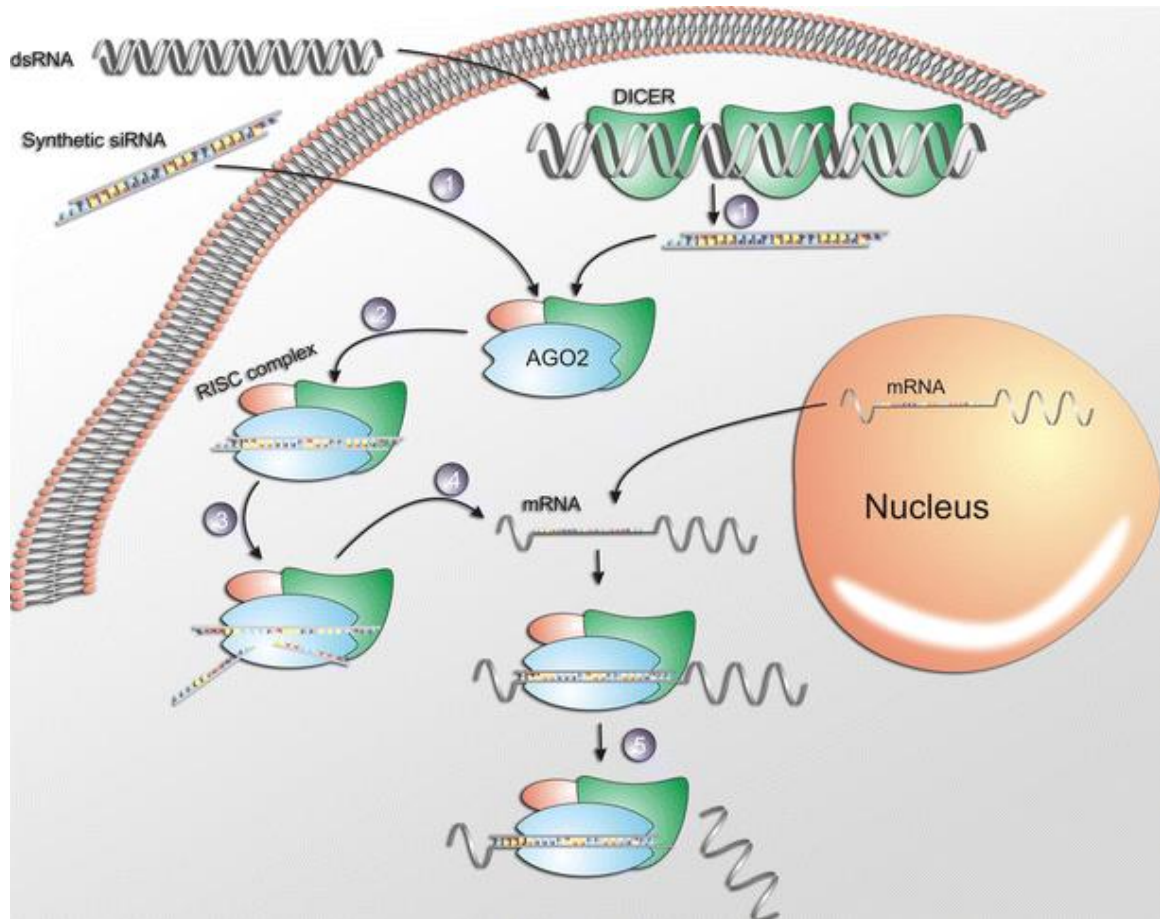


Figure 1.8: Schematics illustrating siRNA mechanism inside the cells. (1) introduction of siRNAs either being taken up from outside the cells or processed from longer regulatory double-stranded RNAs (dsRNAs) inside the cells, (2) formation of the RISC, (3) degradation of the sense (non-guiding) strand of the siRNA, (4) “complexation” of RISC with the target mRNA and (5) cleavage of the target mRNA. Reproduced with permission from Springer [69].

The first miRNA mimic entered clinical trial in 2013 [76]. It utilizes a liposome-based technology to deliver miR-34a in cancer patients (primary or metastatic with liver involvement). Liposomes were exploited for their natural tendency to accumulate in the liver. Interestingly, an miRNA can target multiple proteins involved in different pathways. For example, miR-34a was found to downregulate mRNA expression of several genes, such as ERC1, RRAS, PHF19, WTAP, CTNNB1, SIPA1, DNAJB1, MYCN, and TRA2A [77]. This broad targeting ability can theoretically enhance therapeutic potential, but it also increases propensity for unwanted side effects. The mechanism of miRNA action is similar to siRNAs, described earlier, except that one miRNA can typically modulate more than one gene.

Antisense oligonucleotides modulate gene expression by altering mRNA splicing pattern, blocking mRNA translation (by providing steric hindrance), and inducing degradation of targeted mRNA by the endogenous enzyme RNase H [68, 78]. Since antisense oligos are single-stranded, the aromatic bases are exposed to the outside (unlike double-stranded RNA where aromatic groups are nestled between the strands) [78]. This structure gives antisense oligos a hydrophobic property, which allows some levels of cellular uptake without delivery agents. However, modification and conjugation are still normally performed to promote their stability, cellular uptake, and efficacy. One of the most advanced antisense oligos for cancer in clinical trials (i.e., reaching the NDA filing stage) is Genasense (Genta Inc.). Genasense was developed to block the production of the Bcl-2 protein, one of the key anti-apoptotic oncoproteins in

cancer [79, 80]. It was later rejected by the FDA for approval in melanoma and chronic lymphocytic leukemia, though, because the primary endpoint of improving overall survival was not met [81, 82]. ISIS Pharmaceuticals is another leading company in antisense development. The most advanced antisense in their pipeline for cancer is OGX-011, which targets clusterin in castration-resistant prostate cancer [83, 84]. However, the phase III SYNERGY trial did not show significant improvement in overall survival [85]. Other next-generation antisense drugs for cancer developed by ISIS Pharmaceuticals [78] include ISIS-STAT3-2.5Rx [86] for targeting STAT3 [87] in hepatocellular carcinoma and lymphoma and ISIS-AR-2.5Rx for targeting AR [88, 89] in prostate cancer. ISIS-STAT3-2.5Rx showed some clinical response in lymphoma patients (Phase I, 2014) and has currently progressed to Phase II study [86]. ISIS-AR-2.5Rx is currently in the phase I/II stage and there are no published results yet.

Ribozymes are considered self-processing RNAs in that they do not require proteins for catalysis. Angiozyme (Ribozyme Pharmaceuticals) is the first ribozyme that reached clinical trials for cancer treatment; it is designed to target vascular endothelial growth factor receptor-1 (VEGFR-1) in patients with renal cancer. Phase I results (2005) in patients with refractory solid tumors showed a favorable safety profile, and 25% of patients had stable disease for more than 6 months [90]. Angiozyme was recently evaluated with metastatic breast cancer patients (Phase II, 2012) but did not show clinical efficacy [91].

Aptamers, unlike other non-coding RNAs, rely on their tertiary and quaternary structure for interacting and binding with target proteins [92].

Aptamers can bind proteins in a similar manner to antibodies but with less immunogenicity. Therefore, they are an improved alternative to current therapeutic antibodies.

Like antibodies, most of the aptamer's targets are still confined to only extracellular or membrane proteins [93]. AS1411 (Antisoma PLC) was designed to inhibit nucleolin activity and was the first aptamer to reach a clinical trial for cancer treatment. Extended phase I (2006) and phase II (2014) studies have shown promising outcomes in patients with metastatic renal cell carcinoma [94, 95]. NOX-A12 (Noxxon Pharma), an aptamer conjugated to PEG polymer, was designed to target and block the activity of chemokine CXCL12 [96, 97]. The combination of NOX-A12 and Bendamustine/Rituximab, was evaluated in patients with chronic lymphocytic leukemia (Phase IIa, 2014) [98]. This combination, when compared to the historical data of patients treated with Bendamustine/Rituximab alone, improved the overall response rate and complete remission [99]. Aptamers were also studied as homing targets for other agents. For example, labeling AS1411 with Cu-64 allows it to become a PET tracer and utilized as an imaging agent for non-small-cell lung cancer [100, 101]. Notably, the modification of aptamers must be completed with care so that their three-dimensional structures will not be affected and, in turn, retain their functional properties.

Challenges and Limitations: most applications of oligonucleotides (without delivery platforms) are confined to blood or clearance organs (e.g., liver and kidney). Thus, lymphoma, kidney cancer, and liver cancer are the main

candidates amenable to such technology. However, delivering sufficient therapeutic levels of oligonucleotides to other solid tumors (e.g., breast, prostate, and pancreatic cancer) upon systemic administration remains a challenge. Molecular complexes and nanoparticle platforms have been introduced and widely studied in order to address these unmet needs. The next section reviews the strategy to overcome the short half-life of these small oligonucleotides and help them accumulate more in solid tumors. The progress of translating these technologies to clinical trials/applications in cancer treatment will be presented, with the main focus on siRNA delivery.

Of note, although this dissertation primarily focuses on siRNA delivery, the developed nanoparticle can be used with other types of non-coding oligonucleotides discussed earlier. This is because all of them share the same overall physicochemical feature (i.e., containing negatively charged phosphodiester backbones).

1.6 Clinical translation of siRNA therapeutics

Local delivery of siRNAs was the initial step of siRNA translation to clinical use. Local siRNA delivery is feasible for locally restricted diseases with accessible tissues. Bevasiranib was the first siRNA-based drug that reached Phase III clinical trials. It was designed to modulate VEGF expression upon intravitreal administration to treat age-related macular degeneration. The trial was discontinued because it was deemed unlikely to achieve the primary endpoint of reducing vision loss [102], but since then, a number of siRNA

technologies have advanced towards clinical trials--although, to date, none has made it to the market. For cancer, an example of local siRNA delivery is siG12D encapsulated in biodegradable polymer Local Drug EluteR (LODER) developed by Silenseed Ltd. This siRNA modulates mutant KRAS (KRAS-G12D) expression in pancreatic cancer via injection by endoscopic ultrasound needle [103]. Phase I (2013) showed a favorable safety profile and promising efficacy: reduction in tumor marker CA 19-9 was observed in 64% of the patients with locally advanced non-operable pancreatic cancer [104]. A phase II study was set to start in early 2015 but as of this writing is not yet open for participant recruitment.

Systemic (intravenous) administration of siRNAs is considered more feasible and applicable to target a wider spectrum of cancer, including advanced cancer or metastasis where local treatment is not effective. Systemic delivery of siRNAs must overcome several barriers before reaching its intended site, which is the cytosol of cancer cells. When introduced in blood circulation, though, naked siRNAs exhibit potential for the stimulation of innate immune response and susceptibility to blood enzyme degradation. To solve these issues, siRNAs can be modified using several strategies: (1) backbone modifications such as phosphorothioate or boranophosphate linkages, (2) modifications of 2'-OH group on the pentose sugar such as 2'-fluoro, 2'-O-methyl, 2'-O-(2-methoxyethyl), 2'-O-(2,4-dinitrophenyl), and locked nucleic acids, and (3) modifications of the termini such as 5'-phosphate, 5'-O-methyl, and 3'-deoxythymidine [69, 105, 106]. Because of their small size, siRNAs still suffer a short circulation half-life due to

rapid kidney clearance. These modified siRNAs also still lack the ability to home in on cancer cells.

The next section will review how nanoparticles can be used to overcome challenges and limitations of siRNA delivery. Although viral-based siRNA delivery strategy is effective, concerns regarding immunogenicity response and insertional mutagenesis remain major issues [107]. As a result, this review will focus only on non-viral vectors/platforms for siRNA delivery.

1.7 Nanoparticles for siRNA delivery: common rationale and concepts

Prolonging siRNA half-life cannot be achieved by modifying siRNAs alone. Due to their small size, siRNAs will be cleared rapidly by kidney filtration. At the same time, particles larger than 200 nm can be trapped and cleared by the liver and spleen. Nanoparticles loaded with siRNAs (50-200 nm) can thus potentially prolong systemic clearance [108]. Besides size considerations, surface characteristics also dictate their fates in vivo. Both cationic and anionic nanoparticles can bind with opsonins like immunoglobulin and complement proteins. This binding promotes phagocytosis by means of Fcγ and complement receptors, respectively, in the reticuloendothelial system (RES). This also leads to faster clearance by the liver and spleen. To slow down the nanoparticle uptake by RES and, in turn, extend the systemic circulation time, hydrophilic neutral polymer is often used to shield the surface charge of the nanoparticles. Polyethyleneglycol (PEG) [109, 110] is one of the most often used stealth polymers for nanoparticle-mediated gene delivery. Other polymers that can

shield the surface charge on nanoparticles and prolong nanoparticle circulation include dextran [111-113] and sialic acid [114]. This prolonged circulation of siRNA-nanoparticles will increase the likelihood of their accumulation in tumor and thus their efficacy.

The toxicity of cationic nanoparticles must be taken into account when they are used as a siRNA delivery platform. Although cationic materials (polymer or lipid) are commonly used for siRNA delivery due to their ability to load negatively charged siRNAs, they are considered toxic to cells and notorious for poor blood compatibility. Cellular damage can be caused by direct interactions between the cationic groups and cellular components or indirectly by reactive oxidative species (ROS) formed in the presence of cationic compounds [115, 116]. Further, cationic nanoparticles can interact with red blood cells, causing hemolysis [117]. Since PEGylation of cationic compounds can serve to shield the surface charge of nanoparticles, the stealth effects of PEG also enhance the safety profile and blood compatibility of cationic materials [118-120].

Targeting tumors by nanoparticles can be achieved by two simultaneous strategies. First, passive targeting of nanoparticles to the tumor area relies on the enhanced permeability and retention (EPR) effect [121]. This effect describes tumors that have abnormal molecular and fluid transport dynamics due to leaky vasculature and poor lymphatic drainage. This pathological characteristic allows nanoparticles of size 50-200 nm to remain in tumor tissue. Secondly, active targeting by nanoparticles can be achieved by decorating their outer surface with targeting agents (homing targets) [122] such as monoclonal antibodies, single-

chain variable fragments (scFv), targeting peptides, transferrin, folic acid [113], and aptamers. This strategy utilizes the distinct characteristics of each tumor's overexpressed membrane proteins. As a result, the targeting components on the nanoparticles can enhance the affinity binding to such targeted membrane proteins (and/or receptors) on cancer cells and promote cellular uptake via receptor-mediated endocytosis [123]. For example, breast cancers that overexpress HER2 can be targeted by nanoparticles decorated with HER2-targeted aptamer [124], scFV [125] or antibody [126]. Other examples include cancer cells that overexpress folate [127, 128] or transferrin receptors [129, 130]. In order to deliver cargo to these cancer cells in a more targeted manner, folate or transferrin can be employed as homing targets, respectively.

Endosomal escape is considered a major cellular barrier for siRNA delivery. The primary route of nanoparticle uptake to cells is endocytosis. Upon endocytosis, early endosomes containing siRNA-nanoparticles will later fuse with sorting endosomes, late endosomes and eventually lysosomes in which various nucleases and acidity will degrade siRNAs. To avoid lysosomal degradation, nanoparticles must be capable of compromising endosomal membranes so that siRNAs can escape from the endosome into cytosol, where they can function [131, 132]. Properties of different materials can be utilized to achieve this effect and will be discussed in the next section.

Figure 1.9 summarizes the barriers siRNA-nanoparticles must overcome before reaching the cytosol. To summarize, to be feasible for siRNA delivery, the nanoconstructs must (1) be intravenously injectable and thus dispersible in

saline, (2) have prolonged blood circulation (avoiding rapid clearance by the kidney and liver) so they can seek and accumulate in the tumor, (3) protect siRNAs against blood enzyme degradation, (4) be taken up effectively into cells, (5) escape the endosome and release siRNAs in the cytoplasm, and (6) have low toxicity.

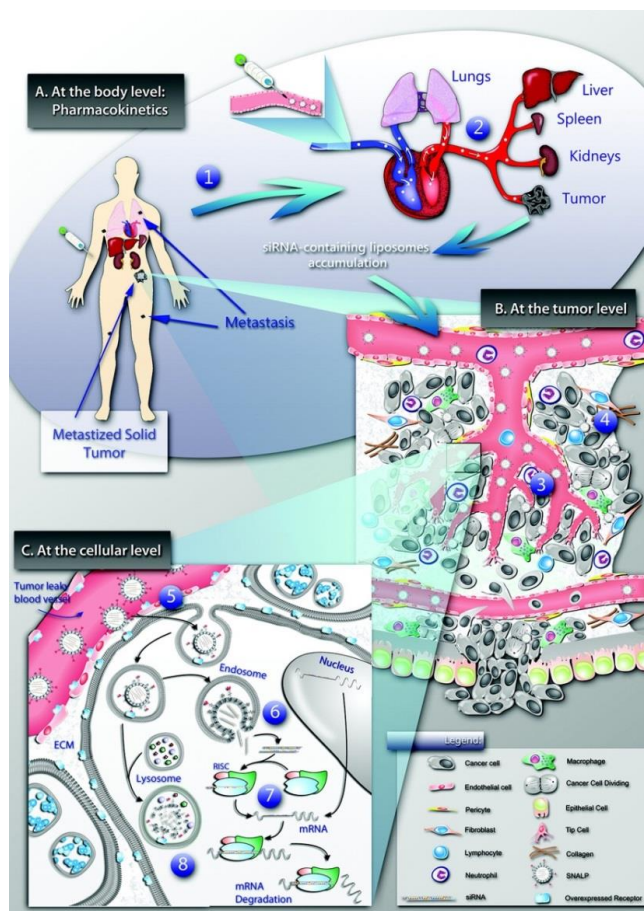


Figure 1.9: Barriers of siRNA delivery upon systemic administration. To overcome several barriers, nanoparticles (e.g., liposomes) are proposed to package and deliver siRNA. (1-2) System level: nanoparticles should avoid the uptake by reticuloendothelial system, prolonging clearance. (3-4) Tumor level: longer circulation time of nanoparticles enhances the chance of accumulation in tumors. (5-8) Cellular level: nanoparticles must be taken up efficiently by cancer cells and able to trigger endosomal escape and deliver siRNAs to their site of action, cytosol. Reprinted with permission from Gomes-da-Silva et al. [133]. Copyright (2012) American Chemical Society.

1.8 Different classes of nanoparticles for systemic delivery of siRNAs

This section summarizes the different classes of materials utilized for siRNA delivery and focuses on those that show efficacy in animal models upon systemic administration. The three main classes of materials under investigation are lipid-based, polymer-based, and inorganic-based nanoparticles.

1.8.1 Lipid-based nanoparticles. As can be seen in the subsequent sections, lipid-based nanoparticles or liposomes are among the earliest material class for systemic siRNA delivery that advanced to clinical trials. A lipid molecule consists of a hydrophilic head group and a hydrophobic tail (**Figure 1.10A**). When put in solution with siRNA, siRNA-liposomes can self-assemble as depicted in **Figure 1.10B**. Cationic lipids [134] that were used to form siRNA-encapsulated liposomes include dioleoylphosphatidyl ethanolamine (DOPE) [135-137], dimethyldioctadecylammonium bromide (DDAB) [136], N-[1-(2,3-dioleyloxy)propyl]-N,N,N-trimethylammonium chloride (DOTMA) [137], 1,2-dioleoyl-3-(trimethylammonium) propane (DOTAP) [135, 136], and oleic acid (OA) [138]. Neutral lipids include 1,2-dioleoyl-sn-glycero-3-phosphatidylcholine (DOPC) [139] and cholesterol. The outer membrane of the liposome can be further functionalized with other components such as PEG and targeting agents. To achieve endosomal escape, liposomes can reorganize and bind the anionic phospholipids on the endosomal membrane. This binding destabilizes the endosome, allowing endosomal escape of siRNAs (flip-flop mechanism) [140].

A majority of lipid-based nanoparticles exploit their natural tendency to accumulate in the liver (major clearance organ) [141-143]. Due to self-assembly one-pot synthesis, liposomes are typically not monodispersed. The specific examples of lipid-based platforms for siRNA delivery in clinical trials will be discussed in the next section.

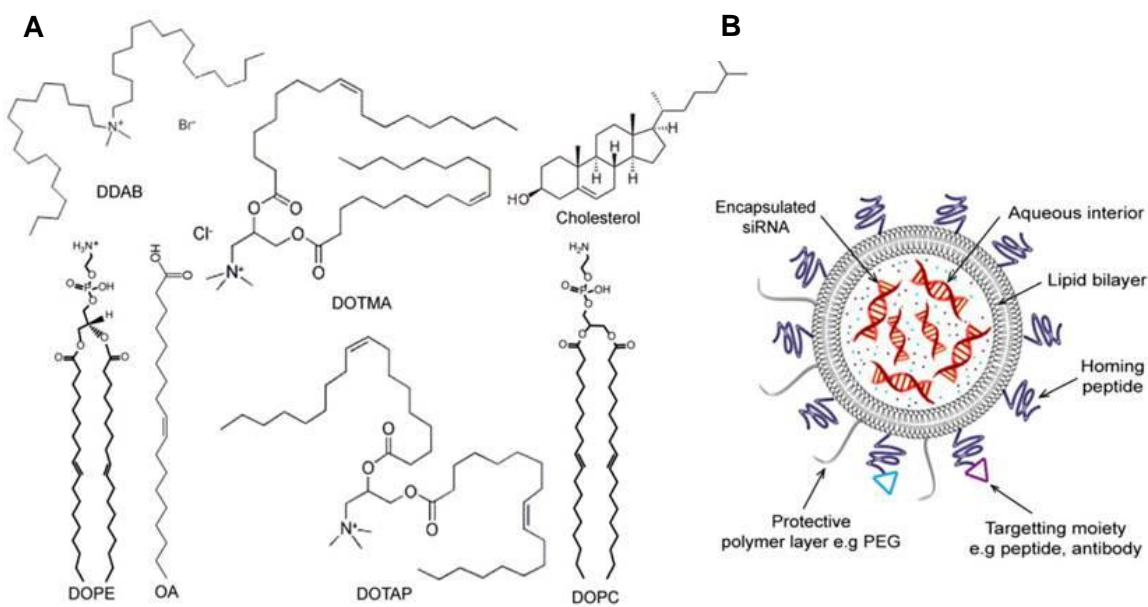


Figure 1.10: Lipid-based nanoparticles for siRNA delivery. (A) Common lipid types and structures used in siRNA delivery. (B) A schematic of lipid-based nanoparticle, e.g., liposome. SiRNA molecules are encapsulated in the aqueous interior of liposomes. Lipid-based nanoparticles can additionally carry a surface protective polymer layer (e.g., PEG) and targeting agents, including homing peptides and antibodies for targeting delivery. Copyright © 2014, Rights managed by Ivyspring International Publisher [134].

1.8.2 Polymer-based nanoparticles. The cyclodextrin-based nanoparticle is the first polymeric nanoparticle that entered clinical trials for systemic siRNA delivery to cancer (see next section) [144]. Since then, there have been several attempts

to develop a polymeric-based platform for siRNA delivery. **Figure 1.11** shows different polymer structures and examples of synthetic and biological polymers. Among these lists, polymers used for siRNA delivery are typically cationic to allow for the loading of negatively charged siRNAs (ionic interaction). In some cases, anionic and neutral polymers can also be used to better condense the polyplex of siRNAs and cationic polymer. Also, siRNAs can be conjugated directly on the polymer. Different strategies to load siRNAs in polymeric construct are summarized in **Figure 1.12**.

Polyethylenimine (PEI) has been a gold-standard polymeric carrier for gene (siRNA and DNA) delivery in vitro. However, the associated toxicity (e.g., oxidative stress, inflammation, and cytotoxicity [145]) is concerning. The strategy to reduce toxicity is to modify PEI and/or use PEI as coatings instead of polyplexes. PEI mediates effective gene delivery due to its high buffering capacity--that is, its ability to resist pH change. Upon siRNA uptake, the buffering capacity of PEI can promote endosomal escape [108, 146]. Briefly, once entering the endosome, PEI buffers the pH conditions and resists the acidification process of endosomal compartments. Hence, in the presence of PEI, to lower the endosomal pH to its natural pH of ~6-6.5, more protons must be sequestered into the endosome through endosomal proton pumps. Each influxed proton is accompanied by influx of one Cl⁻ anion and one water molecule. Ultimately, this process causes the endosome to swell, rupture, and release siRNAs into cytosol. Examples of other amine-containing polymers that can deliver siRNAs utilizing

this proton sponge effect include chitosan, Polylysine (PLL), Polypropyleneimine (PPI), and Polyamidoamine (PAMAM).

A dendrimer is a symmetric and highly branched polymer. Due to its defined structure, dendrimer is of high interest for encapsulating siRNAs. The outer surface of dendrimer can also be further conjugated to other components, such as a PEG stabilizer or targeting agents. The two most commonly used dendrimers that have been studied for in vivo siRNA delivery are PAMAM [147] and PPI [148].

Some examples of polymer used in siRNA delivery (preclinical studies) and their limitations are summarized in **Table 1.1**. Common challenges for polymeric carriers are toxicity concerns, poor siRNA protection ability, and poor scalability and reproducibility.

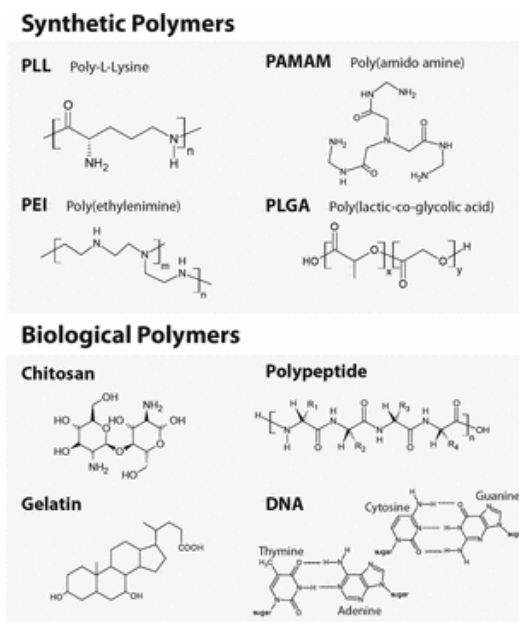


Figure 1.11: Polymeric structure for siRNA delivery. Modified with permission from John Wiley and Sons [149].

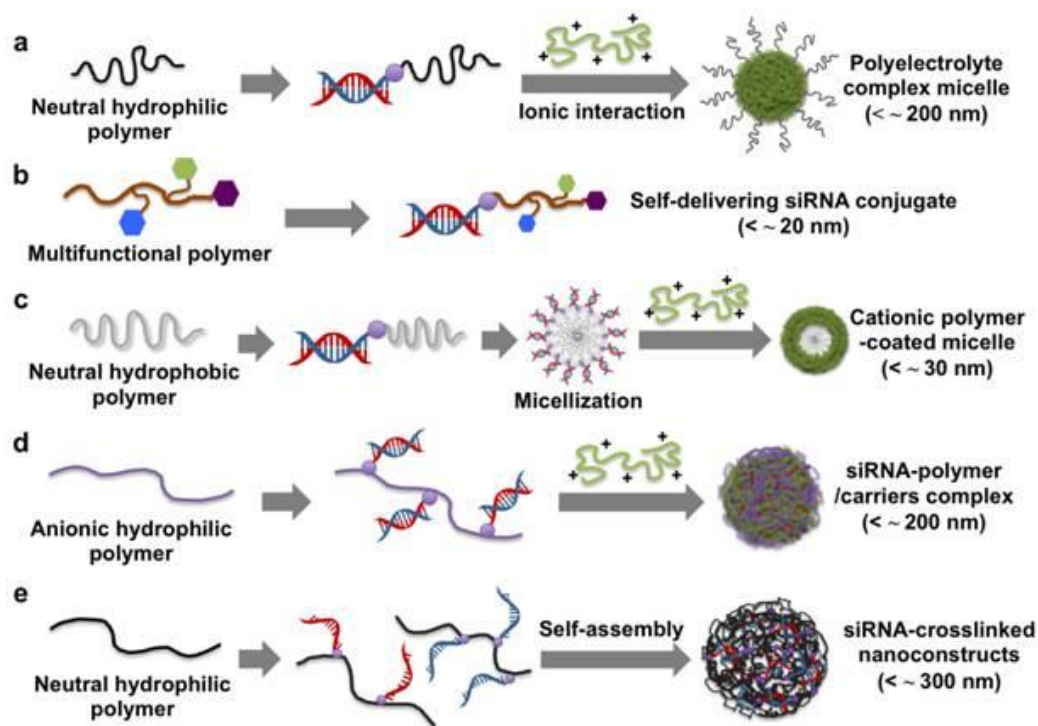


Figure 1.12: Strategies to load siRNAs on the siRNA-polymeric construct.
 Copyright © 2014, Rights managed by Ivyspring International Publisher [150].

Table 1.1 Examples of polymeric construct for siRNA delivery

Material	Year [ref]	Gene target	Homing target	Disease	Limitations
Poly-siRNA/Glycol chitosan self-cross-linked NPs	2012 [151]	VEGF	None	Prostate cancer	Chitosan NPs (not protected with PEG) have been reported to cause toxicity (blood toxicity, cell damage, increase ROS, induce apoptosis, damage embryo development, toxicity is comparable to ZnO)
RGD-labelled chitosan nanoparticles	2010 [152]	PLXDC-1	RGD peptide	Ovarian cancer	
Atelocollagen	2009 [153]	Bcl-xL	None	Prostate cancer	Poor material stability in blood, cannot incorporate targeting component, poor siRNA protection
PEI-g-PEG-RGD/siRNA polyplex	2011 [154]	VEGFR-1	RGD peptide	Colon cancer	Poor protection of siRNAs from blood enzymes (only up to 6 h in 20% serum)

1.8.3 Inorganic nanoparticles exhibit unique tunable properties including large surface-to-volume ratios and the capacity for surface modifications. They are also typically easier to synthesize with high reproducibility and scalability. The rigid formulations afford a better chance of compound stability. Some of the materials that have been used in siRNA delivery include metallic (gold) nanoparticles, carbon nanotubes, quantum dots, magnetic (iron oxide) nanoparticles, silica nanoparticles, and calcium phosphate nanoparticles [155]. In most cases, however, to enable siRNA delivery, inorganic nanoparticles are typically modified or coated with other polymers or lipids, generating a composite compound.

(Mesoporous) silica nanoparticles have many favorable properties as drug delivery carriers such as tailorable mesoporous structures, high specific surface areas, large pore volumes [156], ease of controlling size, and high synthesis scalability. Thus, they have been studied extensively and evaluated for their biomedical applications. Mesoporous silica is biodegradable to non-toxic components (e.g., silicic acid) that can be cleared by kidneys [157]. Silica nanoparticles (C dots) were approved for clinical trials as injectable PET tracers, and the Phase I safety profile was favorable [158]. Therefore, the translation of other silica-based nanoparticles to clinics should be feasible.

Mesoporous silica nanoparticles have been widely researched for siRNA delivery in vitro and in vivo. For those that show efficacy in animals upon systemic administration, MSNPs were coated with cationic polymers including PEI-cyclodextrin [159], PDMAEMA [160], and PEI-PEG [161] for loading siRNAs

and/or aiding in cellular uptake. Shen et al. [159] and Lin et al. [160] loaded siRNAs inside the pores of the nanoparticle before coating with polymer, thus requiring a bigger nanoparticle (80-150 nm MSNP core size). While promising, no significant anti-tumor activity in vivo has been reported for these constructs [159, 160]. Meng et al. reported that the PEG-PEI-MSNP platform co-delivers doxorubicin (in the pore) and siRNAs (on the polymer surface), relying on the EPR effect [161]. However, siRNA loading is low (NP/siRNA mass ratio of 100), and the platform had no targeting component. No MSNP-based platforms have been reported for targeted siRNA delivery upon systemic administration.

Iron oxide nanoparticles have been widely evaluated in biomedical and clinical applications. Examples of the FDA-approved injectable iron oxide nanoparticles include ferumoxtran-10 as an MRI imaging agent and ferumoxytol as an iron replacement product for anemia in patients with chronic kidney disease. Iron oxide nanoparticles are deemed safe because iron exists in and is essential for the body. In addition, iron oxide nanoparticles can be guided to the target site by magnetic drug delivery. Lastly, superparamagnetic iron oxide nanoparticles (SPIONs) can generate heat under alternating magnetic fields and have been explored for magnetic hyperthermia treatment of cancer. Since iron oxide nanoparticles have been approved by the FDA, the translation of this class of materials to clinics is highly feasible.

For these reasons, SPIONs are widely studied as drug/gene delivery platforms. Wu et al. attached to the SPION targeting agents consisting of PEI, PEG, and RGD peptides [162]. Targeted nanoparticles appeared to deliver

survivin siRNA more effectively than their non-targeted counterpart, exemplified by gene silencing activity and apoptotic markers in tumors. In addition, this platform can be monitored under an MRI scan. Tumor growth inhibition was achieved with every-other-day injections of 1.6 mg siRNA/kg.

Calcium phosphate nanoparticles, unlike other inorganic nanoparticles, possess the unique property of being able to induce endosomal escape by themselves. Calcium phosphate can dissolve in acidic conditions [163-165]. This process increases endosomal osmotic pressure and, in turn, causes endosomes to swell and eventually rupture. Yang et al. utilized calcium phosphate nanoparticles coated with lipid bilayer, PEG, and anisamide as a targeting ligand for siRNA delivery [166]. In vivo efficacy (tumor growth inhibition) upon systemic administration was also reported.

Gold nanoparticles are of interest for biomedical applications due to their property of surface plasmon resonance (SPR). They can be utilized for bioimaging diagnosis [167] and photothermal therapy [168]. SiRNA delivery with gold nanoparticles has also been widely studied in vitro. Studies that have evaluated response in animal models upon systemic administration are much less prevalent. For example, relying on passive delivery, Jensen et al. successfully delivered siBcl2L12 to glioblastoma by conjugating siRNAs and PEG directly on gold nanoparticles [169]. The authors suggested loading targeting components on their construct as a next step. Despite the advantages, the translation to clinics might be challenging due to its relatively high price. Also, the safety and biocompatibility of metal nanoparticles requires additional studies.

Carbon nanotubes have also been evaluated as siRNA carriers. However, toxicity is of major concern for this class of material. The mechanisms of carbon nanotube toxicity include oxidative stress, inflammatory responses, and DNA damage [170, 171]. Most studies that employ carbon nanotubes to deliver siRNAs in vivo employ local injection (intratumoral injection) [172, 173]. While carbon nanotubes have been widely studied for drug delivery, in vivo efficacy as siRNA carriers upon systemic administration has not yet been reported for cancer treatment.

Quantum dots have unique electronic and optical properties that are tunable to different sizes and shapes [174, 175]. While they may be useful tools for molecular biology as imaging agents, the toxicity of their components (i.e., cadmium and tellurium) is an issue [176]. This will likely limit the translation of quantum dots to in-human clinical applications in the near future. Non-toxic quantum dots are currently under research in a developmental stage [177, 178]. Quantum dots have not yet been evaluated in vivo for siRNA delivery.

1.9 Translation of systemic siRNA delivery to cancer treatment in clinics

The systemic delivery of siRNAs in their infancy relied on modified siRNAs without carriers. These siRNAs have been chemically modified to enhance their stability and allow cellular uptake. However, due to their small size, a majority of them will be cleared by the kidneys, with a filtration size cutoff of 10 nm. Therefore, these modified siRNAs can be effectively utilized in the field of renal cancer [179].

To overcome kidney clearance, nanoparticle platforms have been developed for siRNA delivery. The first nanoparticle system that reached clinical trial for siRNA delivery to solid tumors was the cyclodextrin nanoparticle system (CALAA-01), developed at Calando Pharmaceuticals. It was designed to deliver siRRM2 (siRNA against the M2 subunit of ribonuclease reductase) to melanoma. The Phase I trial started in 2008 but was terminated in 2013 after a dose-limiting toxicity was observed in some patients [180, 181]. However, this was the first successful proof-of-concept study of targeted delivery of siRNAs by nanoparticles to solid tumors in humans, as successful RNAi activity (in terms of 5' RACE detection and protein knockdown) was evident in patients' biopsy samples [182]. Since then, there have been several developments in siRNA delivery. **Table 1.2** summarizes the nanoparticle systems that have reached clinical trials for cancer treatment upon systemic administration, along with references that describe the technology. It can be seen that a majority of these technologies are lipid-based, exploiting their natural tendency to accumulate in the liver (a major clearance organ) [141-143]. Delivering siRNAs successfully to other solid tumors in humans remains a challenge. For example, Atu027 was designed to modulate PKN3 expression in the vascular endothelium (not cancer cells) [183]. Therefore, it was expected to prevent or limit metastasis by normalizing the physiologic properties of endothelial cells. It is not expected to achieve tumor shrinkage on its own because it does not target tumor cells. In a completed Phase I study, Atu027 was found to stabilize diseases in 41% of the patients with advanced solid tumors at the end of treatment (i.e., 8 weeks) [183]. Accordingly, it will be evaluated in

combination with gemcitabine in patients with pancreatic cancer in the Phase I/II trial (not yet recruiting). While the development of Atu027 signifies important progress in the field of siRNA delivery, it has not yet addressed the need to deliver siRNAs specifically to cancer cells. Other particles are lipid-based nanoparticles, which face the same limitations of liver homing. Clinical trials evaluating these compounds in solid tumors beyond the liver are ongoing (**Table 1.2**), and their efficacy remains to be seen.

Table 1.2 Clinical trials of nanoparticle-mediated siRNA delivery upon systemic administration for cancer treatment. The drug names, companies, material descriptions, targeted diseases, and their clinical status are shown. Details on each material can be found in the cited references. ClinicalTrials.gov Identifier numbers are also shown (NCTXXXXXXXX).

Year	Drug [ref]	Company	Gene target	Description	Diseases/Indications	Clinical status	Clinical Trial ID
2008-2012	CALAA-01 [182]	Calando Pharma.	RRM2	Cyclodextrin-based nanoparticles conjugated with transferrin as a targeting agent	Solid tumor/advanced melanoma	Phase I, terminated	00689065
2009-2011	ALN-VSP02 [184]	Alynlam Pharma.	KSP + VEGF	Stable nucleic acid lipid particles (SNALPs)	Advanced solid tumors with liver involvement	Phase I, completed	00882180
2010-2012						Phase I, completed	01158079
2009-2012	Atu027 [183, 185, 186]	Silence Therapeutics	PKN3	Cationic lipoplex containing siRNA	Advanced solid tumors	Phase I, completed	00938574
2013-2015					Pancreatic ductal carcinoma	Phase I/II, not yet recruiting	01808638
2011-2012	TKM-080301 [187]	Tekmira Pharma.	PLK1	Stable nucleic acid lipid particles (SNALPs)	Solid tumors with liver involvement	Phase I, completed	01437007
2010-2014					Neuroendocrine tumors and adrenocortical carcinoma	Phase I/II, recruiting	01262235
2014-2016					Hepatocellular carcinoma	Phase I/II, recruiting	02191878
2014-2016	DCR-MYC [188]	Dicerna Pharma.	MYC	Lipid nanoparticles	Hepatocellular carcinoma	Phase I/II, recruiting	02314052
2014-2015					Solid tumors, myeloma and lymphoma	Phase I, recruiting	02110563
2015	siRNA-EphA2-DOPC [139]	MD Anderson Cancer Center	EphA2	Neutral liposomes	Advanced cancer	Phase I, not yet recruiting	01591356

No siRNA therapeutics for HER2⁺ breast cancer have ever reached clinical trials. In preclinical studies, there are a few studies of siRNA delivery to HER2⁺ breast cancer. For example, Inoue et al. utilized poly(malic acid) conjugated with HER2 antisense and trastuzumab for targeted delivery [189]. Yao et al. complexed siPLK1 (siRNA against PLK1 protein) with peptide fusion protein containing HER2 scFv (single-chain variable fragment) for targeted siRNA delivery [125]. Despite promising results from both studies, they revealed the efficacy in trastuzumab-sensitive (BT474) tumor models only. As a result, there is still no study that shows siRNA-nanoparticle efficacy in drug-resistant HER2⁺ breast cancer.

1.10 Scope of the dissertation

The focus of this dissertation is to develop a nanoparticle platform that can deliver siRNAs (and potentially other oligonucleotides) to breast tumors and can also elicit therapeutic effects. Due to its overexpression of surface HER2 proteins, HER2⁺ breast cancer serves as an excellent model for the evaluation of this targeted nanoparticle. The nanoparticle under study is based on the mesoporous silica nanoparticle (MSNP). MSNP is surface-decorated with polymer to allow siRNA loading and incorporate a targeting component to enable targeted delivery of siRNAs to HER2⁺ breast cancer. The targeting agent used in this research is the HER2 monoclonal antibody trastuzumab. Another advantage of this developed nanoparticle is that it enables the loading of many cargos simultaneously. Moreover, siRNAs are loaded on nanoparticles by electrostatic interaction, irrespective of their sequences, thus any individual siRNAs can be

loaded onto the nanoparticles effectively. As such, alternative therapeutic siRNAs were also considered and evaluated. In addition to oligonucleotides, the developed nanoparticles can also simultaneously load and deliver chemotherapeutic drugs to cancer cells. This can enable the multiple synergistic therapeutic schemes for these compounds.

The remainder of this dissertation will be segmented into six other chapters. Some of the data in Chapters 2-5 have been published in *Advanced Functional Materials* [190], and the permission to reproduce in a dissertation (full article portion) was granted by John Wiley and Sons. The rationale and nanoparticle design and synthesis will be described in **Chapter 2**. A library of nanoconstructs will be screened for in vitro and in vivo efficacy in **Chapter 3**. During the material development and optimizations, the therapeutic siRNA employed will be siHER2 (siRNA against HER2 mRNA). HER2 knockdown in HER2⁺ breast cancer has great potential to address the resistance of such cancer to current HER2-targeted therapies. As stated above, the combination of HER2-targeted therapies (e.g., pertuzumab and trastuzumab) was shown to prolong survival better than the single agent. This suggests that complete HER2 blockade serves as a promising strategy to address resistant HER2⁺ breast cancer. Another important facet of this technology that aids translation to humans is its inherent safety. As a result, **Chapter 4** describes the in vitro and in vivo safety evaluation of the developed nanoconstruct. Furthermore, scalability and reproducibility of nanoparticles is another hurdle for translation and will be described in **Chapter 5**. Finally, while this dissertation focuses on nanoparticle-

mediated siRNA delivery to breast cancer, a proof-of-concept study for loading chemotherapeutics and additional siRNAs beyond siHER2 is discussed in **Chapter 6**. **Chapter 7** covers the conclusions of the dissertation work and ongoing/future efforts.

Overall, the targeted delivery of siRNAs by nanoparticles has wide applicability in cancer therapy. This technology will enable the modulation of any gene deemed important for a disease state. This platform development coupled with genome analysis and RNAi functional screening could provide a more effective treatment in HER2⁺-refractory breast cancer. Also, the developed nanoparticles can be extended to other types of cancers or diseases by merely using different targeting components and therapeutic cargos.

2. Chapter 2: Material Design, Synthesis and Characterization

This dissertation describes the development of a mesoporous silica nanoparticle (MSNP) construct for the in vivo delivery of siRNAs to breast tumors. Antibody-based targeting of MSNPs carrying chemotherapeutic agents to specific cells have been reported [191-194], but targeted delivery of siRNAs by MSNPs upon systemic administration has not been reported. The MSNPs described herein are functionalized with PEI-PEG co-polymer and targeting antibodies for targeted delivery of siRNAs to HER2-positive (HER2⁺) breast cancer cells. The construct is immunologically targeted to cells that overexpress the HER2 protein by utilizing an antibody against HER2, trastuzumab. This chapter covers the design rationale, synthesis, and characterization of the developed nanoconstructs.

2.1 Materials and Methods

2.1.1 Reagents and siRNAs

TEOS, CTAC, NaH₂PO₄•H₂O, Na₂HPO₄ and TEA were obtained from Sigma Aldrich (MO). Branched-PEI (1.8 or 10 kDa) was obtained from Alfa Aesar (MA). Maleimide-PEG(5kDa)-NHS was obtained from JenKem Technology USA (TX). PBS (pH 7.2) was obtained from Life Technologies (CA). Desalting columns (MW 40 kDa), RNase free water, Traut's reagent, DSP, ethanol, concentrated HCl, sodium hydroxide and siRNAs (see details in Chapter 3) were

obtained from Thermo Fisher Scientific (MA). All reagents are of highest purity grade available.

2.1.2 Synthesis of nanoconstructs

The sol-gel synthesis of uniform mesoporous silica nanoparticle cores (MSNPs) was modified from previous reports [195, 196]. For the 47-nm nanoparticle (NP) core, denoted “S-47”, CTAC (0.15 M) and TEA (350 μ L) were mixed in water (125 mL) at 95 °C. Then, TEOS (3 mL) was added and the mixture was stirred for one hour. Afterwards, the pellets were recovered from suspension by centrifugation, washed with a copious amount of ethanol, and dried overnight. The particles were then re-suspended and refluxed in acidic methanol (HCl (0.6 M) in methanol) overnight to remove CTAC and TEA. Bare MSNPs were then washed with ethanol and dried in a desiccator. TEA was also varied from 200 to 450 μ L to achieve the MSNP sizes of 60 nm and 30 nm, respectively.

Nonuniform MSNPs (O-87) were synthesized by base-catalyzed synthesis (adapted from [161, 197]). CTAB (6 mM) was dissolved in aqueous solution (240 mL, pH 11.0), adjusted by NaOH (2 M). When the temperature stabilized at 80 °C, TEOS (2.5 mL) was added. The reaction continued for 2 h and particles were processed for surfactant removal in the same fashion as explained above.

Coating of PEI on the exterior of the MSNP was carried out in ethanol by shaking MSNP (10 mg) and PEI (2.5 mg) in ethanol solution for 3 h at room temperature. For the version with cross-linked PEI, the MSNP-PEI was pelleted down and resuspended in ethanol solution containing PEI (2.5 mg) and DSP (0.2

mg) as a bioreducible cross-linker. The solution was shaken for another 40 minutes. The particles were pelleted down, washed, and resuspended in PBS (pH 7.2).

For PEG loading, mal-PEG-5kDa-NHS (50 mg) was conjugated to the primary amine of the MSNP-PEI (10 mg) in the PBS buffer under constant shaking (20 h, RT, 300 rpm).

Antibody conjugation of the MSNP-PEI-PEG utilized a thiol-maleimide reaction modified from literature [198, 199]. First, the antibody (trastuzumab (T) or rituximab (R)) was thiolated with Traut's reagent in PBS (pH 8.0) by 50-fold molar excess of Traut's reagent for 2 h and then purified by Zeba spin column – MW-40,000 (Thermo Fisher Scientific). Thiolated antibodies were then mixed with MSNP-PEI-PEG at an antibody:nanoparticle mass ratio of 1:10. The reaction was completed overnight at 4 °C under shaking conditions (300 rpm). The material was pelleted down, resuspended in PBS, and washed with copious amounts of PBS.

Lastly, loading of siRNAs was achieved by mixing MSNP-PEI-PEG-T (designated as T-NP) and siRNAs (at nanoconstruct/siRNA (NP/siRNA) mass ratio of 25 or 50) in PBS solution under shaking (1 h, room temp, 200 rpm).

2.1.3 Characterization of nanoconstructs

MSNPs can be characterized for primary/dry size with TEM (Phillips/FEI CM120/Biotwin TEM) and hydrodynamic size with Zetasizer (ZS-90/Malvern). Surfactant removal of MSNPs was confirmed with Fourier transform Infrared

spectroscopy (FT-IR) analysis. The PEI and PEG loading were analyzed by thermogravimetric analysis (TGA Q50, TA Instruments). Pierce BCA assay kit (Thermo Fisher Scientific) was used to quantify the antibody loading on the nanoparticles, following manufacturer's protocol. The loading of siRNAs was confirmed by monitoring the fluorescent signals of siRNAs labeled with Dylight-677 fluorescent dye.

2.1.4 Buffering capacity measurement

Nanoconstructs were suspended at 0.2 mg/mL in NaCl (150 mM, pH 9 -- pH adjusted with 0.05 M NaOH). Upon stabilization at pH 9.0, HCl (5 μ L, 0.05 M) was added, and the solution was continuously stirred. When reaching steady state, the pH was recorded and the acid was added again. The process was repeated until the pH plateaued at around 3.0. The solution pH was then reported as a function of the amount of acid added.

2.1.5 Serum enzymatic siRNA protection assay

siRNA-nanoconstructs were incubated with human serum (50 v/v% in PBS) for specified time periods (0, 0.5, 1, 2, 4, 8, 24, and 48 h) at 37 °C under continuous shaking. At the end of each time point, the sample was mixed with proteinase K (200 μ g/mL) and frozen at -80 °C to stop the enzymatic reaction. Next, to release the siRNA from the nanoparticles for subsequent gel analysis, thawed samples were spiked with SDS (1.0 wt.%), mixed with an equal amount of 2X loading buffer and loaded onto a 15% TBE-urea gel (BioRad). The gel ran at 100 V for the first 20 minutes, and 150 V for another hour. The gel was then stained with SyBR Gold (Life Technologies) following manufacturer's protocol,

and viewed under the UV chamber. The band intensity was analyzed by ImageJ software. The fraction of intact siRNAs was reported as a function of time that the siRNA-nanoconstructs were in serum (50 v/v% in PBS).

2.2 Results and discussion

2.2.1 Material design and composition

We selected a rigid MSNP core was selected because of its low toxicity, large pore volume (e.g., 0.6-0.9 cm³/g [156]), large surface area (e.g., 500-800 m²/g), and ease of controlling the sizes during synthesis. I loaded MSNP layer-by-layer with PEI, PEG, trastuzumab, and siRNAs as outlined in **Figure 2.1**. This layer-by-layer modification on a rigid nanoparticle enables scale-up production and synthesis reproducibility.

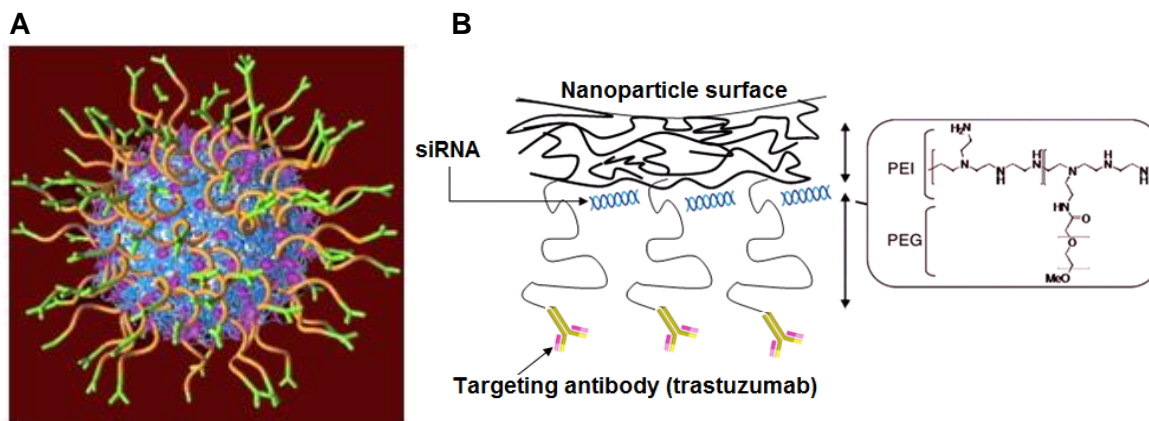


Figure 2.1: Schematic illustration of the nanoconstruct. (A) Nanoparticles are exteriorly modified layer-by-layer with cationic polymer (cross-linked PEI, blue), PEG (orange), antibody (green) and siRNA (magenta). (B) Diagram illustrating the location of each component on the mesoporous silica nanoparticle surface.

PEI, as can be seen from Chapter 1, has been a gold-standard polymer for siRNA delivery. PEI can readily complex with siRNAs by charge interaction of cationic polymer and anionic siRNA. However, PEI is known for its blood toxicity as the cationic charge can interact with blood cells. PEI was thus coated on nanoparticles and further stabilized with PEG polymer to minimize the toxicity, compared to PEI-siRNA polyplex. Another role of PEI is to enhance the endosomal escape by the proton sponge effect. This capability is related to the buffering property of PEI (Chapter 1). The buffering capacity of PEI was shown to be dependent on the number of secondary and tertiary amine groups on PEI [200, 201]. Therefore, branched PEI is shown to be more effective at delivering siRNAs than the linear counterpart. As far as toxicity is concerned, the higher molecular weight PEI (e.g., 25 kDa), despite being more effective at delivering siRNAs, appears to be more toxic than the lower molecular weight counterpart. Therefore, PEI used in this study was limited to 10 kDa and lower. In light of this, to further enhance the efficacy of this nanoconstruct, bioreducible cross-linking between amine groups was performed on the PEI layer. As the buffering capacity is higher with the higher number of secondary and tertiary amines of PEI, I hypothesized that cross-linking the PEI layer on the nanoconstruct that generates more secondary and tertiary amines would enhance the buffering capacity of the nanoconstruct.

PEG was further conjugated on the PEI layer to serve as a stabilizer. PEG provides steric effects to avoid aggregation and non-specific protein binding (e.g., opsonin, which is responsible for rapid hepatic clearance) of cationic

nanoparticles and, in turn, prolongs blood circulation. 5-kDa PEG was used throughout the studies because, as will be shown later, it can be loaded on the nanoconstructs at higher molar contents than other molecular weights tested (2-10 kDa). Ideally, PEG molecules should be densely loaded, maintaining a brush-like conformation. Longer PEG chains can get too bulky to maintain a brush-like conformation, while shorter PEG chains may not be sufficient to prevent non-specific binding and nanoconstruct aggregation. I hypothesized that conjugation with PEG would protect siRNAs on PEI layer from blood enzymatic degradation, enhance blood safety, and prevent adverse immune response.

The targeting antibody (trastuzumab) was conjugated to the end of the PEG chain. Trastuzumab is an FDA-approved HER2 monoclonal antibody. In addition to serving as a homing target, trastuzumab also has therapeutic benefits as reviewed in Chapter 1. Trastuzumab was conjugated on the nanoparticle to target and enhance the uptake to cells that overexpress HER2 proteins.

Nanoparticles loaded with polymer and targeting antibody will be hereafter referred to as “***nan constructs***”. siRNAs were loaded last on the external PEI layer of the nanoconstruct (but protected under the PEG layer) to allow facile siRNA escape from the endosome prior to degradation by the lysosome. siRNAs were loaded last rather than before PEGylation because they can cause aggregation of MSNP-PEI, as will be shown in a later section. In other words, without prior PEG stabilization, siRNAs (negative charge) serve as glue that binds MSNP-PEI (positive charge) together.

The advantages of coating PEI and PEG on the MSNP over siRNA-PEI-PEG polyplex (without nanoparticle cores) are as follows:

1. The MSNP provides a solid support for PEI to bind via electrostatic interaction, thus providing initial size control of material based on a rigid core. This layer-by-layer modification allows ease of reproducibility and scalability, compared to the polyplex self-assembly.
2. High-MW (> 20-kDa) PEI is typically required for siRNA-PEI-PEG polyplex in the literature because it can better form a dense polyplex with siRNAs and gives better transfection efficacy. Lower-MW PEI (e.g., ≤10 kDa) does not show good efficacy but is safer because the toxicity of PEI is dependent on the MW. By coating 10-kDa PEI on MSNP, I showed that the material had an efficacious gene knockdown without having to use 25-kDa PEI.
3. Coating PEI and PEG on the MSNP gives better control of size than polyplex. Our final construct has hydrodynamic size of 117 nm (PDI of 0.2), while the similar siRNA-PEI-PEG polyplex (based on 25-kDa PEI) [202] had the reported size of 241 nm. Higher (doubled) PEI/siRNA mass ratio could be used to achieve the size of below 200 nm (i.e., 192 nm), but was found to be too toxic.
4. Our current constructs afford loading of siRNAs last after surface modifications of the MSNP, in contrast to siRNA-polyplex, which loads siRNAs up front (e.g., during polyplex formation). The nanoconstructs thus

support personalized medicine effectively in case patients may need different types of siRNA cargos that may be determined upon diagnosis.

5. Lastly, the MSNP can be loaded with other components, such as fluorescent dyes, contrast agents, or other drugs, in addition to siRNAs. This allows flexibility of co-delivery of multiple agents for synergistic therapy or theranostic application.

Naming convention: The two molecular weights of PEI used in this study are 1.8 kDa and 10 kDa. Nanoconstructs containing 1.8-kDa PEI and 10-kDa PEI are designated as ***NP^{1.8}*** and ***NP¹⁰***, respectively. In addition, the presence of cross-linking on the PEI layer is designated as C. For example, nanoconstruct containing cross-linked 10-kDa PEI is designated as ***NP^{10C}***. After PEI and PEG loading, nanoparticles were further conjugated with trastuzumab (designated as T) to target cells expressing HER2 or with rituximab targeting CD20 (designated as R) as a negative control. These nanoparticle constructs will be referred to hereafter as ***T-NP*** or ***R-NP***, designating trastuzumab-conjugated PEG-PEI-MSNP or rituximab-conjugated PEG-PEI-MSNP, respectively. Therefore, ***T-siRNA-NP^{10C}*** identifies a nanoconstruct containing cross-linked 10-kDa PEI, PEG, trastuzumab and siRNA. Nanoconstructs always have the same 5-kDa PEG layer. Nanoconstructs without PEG layers will be explicitly labeled with no shorthand nomenclature.

2.2.2 Nanoconstruct development and optimization

The first-generation nanoconstruct is developed on a mesoporous silica nanoparticle core generated by a base-catalyzed synthesis. This material has a size of 87 ± 14 nm (by TEM imaging) and designated as “O-87” (**Figure 2.2**). This material was then coated with 10-kDa PEI, 5-kDa PEG, trastuzumab, and siRNAs as described above. This material can effectively deliver siRNAs and display good efficacy (shown in later chapters). However, the size is polydisperse (not uniform) and rather big after coating with all components (~200 nm). Therefore, to enhance the propensity of the nanoconstructs to accumulate in the tumor, I attempted to create a smaller second-generation material.

In an effort to improve the delivery efficacy, I synthesized a second-generation material in a two-surfactant system. This method can yield core particle sizes of smaller diameter with better monodispersity (more uniformness). With this synthesis method, the materials with core size of 34 ± 3 nm, 47 ± 4 nm, or 61 ± 7 nm were obtained (by varying the ratios of two surfactants, see **Methods**). These MSNP cores are designated as “S-34,” “S-47,” and “S-61,” respectively. Each MSNP core was then coated with PEI, PEG, trastuzumab, and siRNA in the same manner. However, as presented in the next chapter, “S” nanoparticles perform worse than “O-87” (with the same polymer modification) in terms of delivering siRNAs and causing gene knockdown. Smaller-sized nanoparticles carry lower amounts of PEI per particle, thus having lower buffering capacity. To enhance the buffering capacity of “S” material, I introduced a cross-linking strategy on the PEI layer as discussed in **section 2.2.1**.

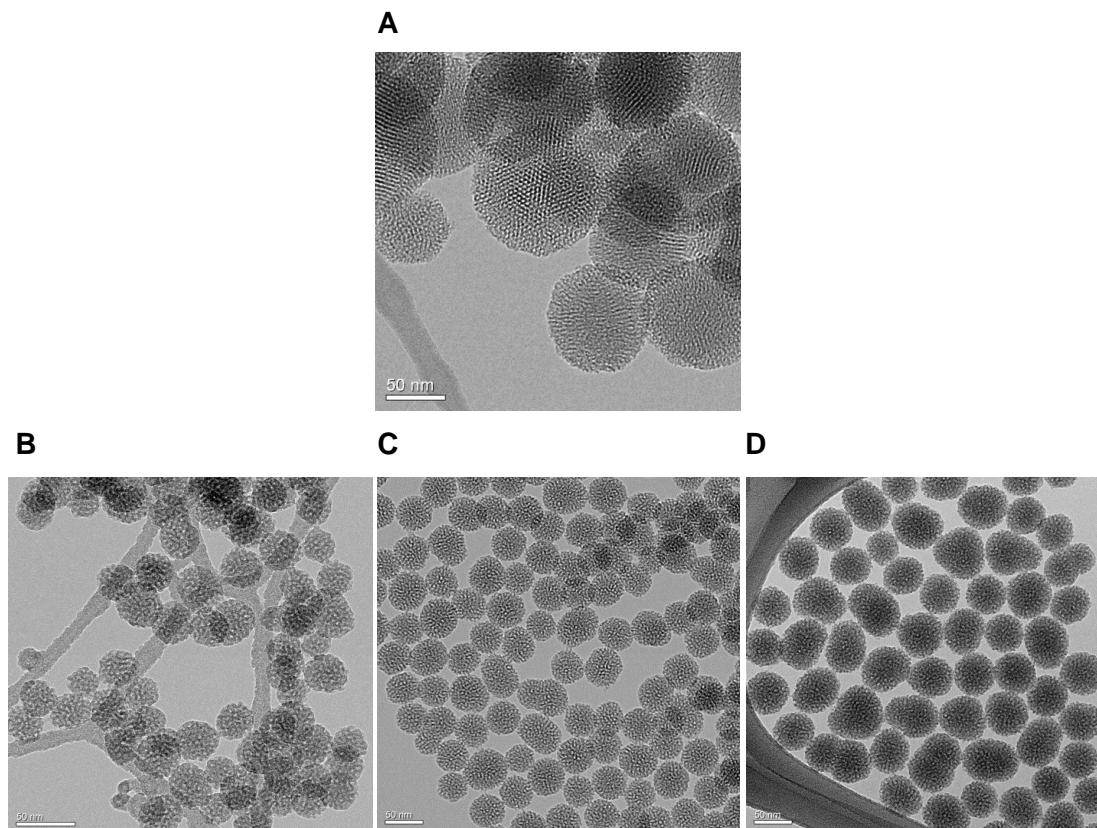


Figure 2.2: TEM images of different mesoporous silica nanoparticles. Representative TEM images of different variations of MSNPs: **(A)** O-87, **(B)** S-34, **(C)** S-47, and **(D)** S-61. Scale bar = 50 nm.

2.2.3 Nanoconstruct characterization

MSNPs were imaged by transmission electron microscope (TEM) to identify their (dry) core sizes, as illustrated in **Figure 2.2**. In addition, as surfactants are used as the templates for mesopores, we also analyzed MSNPs for potential remaining surfactants in the NP cores, using Fourier transform Infrared spectroscopy (FT-IR) (**Figure 2.3**). The graph shows the disappearance of surfactant-associated peaks at 2960, 2870, and 1460 cm^{-1} after the reflux. It

can be seen that the reflux method could remove all surfactants in the mesopores.

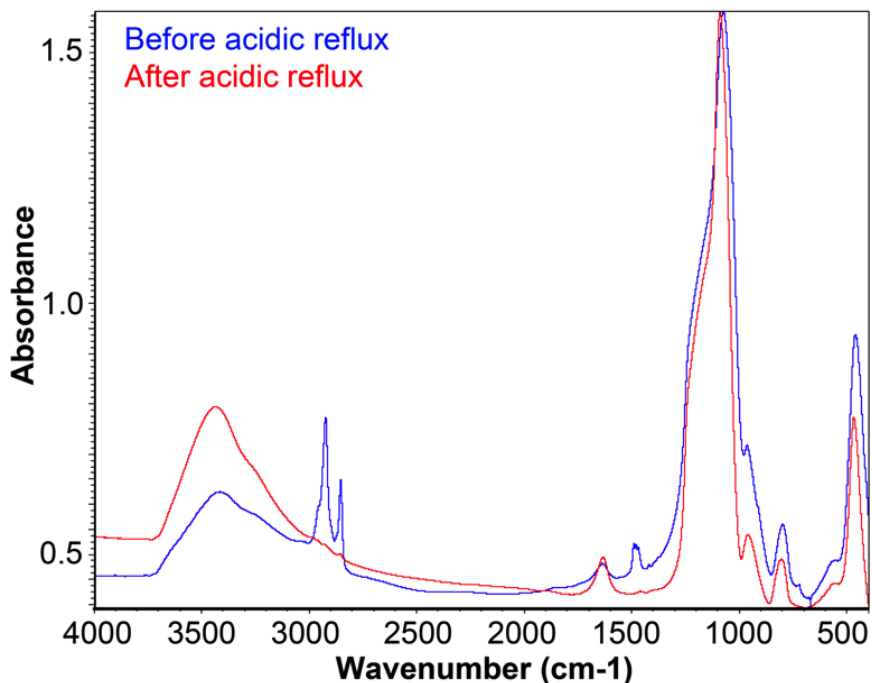


Figure 2.3: FT-IR spectra of MSNP before and after surfactant removal by acidic reflux.

Also, upon coating with polymer and antibody, I characterized nanoconstructs for size and charge in aqueous solution. The nanoparticles had a hydrodynamic size of about 100 nm for the three uniform-sized materials (S-34, S-47, and S-61) and 200 nm for the non-uniform-sized material (O-87) in PBS. All materials were also positively charged after the modification due to the cationic PEI. The hydrodynamic size and zeta potential of the materials after surface modification are shown in **Table 2.1** and **Figure 2.4**.

It can be seen that T-NP^{10C} based on a S-47 core produces nanoconstructs with the best size distribution. As will be seen in the next chapter, this material also gives the best silencing efficacy. Therefore, unless otherwise

specified, S-47 cores will be used throughout this chapter. The zeta potential of the selected construct is ~25 mV, when measured in water (**Table 2.1**). Later, I measured the zeta potential of the T-NP^{10C}-siRNA (S-47) in 10 mM NaCl following the NCL (National Characterization Lab)'s published guidelines, and the zeta potential is ~13 mV. Based on these guidelines, zeta potential values in the range between -10 to +10 mV (measured in 10 mM NaCl) are considered neutral. Therefore, the optimized construct is considered only slightly positive. As will be shown in later sections, despite being slightly cationic, a PEG layer shields this charge effect and thus limits the nanoconstruct interaction with other blood cells or non-targeted cells.

Table 2.1: Hydrodynamic size and zeta potential of six different nanoconstructs.

Material (MSNP core)	MSNP core size (nm) by TEM ^(a)	Surface modification ^(b)	Hydrodynamic size (DLS)		Zeta charge (mV)
			Size (nm) ^(c)	PDI ^(d)	
O-87	87 ± 14	T-NP ¹⁰	214 ± 22	0.22	22 ± 0.5
S-61	61 ± 7	T-NP ¹⁰	113 ± 1.0	0.20	18 ± 0.4
		T-NP ^{10C}	131 ± 0.3	0.20	19 ± 3.7
S-47	47 ± 4	T-NP ^{10C}	117 ± 0.5	0.19	25 ± 0.1
		T-NP ^{1.8C}	117 ± 2.4	0.20	19 ± 4.0
S-34	34 ± 3	T-NP ^{10C}	133 ± 4.1	0.37	19 ± 4.0

(a) Core size measured in dry state, average size of 50 particles.

(b) “10” stands for 10-kDa PEI; “1.8C” and “10C” stand for cross-linked 1.8-kDa and cross-linked 10-kDa PEI, respectively. All PEI-MSNP were then conjugated with PEG, and trastuzumab (T).

(c) Average of three measurements; the z-average diameter and polydispersity index (PDI) values were defined according to International Standard on DLS (ISO13321).

(d) PDI ranges from 0 to 1; smaller number indicates narrower size distribution; e.g., PDI <0.05 is considered monodisperse (one size only), while PDI >0.5 indicates a broad distribution of particle sizes.

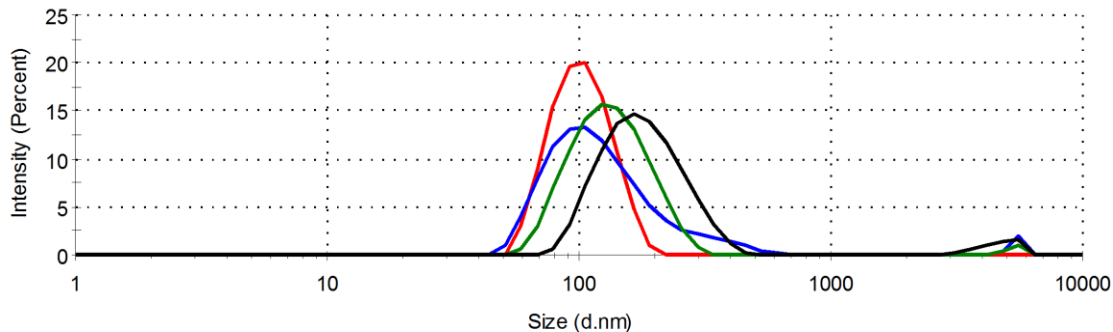


Figure 2.4: Hydrodynamic size of nanoconstructs. Size distribution of nanoconstructs (T-NP^{10C}) based on S-34 (blue), S-47 (red), and S-61 (green) cores and size distribution of nanoconstructs (T-NP¹⁰) based on O-87 (black) core.

2.2.4 Composition analysis of nanoconstructs

I further characterized the nanoconstruct with the best size profile (T-NP^{10C}, based on S-47) for its composition by thermogravimetric analysis (TGA) and BCA protein analysis. Polymer can decompose at high temperature. Thus, weight loss from TGA can be used to quantify the amount of polymer loaded on the nanoparticle (**Figure 2.5**). For example, the PEG content can be deduced from the difference in weight losses of NP-PEI and NP-PEI-PEG. The remaining weight at 800 °C belongs to silica and is used to identify the yield of the synthesis. BCA analysis was used to identify the amount of antibody loaded on the nanoparticle. I also monitored the siRNA loading by the fluorescence signals of unbound siRNAs. siRNAs were loaded in a complete binding condition, thus requiring no further purification after siRNA loading. The composition of T-NP^{10C} can be found in **Table 2.2**.

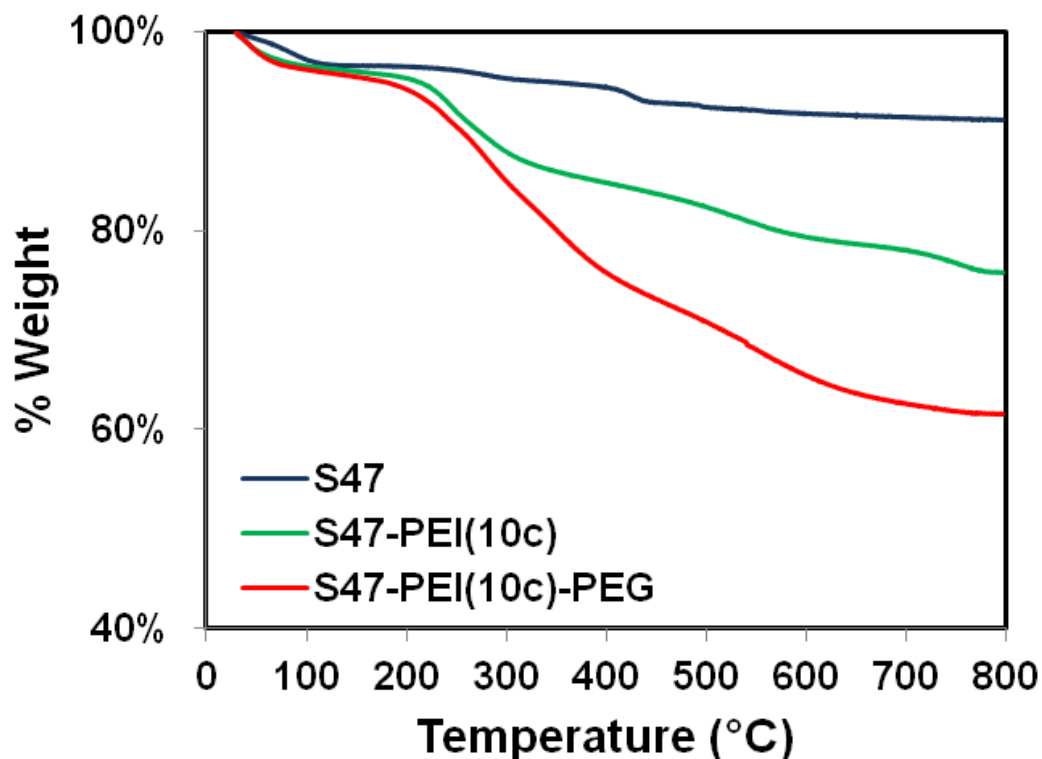


Figure 2.5: Thermogravimetric analysis. Weight versus temperature profile of S-47, S-47 modified with cross-linked-PEI, and S-47 modified with crosslinked-PEI and PEG.

Table 2.2 Composition of T-siRNA-NP (all reported as a percentage by mass of the whole construct)

Material	Surface modification	PEI by TGA [%]	PEG by TGA [%]	Antibody by BCA [%]	NP/siRNA mass ratio (fluorescent method)
S-47	T-NP ^{10C}	13.5	18.2	3	Complete at 25 and 50
S-47	T-NP ^{1.8C}	15.9	6.1	3	Complete at 25 and 50

2.2.5 Engineering endo-lysosomal vesicle escape: Buffering capacity of nanoconstructs

Internalized nanoparticles ultimately end up in the lysosomal vesicles that assemble in the perinuclear region. siRNAs must escape from this environment early to be effective since the nucleases and acidic pH in the lysosomal vesicles

will degrade the siRNA. Polymers that exhibit high transfection efficiencies, such as PEI [203], have buffering capacity in the endo-lysosomal pH range of 5–7 due to the presence of unprotonated secondary and tertiary amines. This buffering is thought to cause an increased influx of hydrated protons and chloride ions that causes the vesicles to swell and eventually rupture, thereby releasing the siRNAs [204] (see Proton sponge effect- Chapter 1).

I tested the possibility that endo-lysosomal escape and gene silencing efficacy of our siRNA-nanoconstructs could be increased by increasing the buffering capacity of the nanoconstructs. First, the buffering capacities of nanoconstructs with cross-linked 1.8-kDa PEI (T-NP^{1.8C}), cross-linked 10-kDa PEI (T-NP^{10C}), and non-cross-linked 10-kDa PEI (T-NP¹⁰) in 150 mM NaCl were measured (**Figure 2.6**). It can be seen that the nanoconstructs had buffering capacity in the order of T-NP^{10C} > T-NP¹⁰ > T-NP^{1.8C}. Clearly, the cross-linking of the PEI creates more secondary and tertiary amines yielding greater buffering capacity than primary amines.

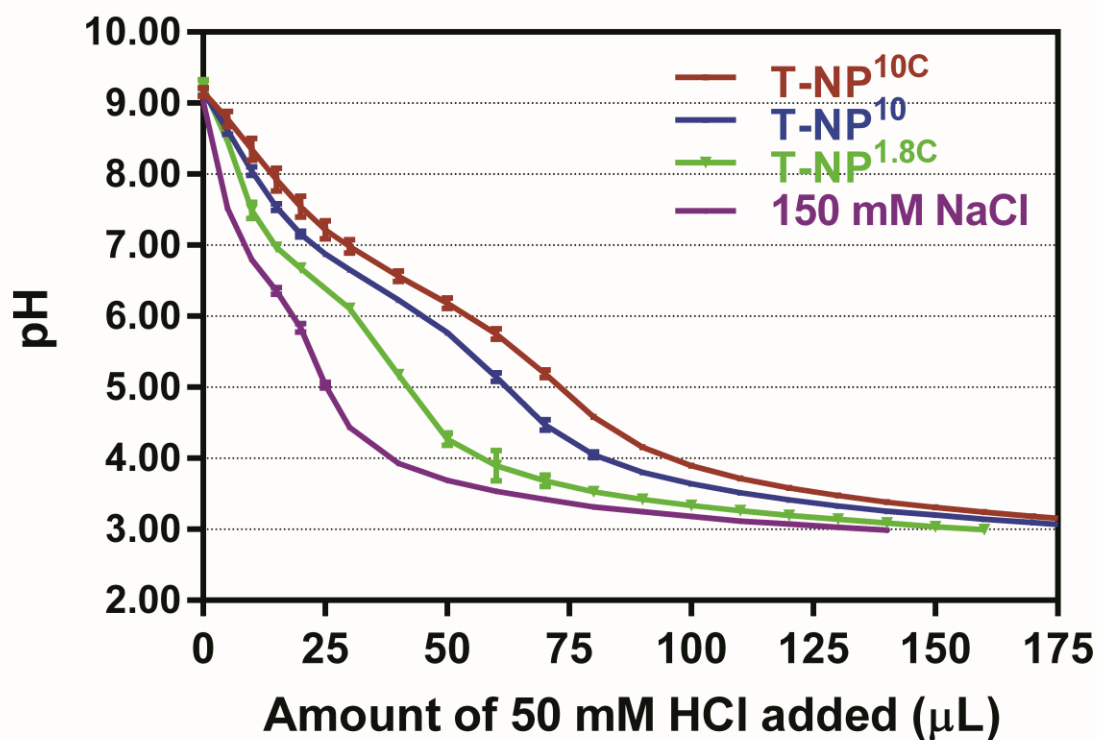


Figure 2.6: Buffering capacity of nanoconstructs. Buffering capacity of three nanoconstructs with crosslinked 1.8-kDa PEI (T-NP^{1.8C}), non-crosslinked (T-NP¹⁰), and crosslinked 10-kDa PEI (T-NP^{10C}) measured in 150 mM NaCl.

2.2.6 Different molecular weights of PEG molecules

To further optimize the nanoconstruct, I tested PEG with different molecular weights (2, 5, 7.5 and 10 kDa). Gref et al. previously showed that 5-kDa PEG has superior stealth characteristics compared with 2-kDa PEG, and PEG of molecular weight of 5-kDa to 20-kDa have the same stealth properties when loaded at the same amount on the nanoparticle [205]. 5-kDa PEG was reported to be a threshold for maximum reduction of protein adsorption in this study. For PEG of molecular weight 5 kDa and above, the loading density becomes the more important factor in that the higher PEG density provides better

'stealth' properties. A longer PEG chain has more chance to collapse on the nanoparticle surface (random coil), resulting in a lower loading of PEG and subsequently less efficient loading of trastuzumab, which binds to the end of the PEG chain. Therefore, I screened for the shortest PEG chain that could still provide the stealth properties for nanoconstructs. I tested PEG with different molecular weights (2, 7.5 and 10 kDa) to see if I could prevent aggregation upon siRNA binding and achieve high PEG loading as I did with 5-kDa PEG. In agreement with the aforementioned study, **Figure 2.7** shows that 2-kDa PEG is not sufficient to prevent siRNA-nanoconstructs from aggregation, as can be seen from a larger hydrodynamic size (red line), compared to other nanoconstructs. A PEG of 5 kDa and above appears to prevent aggregation effectively. I further quantified the amount of PEG loaded on nanoconstructs with 5-, 7.5- and 10-kDa PEG by TGA. The amounts of PEG loaded on the nanoconstructs are 18%, 10% and 12% by mass, respectively. The loading of higher-MW PEGs is low because a brush-like PEG conformation is less likely when the PEG chain is too long and bulky. 5-kDa PEG provided the highest amount of loading on the nanoconstructs among the various PEG molecular weights tested. Thus, this 5-kDa PEG likely provides a more optimum brushlike stealth condition for our nanoconstructs and used throughout the studies. As can be seen in later sections, this 5-kDa PEG layer appears to be effective in stabilizing the size, protecting siRNAs from enzyme degradation and enhancing blood compatibility.

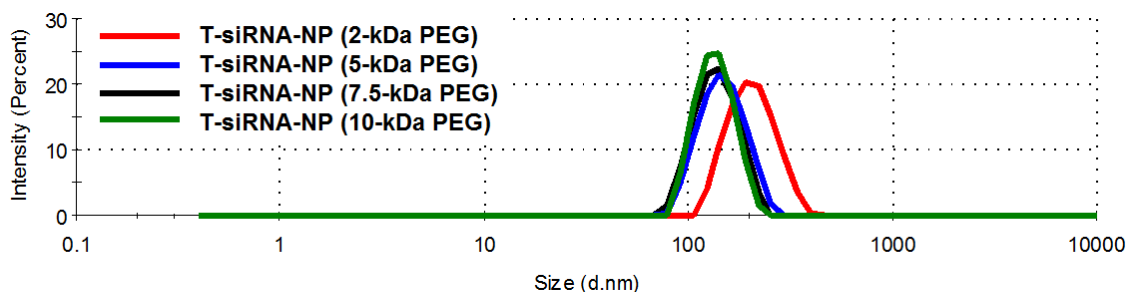


Figure 2.7: Size profile of siRNA-nanoconstructs with different molecular weights of PEG

2.2.7 Protection of siRNAs against blood enzymatic degradation

In order to be feasible for siRNA delivery upon systemic administration, the platform must protect siRNAs from degradation by serum nucleases. I assessed the ability of MSNP constructs (T-NP^{1.8C} vs. T-NP^{10C}) to protect siRNAs (the siRNA against HER2 (siHER2) was used herein) from degradation by blood enzymes by measuring the amount of siHER2 remaining after incubation of siHER2-nanoconstructs for 0 to 48 h in 50% human serum in PBS at 37 °C. These results were compared to those obtained for free siHER2 without nanoparticles. **Figure 2.8A** shows the amount of intact siHER2 that survived enzymatic degradation measured by gel electrophoresis. The corresponding siHER2 quantification based on the band intensity and location is shown in **Figure 2.8B**. Without the nanoconstructs, naked siHER2 was degraded within 0.5 h (observed as bands shifted toward lower molecular weight) and its half-life was about 1 h, in agreement with previous reports for other siRNAs [206, 207]. T-NP^{1.8C} fully protected siHER2 up to 8 h, while T-NP^{10C} fully protected siHER2 up to 24 h. The siRNAs on both of our nanoconstructs experienced much less

degradation than reported cyclodextrin-based nanoparticles that have already shown clinical antitumor efficacy [144]. Those cyclodextrin-protected siRNAs were reported to experience 50% degradation within 12 h and 70% within 24 h under 50% serum conditions [208].

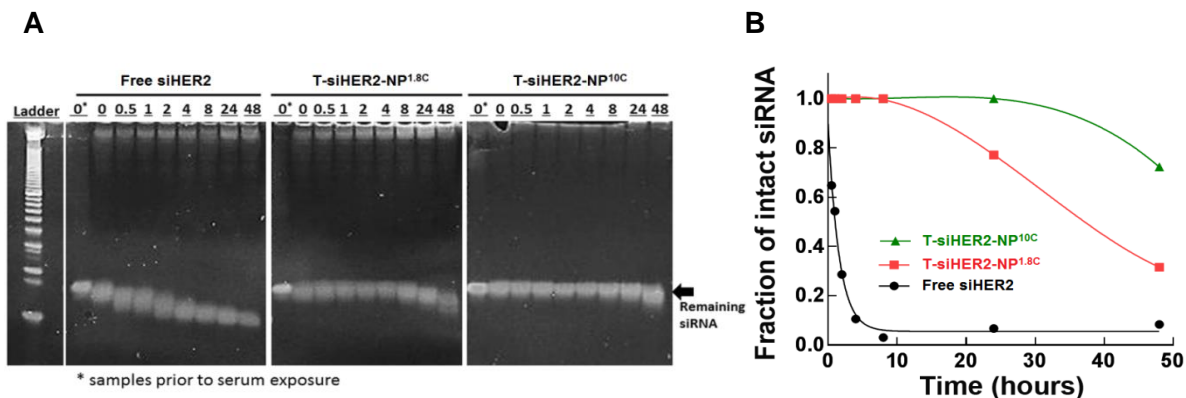


Figure 2.8: SiRNA protection from serum degradation. (A) Residual siRNA against HER2 (siHER2) band after being incubated with human serum (50%) after specified periods of time (37 °C with shaking); conducted with free siHER2, or siHER2 loaded on two nanoconstructs: crosslinked 1.8-kDa (T-siHER2-NP^{1.8C}) and crosslinked 10-kDa PEI (T-siHER2-NP^{10C}). (B) the corresponding siHER2 quantification using ImageJ software.

2.2.8 Significance of a PEG layer

The higher siRNA protection for T-NP^{10C} compared to T-NP^{1.8C} is likely due to the increased PEG content for the higher-molecular-weight PEI of T-NP^{10C}. The PEG contents of T-NP^{10C} and T-NP^{1.8C} were 18.2% and 6.1%, respectively (Table 2.2). Higher PEG content is expected for T-NP^{10C} since it contains more amine groups (thus more reactive sites for PEG binding) than T-NP^{1.8C}. PEG is known to provide a steric blocking effect [209, 210] that reduces enzyme-mediated siRNA degradation [211]. It also reduces binding of blood

proteins to the nanoparticles [210]. In a separate experiment (**Figure 2.9A**), siRNAs on PEI-MSNP without PEG degraded faster than naked siRNAs since positively charged PEI recruited more negatively charged enzymes that degraded the siRNA. In addition, significant aggregation upon siRNA loading on nanoconstructs without PEG (NP coated with PEI alone, **Figure 2.9B**) was apparent, illustrating another advantage of the PEG layer. The PEG layer also improved blood compatibility and reduced immune response as described in the subsequent chapters.

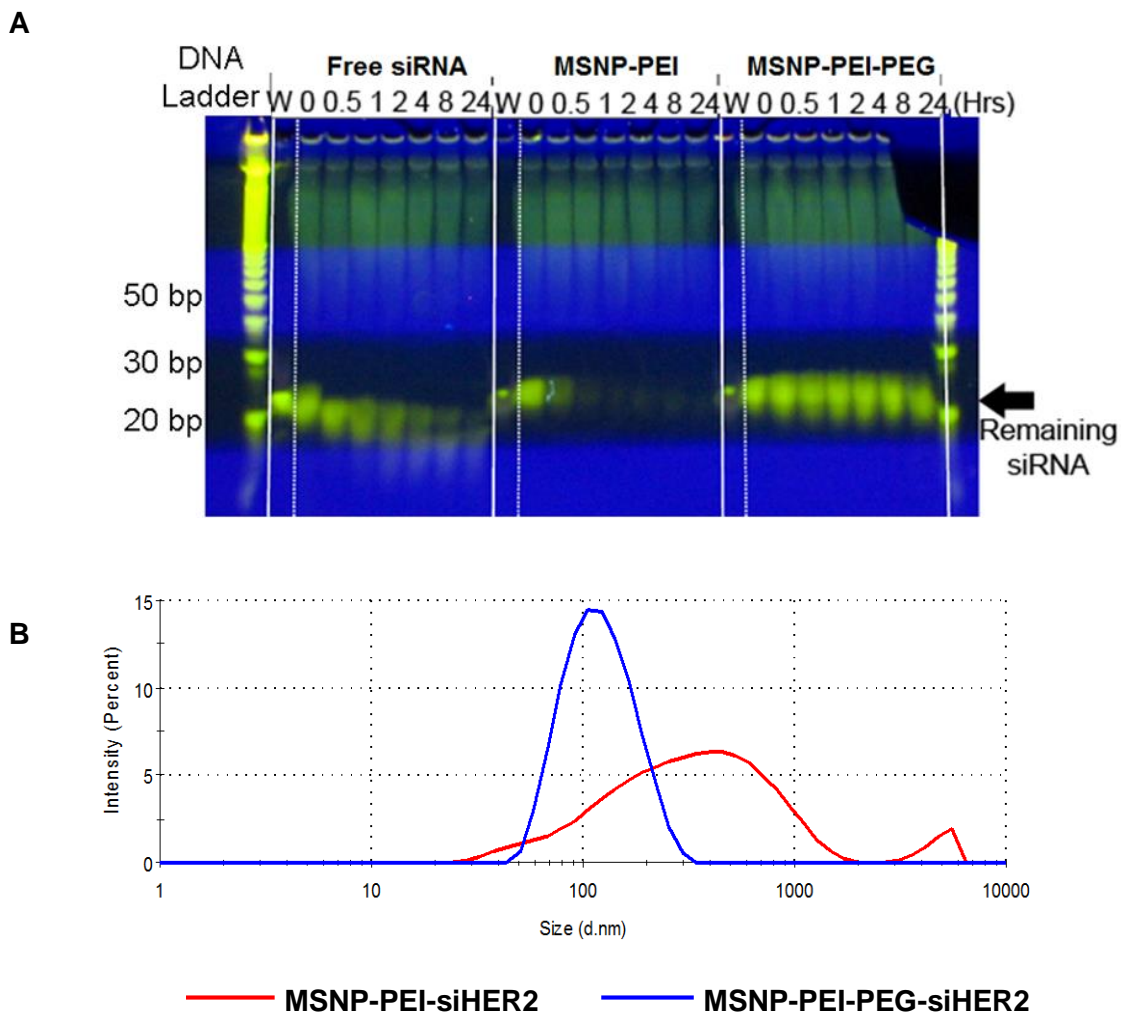


Figure 2.9: Importance of PEG in protecting siRNA from serum enzymatic degradation and preventing aggregation upon siRNA binding. (A) SiRNA against luciferase (siLUC) was loaded on PEI-coated MSNP without PEG (MSNP-PEI) and with PEG (MSNP-PEI-PEG) and subjected to the serum enzymatic degradation assay in the same fashion as **Figure 2.8**. PEI was 10-kDa. (B) Nanoparticle without PEG is shown to aggregate upon siHER2 loading (NP/siRNA of 50), while those with PEG did not show a significant size increase.

2.3 Conclusions

Chapter 2 discusses the design and synthesis procedures of mesoporous silica-based nanoconstructs that will be used throughout the whole dissertation. In addition, this chapter also covers the roles of different components on nanoconstructs. PEI allows siRNA loading and utilizes its inherent buffering capacity to enhance endosomal escape. To further promote this effect, PEI was further cross-linked. In this chapter, PEG was shown to protect siRNAs from serum degradation and stabilize the size of siRNA-nanoconstructs. Nanoconstructs based on S-47 NP cores that were coated with crosslinked 10-kDa PEI, 5-kDa PEG and trastuzumab appear to have the best size profile (Z-average of 117 nm, PDI 0.19) among all of the constructs. Later in this dissertation, I evaluated this mini-library of nanoconstructs for their efficacy and safety as therapeutic agents.

3. Chapter 3: In vitro and in vivo efficacy evaluation of siRNA-nanoconstructs

This chapter describes the evaluation of the library of nanoconstructs synthesized in Chapter 2 with respect to siRNA delivery in both cell lines and an animal model. The siRNA-nanoconstructs were first screened for their ability to silence luciferase proteins in a high-throughput luciferase quantification assay. The nanoconstruct that performed best was selected for subsequent efficacy studies with therapeutic siRNAs. The therapeutic siRNA evaluated for HER2⁺ breast cancer in Chapters 2-5 is siHER2 (siRNA against HER2 mRNA). HER2 was selected as the initial siRNA target because it is a particularly strong and well validated therapeutic target. Amplification of this gene occurs in 15-25% of diagnosed breast cancers [212] and is linked to aggressiveness and poor prognosis [213-215]. Current HER2-targeted therapies are still not sufficient in controlling resistant cancers effectively (see Chapter 1). Thus, additional therapeutic options are needed. Furthermore, Chapter 1 presented evidence that several combinations of existing HER2-targeted therapies work better than a single HER2-targeted therapy. This suggests that more complete inhibition of HER2 proteins could provide a good therapeutic approach for refractory HER2⁺ breast cancer. Silencing HER2 with siRNA in combination with the simultaneous delivery of trastuzumab with our nanoconstructs could provide a new strategy

that may overcome drug resistance, thereby further increasing the survival rate for HER2⁺ cancer patients.

3.1 Materials and Methods

3.1.1. Materials

Trastuzumab, Rituximab, Abraxane and Feraheme were obtained from the OHSU pharmacy. Reagents for cell media were obtained from Life Technologies (CA), unless otherwise specified. DharmaFECT #1 (commercial transfection agent) was obtained from Thermo Fisher Scientific (MA). Several siRNAs were employed in the studies throughout this chapter and dissertation. These are a scrambled siRNA control, designated “siSCR”; an siRNA against luciferase, designated “siLUC”; and a siRNA against HER2, designated “siHER2”. siHER2 and siSCR (without fluorescent dye tag) were custom synthesized (*in vivo* HPLC grade) by Dharmacon, Thermo Scientific (CO). siSCR with Alexa-488 dye was synthesized by Qiagen (CA). siLUC was custom synthesized by Life Technologies (CA). The sequences are summarized in **Table 3.1**.

Table 3.1: siRNA sequences

siRNA	siRNA sequence
siHER2	Sense: 5' CACGUUUGAGUCCAUGCCCAAUU 3' Antisense: 5' UUGGGCAUGGACUCAAACGUGUU 3'
siLUC	Sense: 5' CGGAUUACCAGGGAUUUCAtt 3' Antisense: 5' UGAAAUCCCUGGUAUCCGtt 3'
siSCR	Sense: 5' UGGUUUACAUGUCGACUAA 3' Antisense: 5' UUAGUCGACAUGUAAACCA 3'

3.1.2 Cell lines and media recipes

Cell media recipes for cell lines used in this chapter and throughout the dissertation are summarized in **Table 3.2**

Table 3.2: Cell media recipes for all cell lines used

Cell lines	Cell media recipes
BT474, HCC1954	RPMI-1640 + 10% FBS
BT474-R	RPMI-1640 + 10% FBS + 1 μ M Lapatinib
JIMT1, MCF7, MDAMB231, MDAMB468, HEK293 and	DMEM + 10% FBS
SKBR3	McCoy5A + 10% FBS
LLC-PK1	M-199 + 3% FBS
HUVEC	Endothelial growth medium (Lonza)
MCF10a	Ham's F-12:DMEM + 5% horse serum + 10 μ g/mL insulin + 100 ng/mL cholera toxin + 20 ng/mL EGF + 500 ng/mL hydrocortisone

3.1.3 Luciferase knockdown efficacy

The MDAMB231-H2N-luc cell line (which was genetically modified to overexpress both HER2 and luciferase proteins [216]) was used to assess initial gene silencing efficacy of the nanoconstructs loaded with the siRNA against luciferase (siLUC). Cells were plated at 3000 cells/well in a 96-well plate. One day after seeding, the cells were treated with the siRNA-nanoconstructs, at NP/siRNA 25 or 50 by mass, at a fixed siRNA dose of 30 nM. A commercially available transfection agent, DharmaFECT#1, with the same siRNA dose (following manufacturer's recommended protocol) served as a positive control. After overnight incubation (~20 h), cells were washed once and replenished with complete media. At 48 h post treatment, cells were lysed and analyzed for

luciferase activity by a Luciferase Glow Assay Kit (Thermo Fisher Scientific) and for protein concentration by a BCA protein assay kit (Thermo Fisher Scientific), following manufacturer's protocols. The luciferase activity of the lysate was normalized with the corresponding protein concentration in the same well and reported as a percentage of the untreated control. All treatments were performed in quadruplicate.

3.1.4 Cellular uptake analysis by flow cytometry

Cells were harvested and resuspended in 1 million cells/150 μ L/tube. Each tube was mixed with siSCR(tagged with Alexa-488)-nanoparticles (100 μ g) in PBS (150 μ L). Upon addition of siSCR-nanoparticles, cells were placed on a rocker in the cell incubator (37 $^{\circ}$ C, 5% CO₂) for 0.5 or 2.0 h. After the specified incubation time, cells were washed (centrifuge at 115g, 5 min) with FACS buffer (1mL, 1X Phosphate Buffered Saline (Ca/Mg⁺⁺ free) + 1mM EDTA + 25mM HEPES pH 7.0 + 1% Fetal Bovine Serum (Heat-Inactivated)) three times. Cells were then resuspended in FACS buffer (550 μ L) and transferred to 5-mL BD FACS tube. Cells were kept on ice until analysis. For cells stained with free antibody (for gating purpose), antibody labeling was performed on ice and under rocking conditions. Cells were stained with the primary antibody (trastuzumab or rituximab: 2 μ g per tube) for an hour, washed (centrifuge at 115g, 5 min) with PBS one time, stained with the secondary antibody (Anti-human Alexa 488: 2 μ g per tube) for 45 minutes, then washed 2 times with PBS, and resuspended in FACS buffer (550 μ L) before analysis. All tubes were counter-stained for cellular DNA with DRAQ5 (2 μ L, 5 mM, Cell Signaling) for 15 minutes on ice. Then all

tubes (except antibody-labeled cells for gating purpose) were quenched with Trypan Blue (500 μ L, 0.4% in PBS; Hyclone) to remove signals outside of the cells, and subjected to flow cytometry analysis. 10,000 events (cells) were analyzed for each sample. The intensity was processed with FlowJo software (FlowJo LLC).

3.1.5 In vitro efficacy: HER2 protein knockdown and cell viability

BT474, SKBR3 and HCC1954 were seeded in a 96-well plate for 24 h prior to treatment. Nanoparticles were loaded with siHER2 or siSCR at NP/siRNA 50. The siRNA dose was fixed at 60 nM. Media were switched to complete media after overnight incubation. Three days after treatment with siRNA-nanoconstructs, cells were fixed and analyzed for HER2 protein expression by the immunofluorescence method. HER2 mRNA and β -actin mRNA levels were analyzed at 48 h post treatment using the Quantigene 2.0 Reagent System (Panomics) following the manufacturer's protocol. The HER2 mRNA level was then normalized with β -actin mRNA (housekeeping gene) and reported as a percentage of the untreated control. Cell viability and apoptosis were analyzed four days post treatment using the CellTiter-Glo[®] Luminescent Assay (Promega) and Caspase-Glo[®] 3/7 Assay Systems (Promega), respectively. Caspase activity was normalized with the cell viability. Both were reported as a percentage of the untreated control.

3.1.6 Immunofluorescence staining and microscopy

Cells were washed two times with dPBS (Dulbecco's Phosphate Buffered Saline, Life Technologies), fixed with 100% ice-cold methanol for 15 minutes at room temperature, and washed two times with dPBS. Then, cells were washed three times with 1X TBST (Tris Buffered Saline with Tween 20, Cell Signaling), two times with blocking buffer (1X PBS + 5% Goat Serum) and incubated for one hour in the blocking buffer at room temperature. Blocking buffer was then removed, and primary antibodies (anti-HER2 (50 μ L, 1:200, Abcam)) in blocking buffer solution were added and incubated overnight at 4 °C. Following a series of PBS washes (5 times), blocking buffer was added and incubated for 10 minutes. Blocking buffer was removed, and secondary antibodies (Alexa-488 goat anti rabbit (50 μ L, 1:500, Life Technologies)) were incubated at 37 °C for 30 minutes. Cells were then washed five times with blocking buffer. Cell nuclei were visualized by DAPI (Life Technologies) following manufacturer's protocol. Fluorescence images were obtained with the EVOS FL cell imaging system (Life Technologies). All images were processed for signal intensity by CellProfiler image analysis software (Broad Institute).

For the tumor tissue immunofluorescence study, tumors were harvested and paraffinized until the time of analysis. At this point, the tumor sections were deparaffinized and incubated with antibodies under the same conditions as detailed above. Fluorescence images were obtained and analyzed the same way.

3.1.7. Animal studies: a mouse tumor model and in vivo efficacy studies

All animals were recruited and used under an approved protocol of the Institutional Animal Care and Use Committee (IACUC) of Oregon Health and Science University. All animal experiments were carried out under the auspices of the OHSU Department of Comparative Medicine. In vivo gene silencing studies were performed in an orthotopic mouse tumor model generated by implanting HCC1954 (4×10^6 cells) into the mammary fat pads of 5-week-old SCID mice (Charles River). Tumors were allowed to grow to an average size of $\sim 250 \text{ mm}^3$. Mice were then grouped and received a single injection (tail vein) of the nanoconstructs (T-siHER2-NP^{10C} or T-siSCR-NP^{10C}, S-47 cores, 1.25 mg siRNA/kg), or the PBS control. The tumors were harvested four days after treatment and analyzed for HER2 protein expression by immunofluorescence. A subsequent study evaluated tumor growth reduction in the orthotopic HCC1954 tumor model. Tumors were allowed to grow to 150 mm^3 prior to treatments (by tail vein injections) with siHER2 or siSCR (1.25 mg siRNA/kg) delivered with T-NP^{10C} (S-47 core) as indicated in **Figure 3.8**.

3.1.8 Statistical analysis

Pairwise statistical comparisons and tumor growth curves were performed using unpaired, two-tailed Student's t tests. Statistical significance was established at $P < 0.05$. Graphpad Prism 6.0 software (GraphPad software Inc.) was utilized for statistical analyses.

3.2 Results and discussion

3.2.1 In vitro gene knockdown by siRNA-nanoconstructs

As detailed in Chapter Two, I found that the nanoconstructs had buffering capacity in the order of T-NP^{10C} > T-NP¹⁰ > T-NP^{1.8C}. I hypothesized that gene silencing efficacy would correlate to buffering capacity, since siRNA endosomal escape is mediated by the proton sponge effect.

I evaluated the gene silencing ability of siLUC on various nanoconstructs (four core sizes, loaded with PEI of 1.8-kDa or 10-kDa, cross-linked or no cross-linked). Specifically, I measured luciferase silencing activity at 48 h post-exposure to the siLUC-nanoconstructs on the MDA-MB-231-H2N-luc breast cancer cell line. **Figure 3.1** shows the luciferase silencing (vs. siSCR) of all nanoconstructs. Complete siRNA binding was achieved for all materials at NP/siRNA mass ratio of 25 and above (confirmed by no remaining unbound siRNAs in the solution phase after the loading step, **Table 2.1**). However, materials with NP/siLUC of 50 offered better efficacy (per the same dose basis of siLUC) (**Figure 3.1B**) than those with NP/siLUC of 25 (**Figure 3.1A**). This can be attributed to the increased density of nanoparticles on a per cell basis. NP/siRNA ratio of 50 was used throughout this study unless specified otherwise. It can be seen that smaller particles had reduced silencing efficacy compared to larger ones (see S-61 vs. O-87, both were modified with 10-kDa PEI, designated as T-NP¹⁰ in **Figure 3.1B**). This is likely due to poorer endo-lysosomal escape of the siLUC from the smaller particles. But since large particles are less desirable for tumor delivery using EPR effects (Chapter 1), I tested the possibility that the

siRNA endosomal release from smaller particles could be increased by PEI cross-linking, which effectively increases the buffering capacity, as shown in **Figure 2.6**. **Figure 3.1** shows that the silencing efficacy was indeed improved with cross-linked materials compared to the non-cross-linked material (see T-NP^{10C} vs. T-NP¹⁰, from S-61 cores).

The highest silencing efficacy (76%) was achieved with the nanoconstructs that were developed from the S-47 core. This S-47 material also yielded the best size distribution without large aggregates unlike other materials (**Figure 2.4**). The S-47 modified with 10-kDa PEI was more effective than that modified with 1.8-kDa PEI (76% vs. 60% silencing efficacy). The latter material may be safer, however, and can be used at a higher dose to enhance the efficacy, hence warranting further investigation. The S-47 core material with cross-linked PEI was used for all subsequent experiments based on these results.

3.2.2 Targeted cellular uptake of the siRNA-nanoconstructs

Next, I assessed two test siRNA-nanoconstructs (with 1.8-kDa PEI and 10-kDa PEI, both made from the S47 core) conjugated with the antibody trastuzumab (T) for their uptake into cells that overexpress the HER2 protein. Scrambled control siRNA was used (siSCR). These particles are designated hereafter as T-siSCR-NP^{1.8C} and T-siSCR-NP^{10C}, respectively. Two siRNA-nanoconstructs with the control antibody, rituximab targeting CD20, are designated as R-siSCR-NP^{1.8C} and R-siSCR-NP^{10C}, respectively.

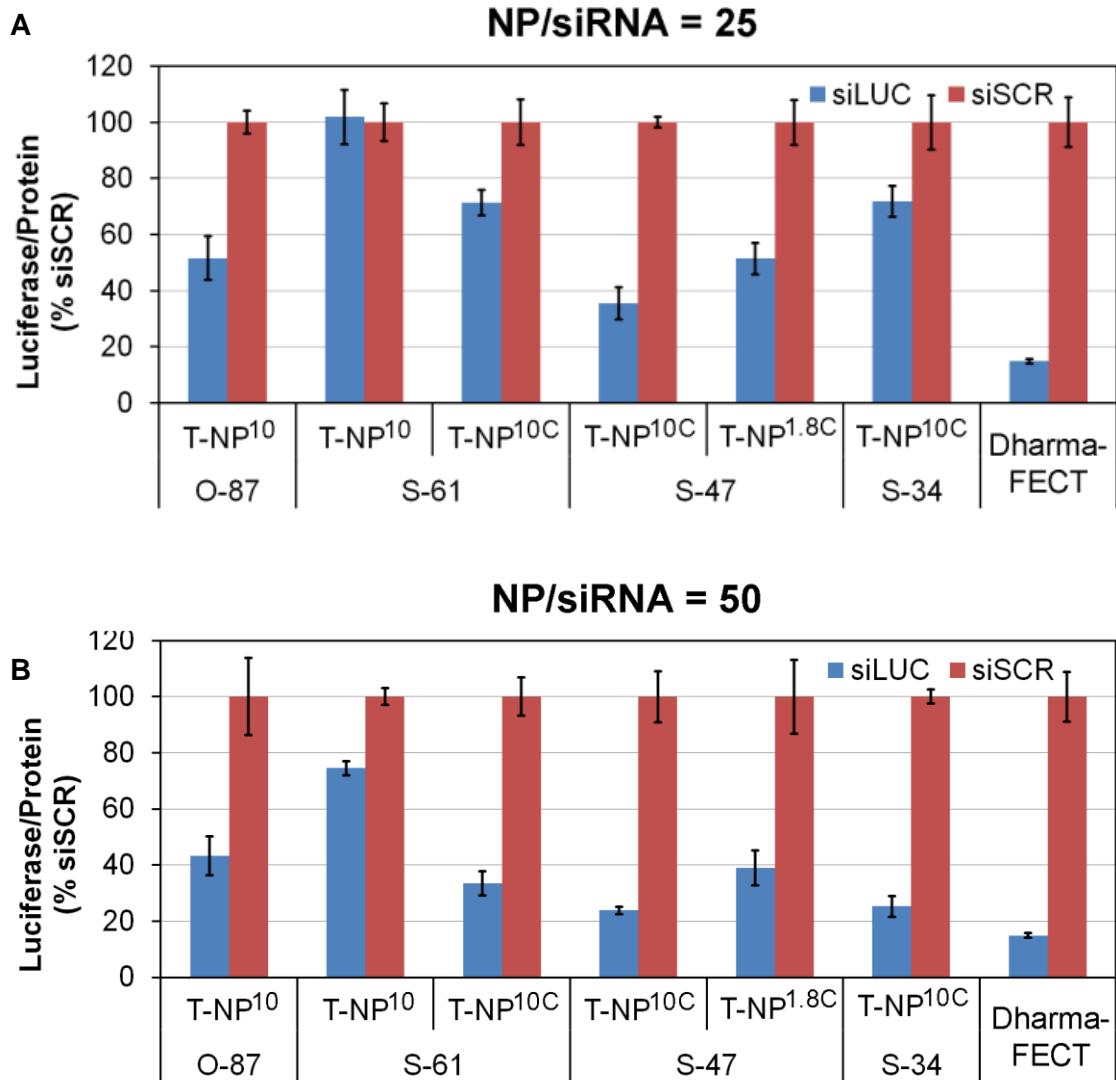


Figure 3.1: Luciferase silencing efficacy of nanoparticles. Silencing of luciferase in MDA-MB-231-H2N-luc (high HER2, high luciferase) upon treatment with 30 nM siLUC on nanoconstruct at NP/siRNA weight ratio of **(A)** 25 and **(B)** 50 was measured at 48 h post-transfection (with overnight media change).

I measured the cellular uptake of T-siSCR-NP^{10C} and T-siSCR-NP^{1.8C} in HER2⁺ breast cancer cells (BT474 and SKBR3) and the HER2⁻ cell line (MCF-7) at 0.5 or 2.0 h post-exposure to the nanoconstructs. The siSCR was tagged with the fluorescent reporter Alexa 488 to enable quantitative analysis of siSCR uptake. R-siSCR-NP^{10C} and R-siSCR-NP^{1.8C} nanoparticles served as a negative

control, since BT474, SKBR3 and MCF-7 cells weakly express CD20. The amount of Alexa 488-tagged siSCR in the interior of individual cells was measured using flow cytometry after quenching fluorescence from Alexa 488-tagged siSCR on the external cell membrane using Trypan blue.

Figure 3.2A-C shows that T-siSCR-NP^{10C} were taken up effectively (>90%) into HER2⁺ cells (BT474 and SKBR3), but not HER2⁻ cells (MCF7) and that uptake increased with time from 0.5 h to 2 h. Furthermore, uptake of T-siSCR-NP^{10C} was greater than T-siSCR-NP^{1.8C}.

Figure 3.2 shows that R-siSCR-NP^{10C} and R-siSCR-NP^{1.8C} nanoconstructs were not taken up efficiently by any of the cell lines. This confirms that nanoconstructs enter cells primarily by HER2-receptor mediated endocytosis mechanism and not by adsorptive endocytosis of positively-charged particles, as reported for PEI-MSNP [217]. Fluorescence distributions are shown in **Figure 3.3**.

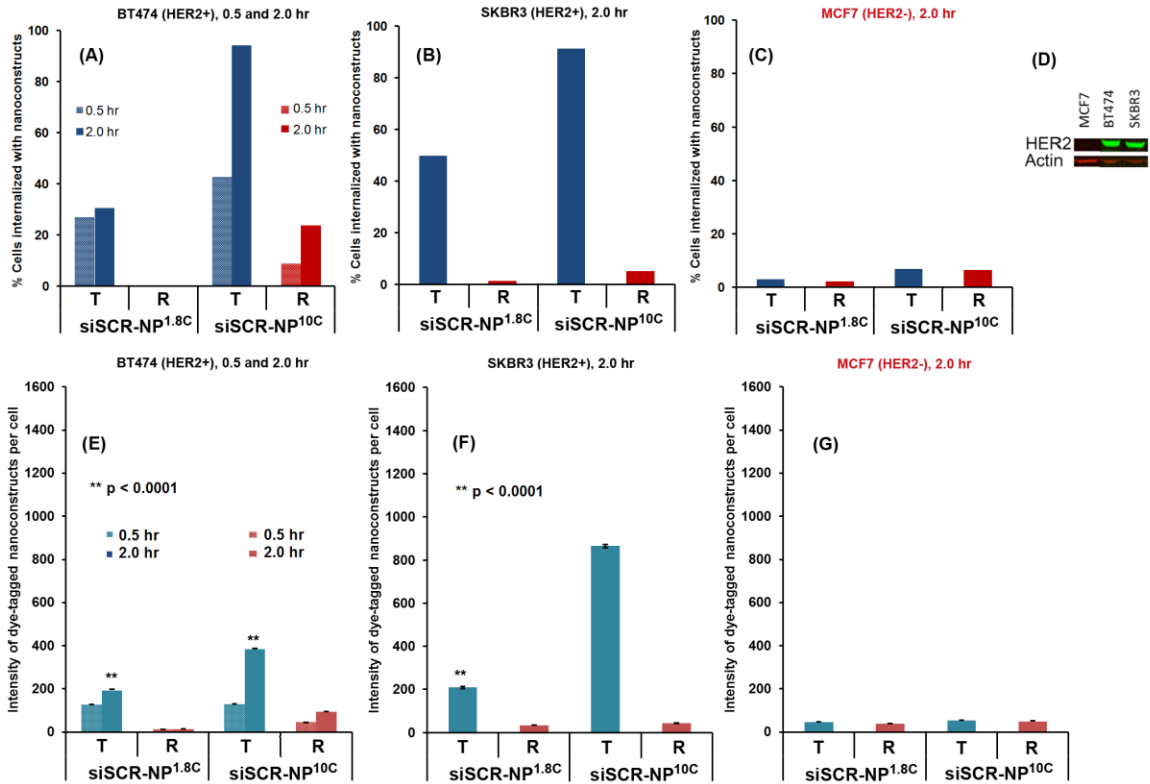


Figure 3.2: Cellular uptake of siRNA–nanoconstructs. Percentage of **(A)** BT474 (HER2⁺), **(B)** SKBR3 (HER2⁺) breast cancer cells, and **(C)** MCF7 (HER2⁻) breast cancer cells, that were internalized with fluorescent dye-tagged scrambled siRNA (siSCR)–nanoconstructs having either cross-linked 1.8-kDa (NP^{1.8C}) or cross-linked 10-kDa PEI (NP^{10C}), and conjugated with either trastuzumab (T) or rituximab (R), **(D)** western blot confirming HER2 content of these three cell lines, and **(E)–(G)** the corresponding intensity (per cell) of dye-tagged siSCR–nanoconstructs internalized into the cells. Data were presented as mean ± SEM. All were performed with 1 × 10⁶ cells and 100 µg of nanoconstructs in 0.3 mL of cell culture media and exposure time of 0.5 or 2 h.

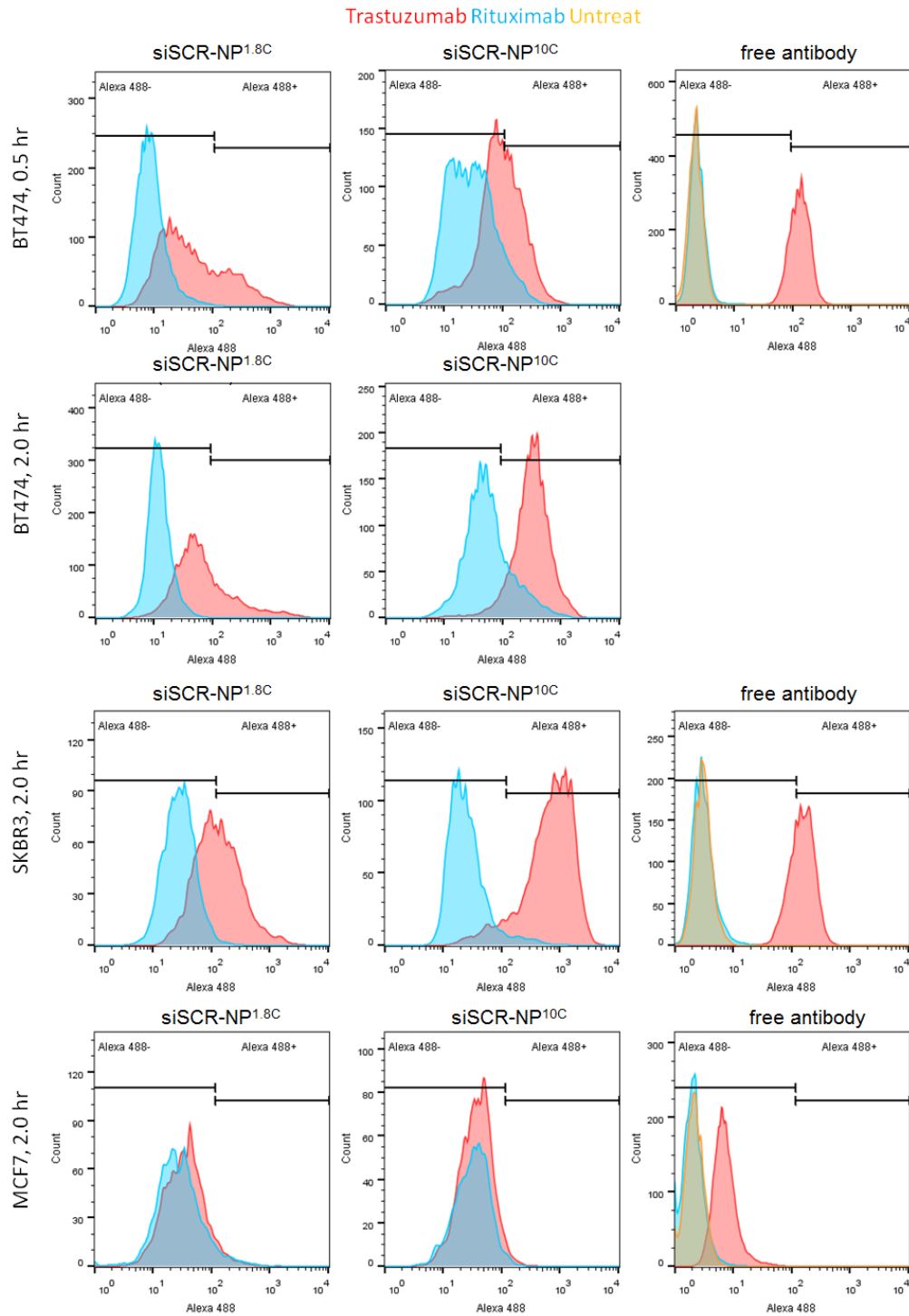


Figure 3.3: Flow cytometry histograms demonstrating the uptake of fluorescent-labeled siRNA-nanoconstructs in breast cancer cells. The corresponding bar chart was presented in Figure 3.2.

The data suggest some minimal non-specific cell uptake of the nanoconstructs (T-siSCR-NP^{10C}). I hypothesize that this uptake in non-targeted cells is due to the slightly positive charge on the nanoconstructs. To test this hypothesis, I will need to perform the cellular uptake study at 4 °C, where receptor-mediated (energy-dependent) endocytosis is halted [218, 219], and, thus, only non-specific (charge-mediated and energy independent) intracellular uptake will be detected. This will show the relative contribution of non-specific uptake for the nanoconstructs. Further, studies have shown that the proteoglycan component heparan sulfate (HS) can cause release of siRNAs from PEI in the cell [220], and the heparan sulfate proteoglycan (HSPG) on the cell membrane can interact with PEI and mediate another form of active (energy-dependent) uptake [221, 222]. A certain degree of this uptake could also happen with our nanoconstructs since PEI is one of the components of the construct. To test that PEI-HS-mediated uptake could also occur in our system, uptake experiments will be conducted across HER2⁻ cell lines with varying HSPG expression. This will allow me to evaluate and potentially correlate uptake with HSPG level on the cell membrane. Any observed correlation can then be substantiated by performing uptake experiments under concurrent inhibition of HSPG activity and monitoring potential interference. This can be done with conventional knockdown (siRNA or shRNA against HSPG) or by blocking its activity with antibodies. Interestingly, HSPG expression was reported to correlate with cancer tumorigenesis [223]. Should this mode of uptake happen, it could also potentially serve as another targeting strategy for cancers.

3.2.3 HER2 knockdown efficacy and therapeutic effects

I evaluated the efficiency of T-siHER2-NP^{10C} and T-siHER2-NP^{1.8C} in inhibiting HER2 mRNA levels and HER2 protein expression in HER2⁺ breast cancer cells (BT474, SKBR3, and HCC1954). I used quantitative immunofluorescent imaging (IF) to assess HER2 protein levels (**Figure 3.4A**), the Quantigene RNA assay for HER2 mRNA levels (**Figure 3.4B**), cleaved Caspase 3 and 7 assay for apoptotic markers (**Figure 3.4C**), and cellular ATP level assay for cell viability (**Figure 3.4D-E**) following treatment.

Figure 3.4A shows that T-siHER2-NP^{10C} reduced HER2 levels by 81-93% compared to T-siSCR-NP^{10C}. **Figure 3.5A** shows that the T-siHER2-NP^{10C} was more effective than T-siHER2-NP^{1.8C} at an equivalent siRNA dose. Also, **Figure 3.5B** shows that doubling the dose of T-siHER2-NP^{1.8C} reduced HER2 protein levels by 79-83% in SKBR3 and HCC1954 but even that was not effective in BT474 cells. Therefore, T-siHER2-NP^{10C} is deemed to be a better material than T-siHER2-NP^{1.8C} in terms of protein silencing. Encouragingly, the T-siHER2-NP^{10C} outperformed DharmaFECT in all cell lines as shown in **Figure 3.5C**. Quantitative interpretation of these results is complicated by the fact that treatment with T-siSCR-NP^{10C} also reduced HER2 levels and killed HER2⁺ breast cancer cells (**Figure 3.5D**). This is due to the high levels of trastuzumab on the nanoconstructs (3% by weight), since trastuzumab by itself is known to impact HER2 expression and cell viability independent of the siHER2 [224]. **Figure 3.5D**, for example, shows that HER2 levels in BT474 were reduced by 41% with T-siSCR-NP^{10C} and by 87% with the T-siHER2-NP^{10C}. Likewise, **Figure 3.4D**

shows that cell viability was reduced 59% by T-siSCR-NP^{10C} and 86% by T-siHER2-NP^{10C}. Hence, to evaluate solely the effect of siRNAs, the results were normalized to the siSCR control instead of the untreated control. I also assessed T-siHER2-NP^{10C}-induced change in HER2 mRNA levels in BT474 at 48 h after treatment with these same nanoconstructs. **Figure 3.4B** shows a 44% reduction in the HER2 mRNA level relative to the siSCR control. This compares with a 58% reduction using DharmaFECT#1 (positive control). Interpretation of these results may be affected by the high cell death induced by the T-siHER2-NP^{10C} since cells that are most strongly affected will be preferentially lost. Accordingly, I evaluated the knockdown efficiency in cells that are more resistant to trastuzumab, such as JIMT1 and HCC1954. In **Figure 3.6**, the mRNA reduction induced by T-siHER2-NP^{10C} and DharmaFECT were more comparable; 69% vs. 72% in JIMT1 cells and 57% vs. 63% in HCC1954 cells.

T-NP^{1.8C} was shown to have poorer silencing efficacy when compared to T-NP^{10C}. I hypothesize that this reduced efficacy is directly related to both its reduced buffering capacity and poorer cellular uptake, as shown in **Figure 2.6** and **Figure 3.2**, respectively. To confirm this hypothesis, I first need to identify conditions that will essentially normalize the amount of the T-siHER2-NP (both 10C and 1.8C) delivered to the cells. I will need to monitor intracellular levels upon careful titration of each nanoconstruct and assess the silencing efficacy at doses deemed equivalent with respect to intracellular amounts. Thus, any differences in silencing efficacy cannot be attributed to enhanced uptake of T-NP^{10C} over T-NP^{1.8C}. I will also need to validate the enhanced buffering capacity

and its ability to improve the endosomal escape of siRNAs in cells. One strategy is to utilize the siRNA tagged with two dyes. One dye is pH-sensitive (i.e., the fluorescence emission intensity is dependent on the pH of its local environment) and will be used to track the siRNA transit in relation to intracellular pH (e.g., neutral pH represents cytosol, and acidic pH represents endosomes (pH 5.5-6.5) and lysosomes (pH 4.5-5.5) [225]). The other standard pH-insensitive dye will be used for normalization purposes. Another strategy is to stain the cells with different endosome (e.g., anti-EEA1) and lysosome (e.g., anti-LAMP1) markers and monitor dye-tagged siRNAs at high resolution to see the spatial location of siRNAs in different cellular compartments. Thus, co-localization of siRNAs and labeled proteins will capture endosomal escape events (i.e., the time and extent of siRNAs that end up in the cytosol). These methods will confirm whether T-NP^{10C} does indeed have better ability to escape endosomes.

Figure 3.4C shows that apoptotic activity was three-fold greater after treatment with T-siHER2-NP^{10C} than with T-siSCR-NP^{10C}, corresponding to less cell viability in **Figure 3.4D**. I also measured cell viability after treatment with T-siHER2-NP^{10C} in a panel of HER2⁺ cells, HER2⁻ cells, and nonmalignant epithelial cells. **Figure 3.4E** shows that treatment with T-siHER2-NP^{10C} reduced viability more strongly in HER2⁺ breast cancer cells (BT474, SKBR3, HCC1954, and JIMT-1) than in HER2⁻ breast cancer cells (MCF-7, MDA-MB-231, and MDA-MB-468) or non-tumorigenic breast epithelial (MCF-10a) or liver epithelial cells (HepG2).

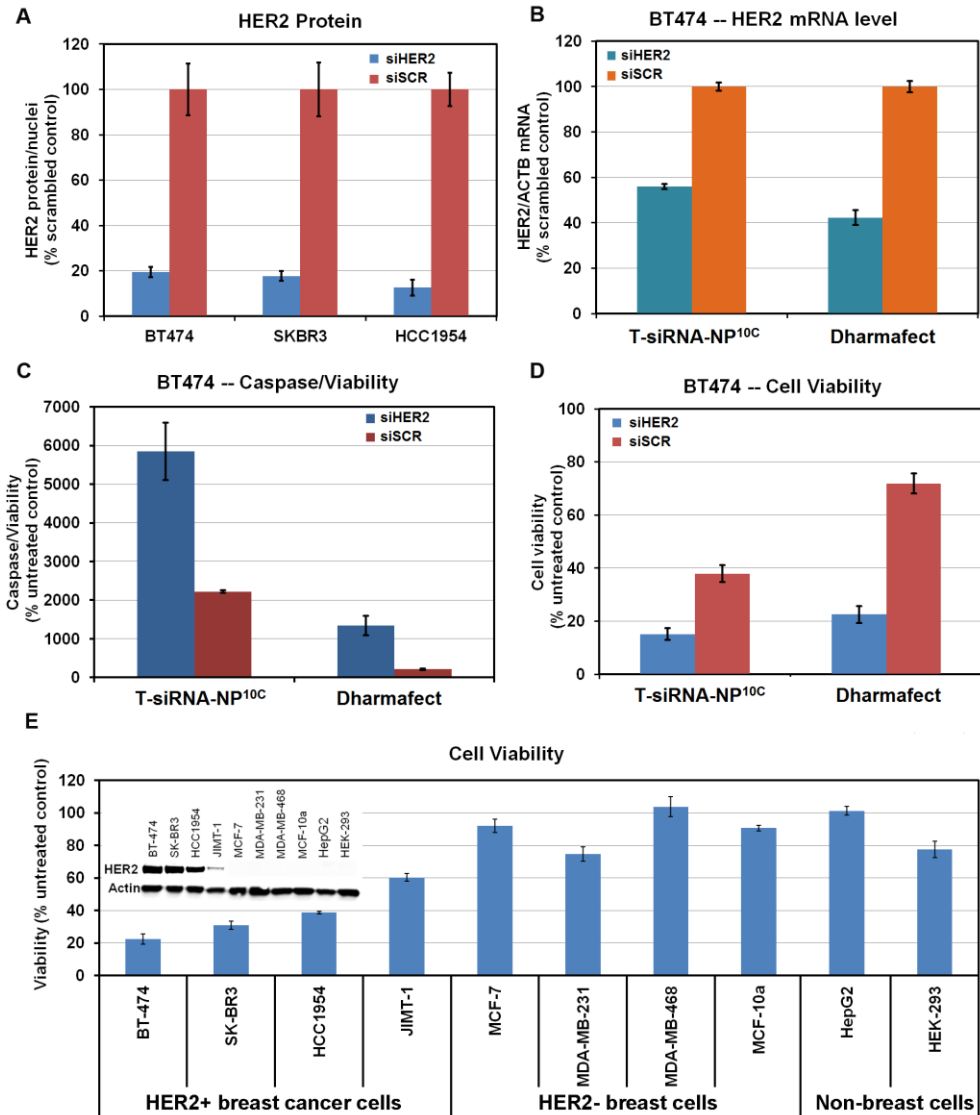


Figure 3.4: HER2 knockdown by siHER2–nanoconstructs and therapeutic responses. (A) HER2 expression of three HER2⁺ breast cancer cells at 72 h post-treatment with siHER2 or siSCR (60 nM) on T–NP^{10C}. (B) HER2 mRNA level (48 h), (C) apoptotic activity (four days) and (D) cell viability (four days) of BT474 cells treated the same way as (A). (E) Cell viability after treatment with T–siHER2–NP^{10C} for four days in various cell lines. All cells exposed to siRNA–nanoconstructs overnight and media changed. Inset of (E) shows HER2 levels of all cells tested.

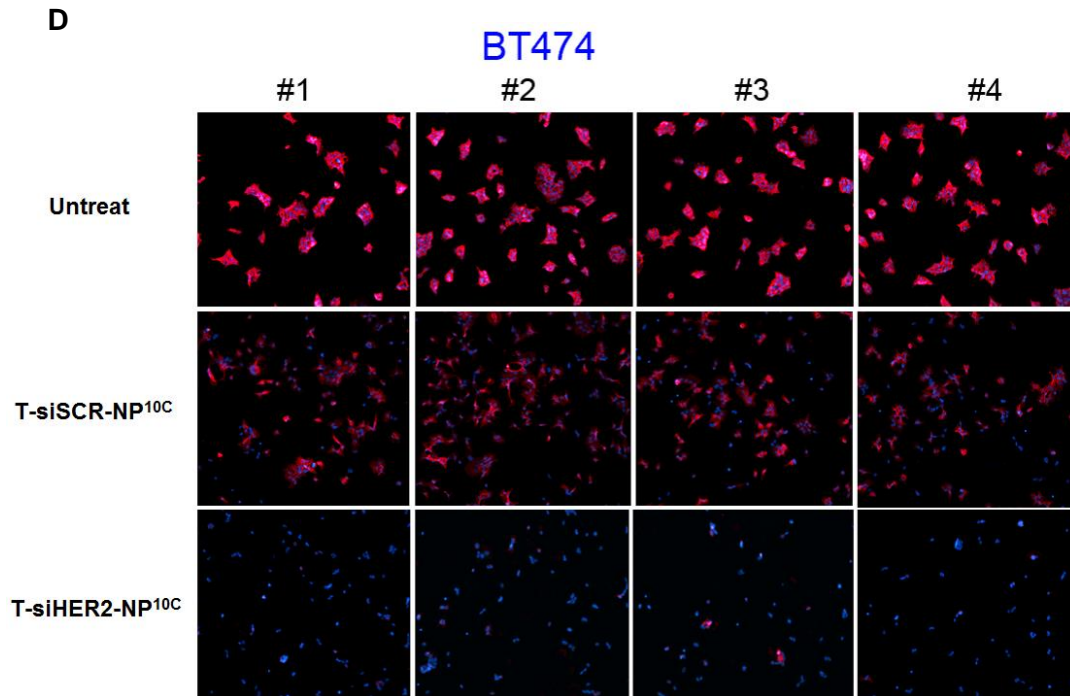
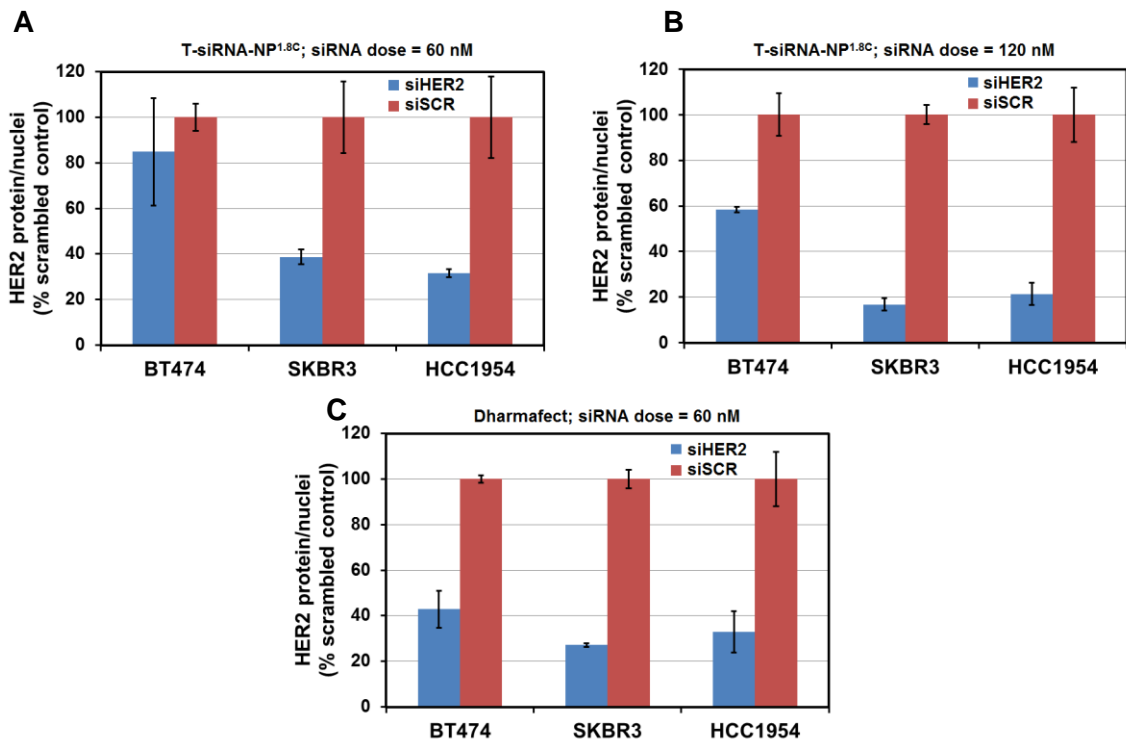


Figure 3.5: HER2 protein reduction analyzed by Immunofluorescence imaging. Fluorescent detection of HER2 and quantification per cell in three HER2⁺ cell lines after treatment with siHER2 or siSCR on nanoconstructs with (A)-(B) cross-linked 1.8-kDa PEI, or (C) DharmaFECT. The experiment was conducted in the same manner as **Figure 3.4A**. All values were normalized with the scrambled siRNA control. (D) Representative immunofluorescent images of HER2 (red) and nuclei (blue, DAPI stain) of BT474 cells treated with 60 nM of siHER2 or siSCR, delivered by the most optimal nanoparticles (T-siRNA-NP^{10C}, **Figure 3.4A**), compared to the untreated control. All were performed in 4 replicates (wells). Cells were fixed and stained for IF analysis at 72 h after treatment (nanoparticle exposure was the first 20 h). Signal intensity was processed by CellProfiler image analysis software. Only HER2 (red) signal associated with nuclei was accounted for. HER2 signal was reported per number of cells (nuclei).

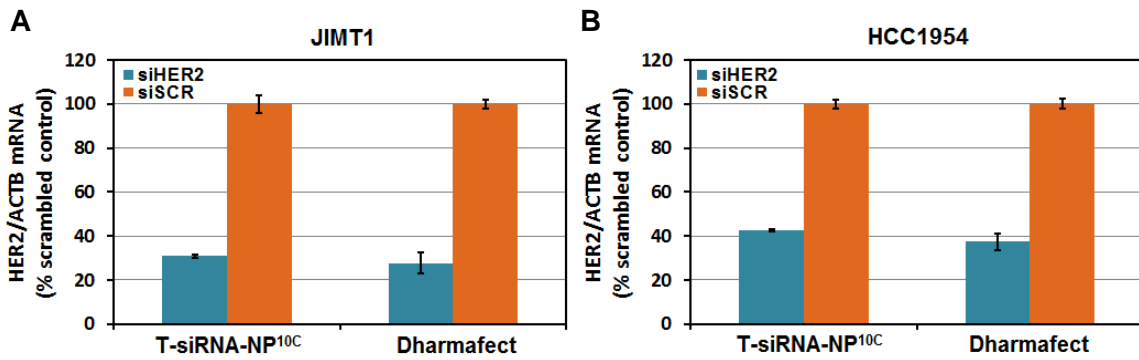


Figure 3.6: HER2 mRNA reduction in JIMT1 and HCC1954. HER2 mRNA level (normalized by β -actin mRNA) of (A) JIMT1 and (B) HCC1954 after treatment with siHER2 or siSCR on nanoconstructs with cross-linked 10-kDa PEI (T-siRNA-NP^{10C}). The experiment was conducted in the same manner as **Figure 3.4**. All values were normalized with the scrambled siRNA control.

T-siHER2-NP^{10C} is hypothesized to serve specificity two-fold. First, T-NP^{10C} should have preferential uptake in HER2⁺ breast cancer cells. Secondly, siHER2 should mainly affect the viability of HER2⁺ cancer cells. As can be seen from **Figure 3.4E**, the treatment response showed positive correlation with HER2 levels in the respective cells.

To dissect these hypotheses, first, I will need to study the uptake of T-siSCR-NP^{10C} (dye-tagged siSCR loaded on trastuzumab-nanoconstructs) in a larger panel of cells with varying expression of HER2 protein. This will confirm whether the level of cellular uptake of T-siSCR-NP^{10C} correlates with the membrane HER2 protein level. Secondly, I will need to use the standard transfection method (e.g., DharmaFECT) to deliver equal amounts of siHER2 to these cells. This will require careful titration of siHER2 concentration since all cells do not uniformly take up DharmaFECT. This will confirm whether knocking down HER2 protein with siHER2 has greater effects in cells with higher levels of HER2 protein. It is likely that the specificity of treatment depends on both HER2⁺ cell targeting mediated by trastuzumab and specificity of siHER2. In this case, I should see both higher cell uptake and response to siHER2 in cells with higher expression of HER2 protein.

Besides serving as a targeting component, trastuzumab also serves a therapeutic potential. To address this role, I will also need to study the effects of trastuzumab on cell viability of the same extended panel of cells, so I could detect cells that are responsive to trastuzumab and correlate the effects to trastuzumab on nanoconstructs.

I hypothesize that the moderate reduction in cell viability found in MDA-MB-231 and HEK-293 (HER2⁻ cells) upon treatment (**Figure 3.4E**) were likely due to 1) slightly positive charges on nanoconstructs and, in turn, non-specific uptake and 2) the low baseline HER2 levels in these cells which may affect the uptake of T-siHER2-NP^{10C} or may indicate functional importance of HER2 protein in these cells. To test the first hypothesis, I will need to correlate the uptake level of T-siSCR-NP^{10C} in these non-targeted cell lines with cell viability after treatment. This will show whether MDA-MB-231 and HEK-293 could take up more T-siSCR-NP^{10C} than other cells whose viability appears unaffected. Another possibility for preferential uptake could be HSPG-mediated uptake as discussed earlier in **section 3.2.2**. I will also need to profile the HSPG expression and see whether I can correlate the T-siSCR-NP^{10C} uptake level to the HSPG level of these cells. Secondly, to test whether the baseline HER2 level is responsible for any preferential receptor-mediated uptake, I will need to stably knock down HER2 protein in these cell lines (e.g., with shHER2 (shRNA against HER2)) and monitor whether the cell uptake of T-siSCR-NP^{10C} in these cells and subsequent cell viability upon treatment are affected, compared to naïve (no knockdown). Further, I will also monitor the cell viability in these non-targeted cells upon knocking down HER2 protein (with standard non-selective transfection: DharmaFECT) in case these cells rely on HER2 pathway and, in turn, are sensitive to siHER2 treatment.

3.2.4 Impact of T-siHER2-NP^{10C} on trastuzumab-resistant cells

Data presented thus far illustrate the efficacy of the T-siHER2-NP^{10C} construct in intrinsic trastuzumab-resistant HER2⁺ cell lines, HCC1954 and JIMT1. In line with the acquired resistance observed in the clinics, I also compared the efficacy of T-siHER2-NP^{10C} in the HER2⁺ cell line, BT474-R, a derivative of the BT474 cell line that was made lapatinib-resistant by long-term treatment of BT474 with 1 μ M lapatinib. **Figure 3.7A** shows that the BT474-R cells were also less responsive to trastuzumab compared to parental BT474. However, **Figure 3.7B** shows that both cell lines were responsive to T-siHER2-NP^{10C} in the same manner compared to the T-siSCR-NP^{10C} control.

In **Figure 3.7C**, under the same treatment with siHER2-nanoconstructs, the viability of BT474 was 26.9% (vs. untreated), while that of BT474-R was 38.3% (vs. untreated). This difference was attributed to the fact that BT474-R was resistant to trastuzumab (on the nanoconstructs).

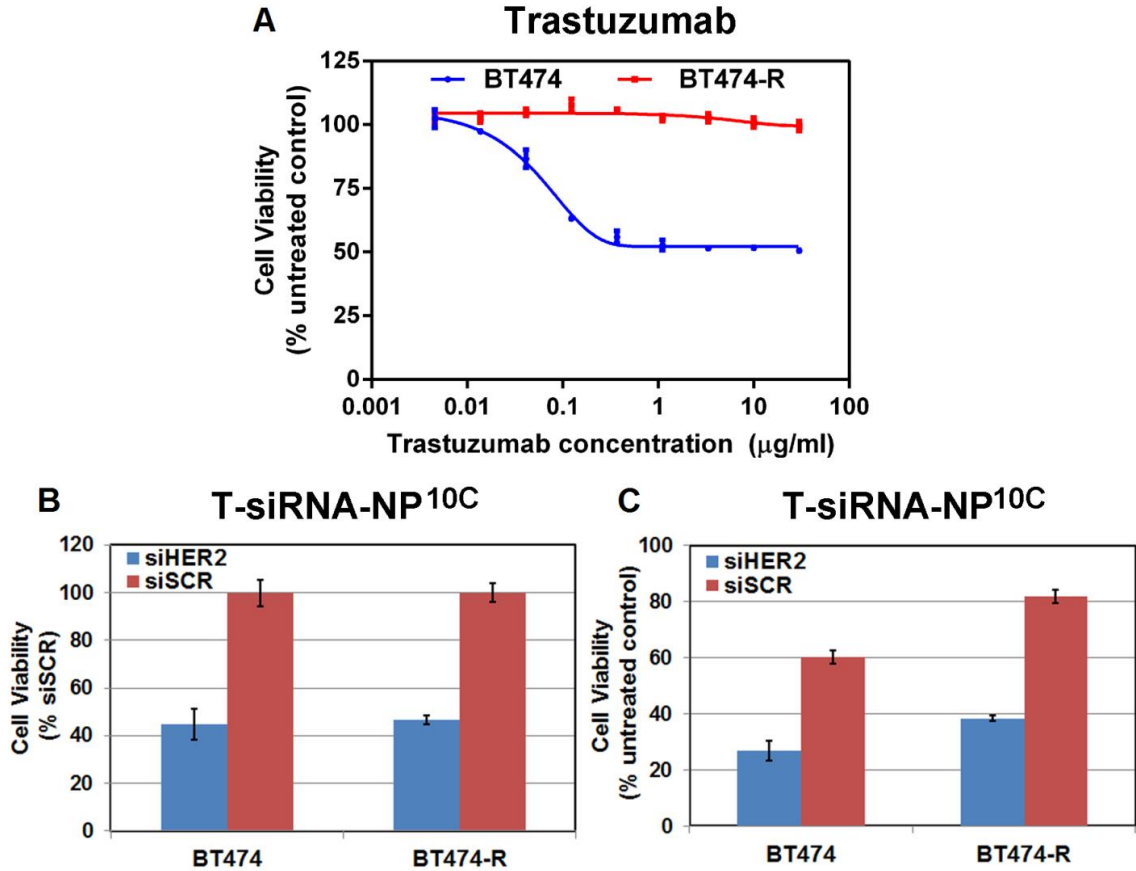


Figure 3.7: In vitro evaluation of siHER2-nanoconstructs on HER2 silencing and ability to overcome trastuzumab resistance. (A) Trastuzumab dose response (as 5-day cell viability) of BT474 and BT474-R (trastuzumab and lapatinib-resistant cell line derived from prolonged treatment of BT474 cells with lapatinib(1 µM)). **(B)-(C)** BT474 and BT474-R were treated with one dose of T-NP^{10C} loaded with siHER2 or siSCR (60 nM siRNA) and cell viability was monitored at 5 days post-treatment and reported as a percentage of siSCR control (B) or untreated control (C).

3.2.5 In vivo HER2 silencing efficacy and tumor growth inhibition in an orthotopic mouse tumor model

T-siHER2-NP^{10C} (with S-47 MSNP core) was chosen over T-siHER2-NP^{1.8C} because it yielded higher siRNA protection, better cellular uptake, higher

gene knockdown, and better cell killing efficacy, without greater toxicity concerns over the T-siHER2-NP^{1.8C}. We then evaluated T-siHER2-NP^{10C} for in vivo gene knockdown efficacy study using the orthotopic HCC1954 xenograft mouse model following a single dose administration. Tumors were allowed to grow to 250 mm³ before treatment (n = 4 per group). Following a single dose of our siHER2-nanoconstructs (1.25 mg siRNA/kg bolus, i.v. administration via tail vein), tumors were harvested at 4 days post-dosing and analyzed. HER2 protein levels in the HCC1954 tumors were significantly reduced by 58.6% versus the saline control (p < 0.0013) and by 46.5% versus the siSCR control (p < 0.015) (**Figure 3.8A-B**). It should be noted that 22.7% (p = 0.27 vs. saline control) HER2 reduction in the siSCR control is likely due to trastuzumab on the nanoconstructs.

In a separate study in our lab, we have established an efficacious dose of T-siRNA-NP^{10C} to be used for effective gene silencing in vivo. For this study, we used mice bearing luciferase-expressing tumors and administered a single i.v. dose of 0.625 or 1.25 mg siLUC/kg. We subsequently monitored the levels of luciferase activities by IVIS imaging at various time points. We found that 1.25 mg siLUC/kg could knock down the luciferase activity by 59%, 53% and 51% at days 1, 2 and 3, respectively, compared to the scrambled controls. Yet, 0.625 mg siRNA/kg did not show a significant knockdown after one bolus dose. Hence, I selected 1.25 mg siRNA/kg as a starting point for in vivo efficacy evaluation.

Next, we performed a tumor growth inhibition study with the same material, T-siHER2-NP^{10C}, as shown in **Figure 3.8C** using the same HCC1954 mouse model. Tumors were allowed to grow to ~100-150 mm³ in size prior to

group randomization (n = 5 per group). The HCC1954 cell line was also recognized as multiple-drug (e.g., cisplatin [226], trastuzumab [227] and pertuzumab [228]) resistant in vitro and/or in mice. In agreement with the literature, we found it to be resistant to trastuzumab (**Figure 3.9A-B**) and the combination of trastuzumab and paclitaxel (**Figure 3.9C**) in mice. After a multiple dose administration (1.25 mg siRNA/kg, via tail vein injection over a period of three weeks), the tumors responded well to T-siHER2-NP^{10C} while little response was found with T-siSCR-NP^{10C} compared to the saline treatment.

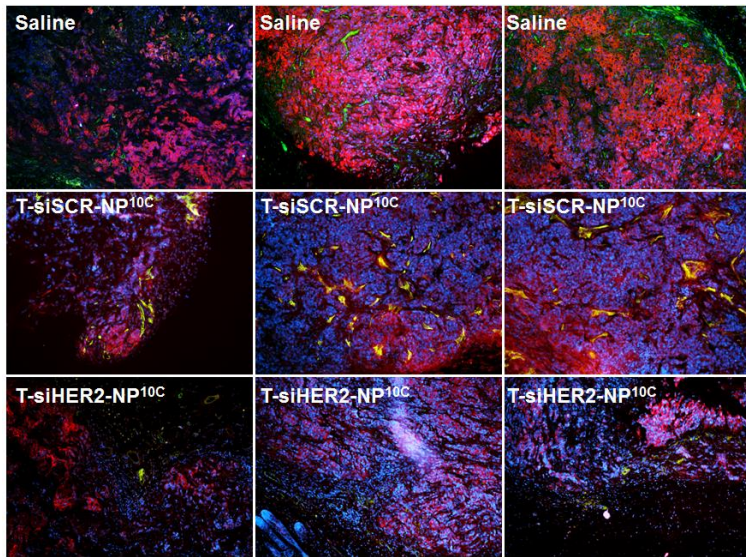
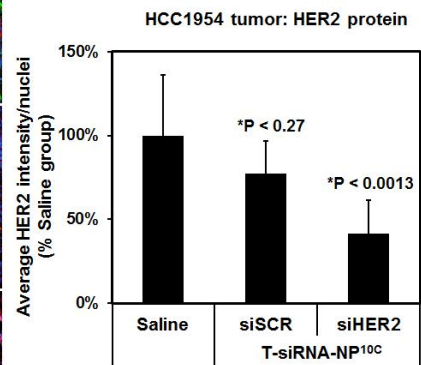
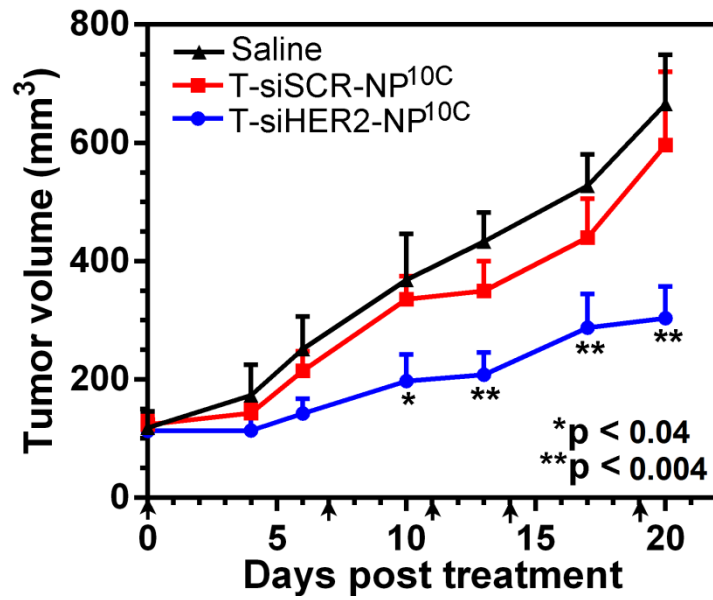
A**B****C**

Figure 3.8: In vivo HER2 reduction and growth inhibition of orthotopic HCC1954 tumors. (A) Representative immunofluorescent images of tumor tissues collected from mice (n = 4/group) at 4 days after i.v. injection with one dose of T-NP^{10C} loaded with siHER2 or siSCR (1.25 mg siRNA/kg, NP/siRNA of 50) or PBS control. **(B)** Quantitative HER2 levels of the tissues. Images were analyzed by CellProfiler; red = HER2 protein; green = CD31 endothelial marker; blue = DAPI staining cell nuclei. **(C)** Tumor growth in mice bearing orthotopic HCC1954 tumor xenografts (n = 5/group) receiving the same treatments as (A) but multiple doses (days of injection are indicated by arrows). All data are presented as means ± SEM. Specified p-values are against the saline control.

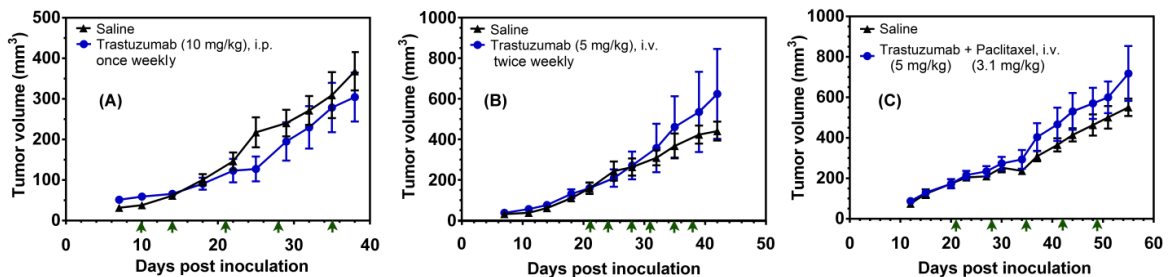


Figure 3.9: Drug resistance in HCC1954 in vivo. Tumor growth in mice bearing orthotopic HCC1954 tumor xenografts. **(A)** Mice (n=7/group) were injected intraperitoneally with trastuzumab (10 mg/kg) or saline. **(B)** Mice (n=5/group) were injected via tail vein with trastuzumab (5 mg/kg). **(C)** Mice (n=9/group) were injected via tail vein with trastuzumab (5 mg/kg) and paclitaxel (3.1 mg/kg). Arrows indicate days of injection.

The complete eradication of tumors was not achieved in my investigations. I hypothesize that the heterogeneity of HER2 expression in tumors could affect the tumor response mediated by HER2 targeting. To test this hypothesis, we need to study co-localization of siRNA uptake (e.g., fluorescently-tagged siHER2) and cellular HER2 status in tumor cells at different time points (e.g., 1, 2, 4, 10, and 24 hours). Another possible hypothesis is that knocking down HER2 protein alone is not sufficient to elicit death in all cells across the population. Certain cells

may be able to escape HER2 pathway (e.g., by PIK3CA mutation). To test this hypothesis, I will need to perform more complete and permanent inhibition of HER2 protein (e.g., shHER2) and see whether the cells can still survive. The surviving cells will then be evaluated for downstream mutation profiles and protein expression profile (overexpression or suppression of certain proteins) to aid in designing additional therapeutic hits to elicit death in these cells. Therefore, a cocktail of siRNAs might be needed to more completely inhibit tumor growth. The other possible limitation is the delivery barrier. The distribution within a tumor might not be uniform and may be restricted near vasculatures. We need to look at the distribution of siRNAs within the tumor areas in different cross-sections and relative to the locations of vasculature. Also, staining for other stromal components to correlate the degree of those stroma barriers with siRNA distribution should shed more light on the phenomenon and, in turn, lead to a better design of the carrier.

3.3 Conclusions

This chapter covers the assessment of the in vitro and in vivo efficacy of the developed MSNP-based nanoconstruct for siRNA delivery. T-NP-PEI^{10C}, based on the S-47 core, appears to be the most effective and is used for the rest of the dissertation. In this chapter, the lead nanoconstruct was shown to have cell uptake specificity upon the loading of targeting antibodies. In particular, HER2-targeted nanoconstructs were taken up significantly more in HER2⁺ cells than HER2⁻ cells (>80% difference). Also, the delivery of siHER2 by HER2-targeted nanoconstructs can cause HER2 knockdown at both mRNA and protein levels

and, in turn, elicit death in HER2⁺ cancer cells, while sparing HER2⁻ cells. In vivo delivery upon systemic administration results in HER2 protein knockdown in tumor and resultant growth inhibition of the drug-resistant HER2⁺ breast tumors. In the next chapter, I evaluated the safety profile of this material.

4. Chapter 4: In vitro and in vivo safety evaluation of siRNA-nanoconstructs

In addition to efficacy, safety is another major consideration for nanoparticles being developed for human use. This chapter covers the potential cytotoxicity of siRNA-nanoconstructs in a panel of normal and cancer cells. Various types of inorganic nanoparticles, including mesoporous silica, have been reported to induce cellular reactive oxygen species (ROS). Therefore, ROS was measured in cells upon the siRNA-nanoconstruct treatment. In addition, blood compatibility of nanoconstructs is examined, as this is an essential property for systemically administered nanoconstructs. Potential immune responses to nanoconstructs were also evaluated. Lastly, the serum biochemistry profiles of mice after multiple-dose treatment with siRNA-nanoconstructs are reported.

4.1 Materials and Methods

4.1.1 Materials

Abraxane and Feraheme were obtained from OHSU Pharmacy. Acetaminophen (APAP) and menadione were obtained from Sigma Aldrich (MO).

4.1.2 Assessment of cytotoxicity and ROS generation in cell lines

Cells were seeded in a 96-well plate for 24 h prior to treatment (see media recipe in **Table 3.2**). Nanoconstructs were loaded with siHER2 at NP/siRNA mass ratio of 50. The siRNA dose was either 30 or 60 nM. Cell viability was evaluated at 24 h post-treatment with CellTiter-Glo assay (Promega) following

the manufacturer's protocol. Cytotoxicity in terms of cell membrane rupture was measured as the amount of the dehydrogenase (LDH) enzyme that leached into cell culture supernatant at 24 h post-treatment using an LDH assay kit (Thermo Scientific) following the manufacturer's protocol.

At 24 h post-treatment, a subset of cells treated as aforementioned was used to measure levels of reactive oxygen species (ROS) in the cells. The cellular ROS were probed by CellROX Green reagent (Life Technologies). The cell-permeant dye is not fluorescent while in a reduced state, but it exhibits bright green photostable fluorescence upon oxidation by ROS (e.g., hydrogen peroxide, hydroxyl radical, superoxide anion). Fluorescence images were obtained with the EVOS FL cell imaging system (Life Technologies). All images were processed for signal intensity by CellProfiler image analysis software (Broad Institute). The fluorescent signals were averaged by the number of cells being analyzed (measured by cell counts with DAPI stains).

4.1.3 Blood compatibility of nanoconstructs: hemolysis, thrombogenesis, and platelet aggregation

Studies on blood compatibility were performed following or with minor modifications from the Nanotechnology Characterization Laboratory (NCL)'s published protocols. Concentrations of nanoconstructs in the studies herein were based on the estimated concentration of nanoconstructs in human blood, using "animal-to-human equivalent dose" table provided by the FDA. "1X" dose level is an estimated material concentration in human blood, assuming a body weight of 70 kg and blood volume of 5 L. "5X" dose level 5 times the "1X" dose level.

Hemolysis. In vitro hemolytic property of the nanoparticles was evaluated with some modifications from other works [229]. Briefly, human blood was collected in the presence of EDTA, and serum was removed. Red blood cells were suspended at 1×10^9 cells per mL and exposed to nanoconstructs (final concentrations of 70 or 350 $\mu\text{g/mL}$ for 1X or 5X, respectively) for 4 h and 37°C . Following centrifugation, absorbance of hemoglobin in the supernatants (542 nm) was measured and used to quantify percent hemolysis. Abraxane (Celgene) (94 $\mu\text{g/mL}$ for 1X and 470 $\mu\text{g/mL}$ for 5X, calculated from the prescribed dose assuming a typical human's body weight of 70 kg and 5 L of blood) was used as the FDA-approved nanoparticle-based drug benchmark.

Coagulation (thrombogenesis) assay. Platelet-poor plasma (PPP) was obtained following a two-step centrifugation of isolated blood (diluted in 3.2% sodium citrate, 1:10). After the first spin (2150 g, 10 min), the top portion of plasma (~75% of the total volume) was collected without disturbing the plasma at the bottom. The collected portion was centrifuged again at the same speed for 10 minutes, and the top portion (~75% of the total volume) was collected as PPP. Nanoconstructs (70 or 350 $\mu\text{g/mL}$) were mixed with PPP (0.15 mL). The tubes were incubated for 30 minutes at 37°C . After the 30-minute incubation, APTT-xl reagent (0.05 mL) was added and incubated for 3 minutes in the Trinity Biotech KC-4 coagulation analyzer. After which, CaCl_2 (8.3 mM) was added, and the time until the onset of coagulation was recorded. Abraxane at 1X and 5X was used at the same doses as the above (see hemolysis section). Likewise, Feraheme

(AMAG Pharmaceuticals), another FDA-approved nanoparticle-based drug, (102 µg/ml for 1X and 510 µg/ml for 5X) was also compared in parallel.

Platelet aggregation assay. Platelet-rich plasma (PRP) was obtained following centrifugation of isolated blood (diluted in 3.2% sodium citrate, 1:10). The isolated blood was centrifuged at 200g for 20 minutes. The supernatant (which contains PRP) was collected and maintained at room temperature prior to treatment. Following a 1-min incubation at 37°C (baseline), reactions were initiated by addition of nanoconstructs (70 or 350 µg/mL) or collagen related peptide (CRP; 100 µg/ml) and monitored for three minutes for optical density via an aggregometer (Chrono-log Corp). Abraxane at 1X and 5X as entailed above was also used as a benchmark.

4.1.4 Immune response: peripheral blood mononuclear cell (PBMC) cytokine release assay.

A PBMC cytokine release assay was conducted according to the recommendations and method outlined by the Nanotechnology Characterization Lab (NCL) of the NCI for immunological studies of nanoparticles. The in vitro cell-based assay evaluated cytokine production by PBMCs (200,000 cells/well) following a 24-h exposure to the test materials. Test materials included nanoconstructs with and without siHER2 to investigate the potential impact of siRNA-mediated immune response. Following incubation, cell culture supernatants were collected and analyzed for IL-1 β , IL-6, IFN- α , and TNF- α by a cytometry bead array (Milliplex Magnetic Bead) following the manufacturer's protocol. Abraxane (Celgene, NJ) and Feraheme (AMAG Pharmaceuticals, MA)

were used as FDA-approved nanoparticle-based drug benchmarks since there's no siRNA-based nanoparticle drug in the market. Nanoconstructs were tested for the presence of endotoxin with the LAL gel-clot assay (Lonza, NJ), following the manufacturer's protocol.

4.1.5 Serum biochemistry profiles: kidney and liver functions

Serum was collected from terminal animals that participated in the multiple dose efficacy study (see section 3.1.7). Serum was analyzed for markers of kidney function (Blood urea nitrogen (BUN) and creatinine (CRE)) of liver function (Alanine transaminase (ALT), Aspartate transaminase (AST), and total bilirubin (TBIL)) by DRI-CHEM 4000 Analyzer (Heska Corporation) following the manufacturer's protocol. Liver and kidney samples were sectioned and stained with hematoxylin and eosin as serviced by the OHSU histopathology core. The slides were imaged with optical microscope (EVOS FL cell imaging system (Life Technologies)).

4.2 Results and discussion

4.2.1 Cytotoxicity

I evaluated the cytotoxicity profile of T-siHER2-NP^{10C} in five "normal/non-tumorigenic" cell lines, including LLC-PK1 (pig kidney epithelial cells), HEK-293 (human embryonic kidney cells), HepG2 (human liver hepatocellular cells), MCF-10a (human mammary epithelial cells), and HUVEC (human umbilical vein endothelial cells). The first three cell lines have been recommended by the NCL for cytotoxicity studies of nanoparticles since kidney and liver are clearance or

homing organs for nanoparticles. MCF-10a is considered a normal counterpart of breast cancer, and HUVEC is a relevant cell model for intravenous administration of nanoparticles. The cell viability was measured with the CellTiter-Glo assay, which measures adenosine triphosphate (ATP) as an indicator of metabolically active cells. Cell viability was measured at 24 h post-treatment and is shown in **Figure 4.1**. Acetaminophen (APAP, Tylenol) is a drug benchmark (used according to NCL's protocol), while our T-siHER2-NP^{10C} was tested at efficacious doses (30-60 nM as siRNA, or 21-42 µg/mL as nanoconstructs). **Figure 4.1** shows that T-siHER2-NP^{10C} did not elicit significant cytotoxicity in any cell line tested (< 10% cell death for all cell lines tested, except 20% for LCC-PK1). T-siHER2-NP^{10C} appeared safer than the positive control, APAP, for all cells.

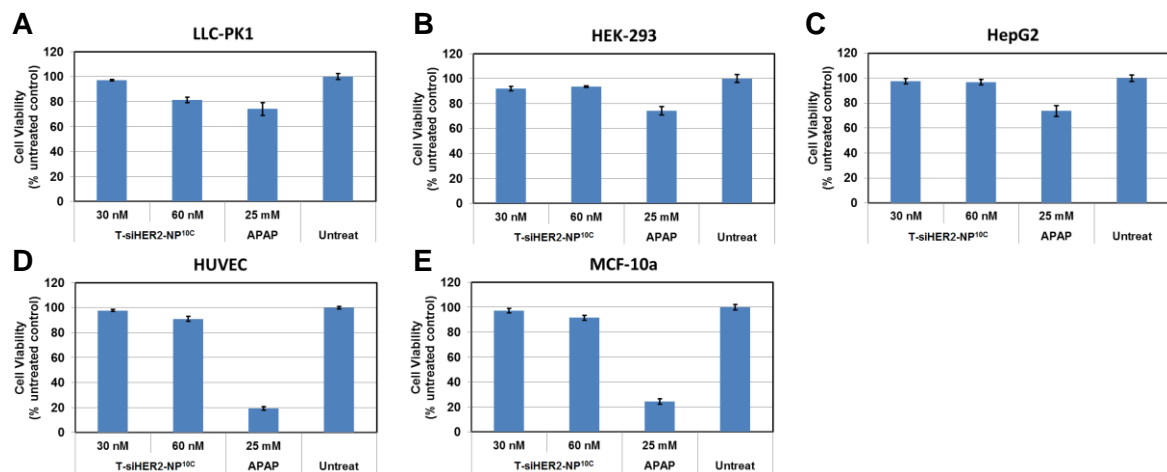


Figure 4.1: Cytotoxicity (cell viability). A panel of non-tumorigenic epithelial cell lines ((**A**) LLC-PK1, (**B**) HEK-293, (**C**) HepG2, (**D**) HUVEC and (**E**) MCF-10a) was treated with T-siHER2-NP^{10C} (30 or 60 nM siRNA) and APAP (25 mM) as a benchmark. Cell viability was measured at 24 h after the treatment. Cell viability is reported as the percentage of the untreated control.

The cytotoxicity of APAP in various cell lines depends greatly on the cytochrome P450s present, which effectively metabolizes acetaminophen to the reactive metabolite NAPQI, as well as the initial and depleted levels of glutathione [230].

In addition, cell membrane integrity was monitored by the lactate dehydrogenase (LDH) enzyme levels in cell culture supernatants. LDH is a cytosolic enzyme that is released into the cell culture media upon cell lysis. LDH enzyme levels were measured at 24 h post-treatment and are shown in **Figure 4.2**. It can be seen that most data agree well with cell viability data in **Figure 4.1**. T-siHER2-NP^{10C} did not elicit significant membrane damage in any cell line tested (< 10% LDH leakage for all cell lines tested) at both dose levels; APAP (at NCL's recommended dose) did worse across the 5 cell lines.

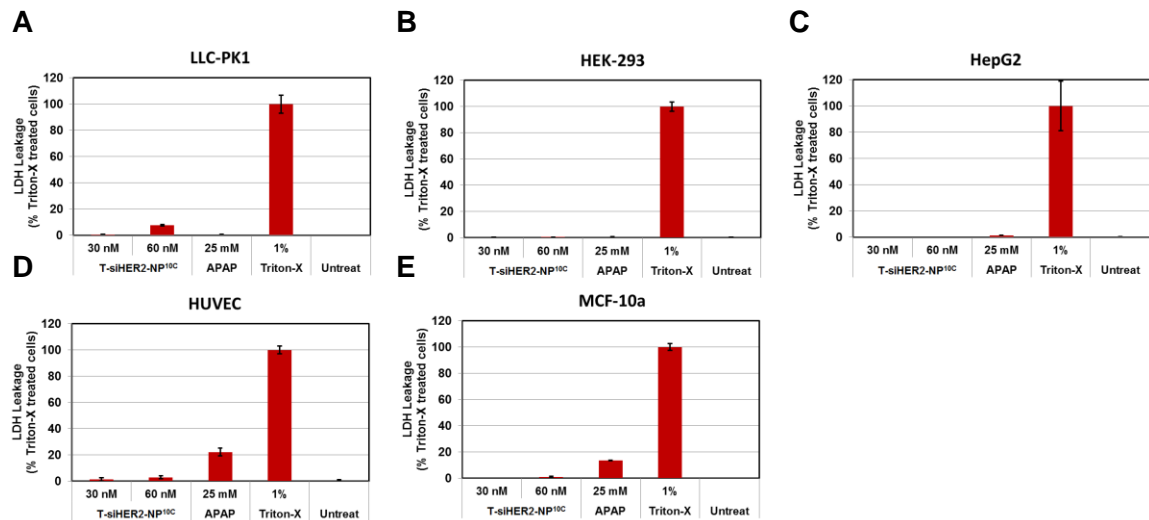


Figure 4.2: Cytotoxicity (LDH leakage). A panel of non-tumorigenic epithelial cell lines ((**A**) LLC-PK1, (**B**) HEK-293, (**C**) HepG2, (**D**) HUVEC and (**E**) MCF-10a) was treated with T-siHER2-NP^{10C} (30 or 60 nM siRNA) and APAP (25 mM) as a benchmark. LDH activity in supernatant was measured at 24 h after the treatment. LDH leakage is reported as the percentage of the complete lysis with 1% Triton-X (positive control).

4.2.2 Reactive Oxygen Species

I further evaluated the nanoconstructs for their ability to generate oxidative stress through the production of ROS. The cellular ROS were probed by CellROX Green reagent. Using similar experimental conditions as in the **Cytotoxicity** study, ROS were monitored in two relevant cell lines at 24 h post-treatment with the siHER2-nanoconstructs. HepG2 cells are recommended by the NCL for evaluating ROS generation by nanoparticles. MCF-10a was included since it is relevant to the breast cancer application. ROS generation 1 h after treatment with 100 μ M menadione (which is known to generate intracellular ROS and apoptotic cell death) was used as a positive control. **Figure 4.3** shows that T-siHER2-NP^{10C} did not induce oxidative stress in the two cell lines tested (levels are comparable to that of the untreated control). In contrast, menadione induced oxidative stress via ROS generation, reflected as a 1.5- to 2-fold increase relative to the untreated control. This agrees well with the cell viability data in **Figure 4.1**. In conclusion, T-siHER2-NP^{10C} was not toxic to cells, and it did not damage (lyse) cells or increase the ROS of cells.

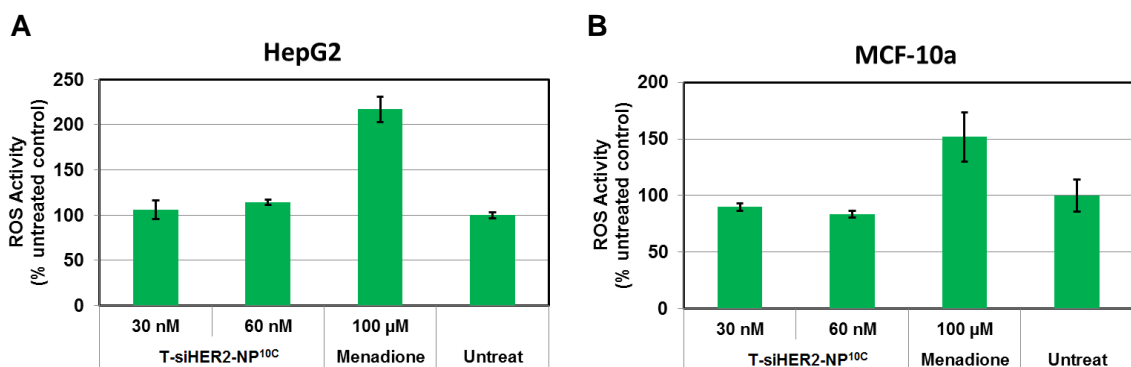


Figure 4.3: ROS activity. HepG2 (**A**) and MCF-10a (**B**) were treated with T-siHER2-NP^{10C} (30 or 60 nM siRNA) and menadione (100 μM). ROS activity was measured 24 h after the treatment, except for menadione, which was treated for only 1 h before analysis. ROS signals were normalized with cell viability and reported as a percentage of the untreated control.

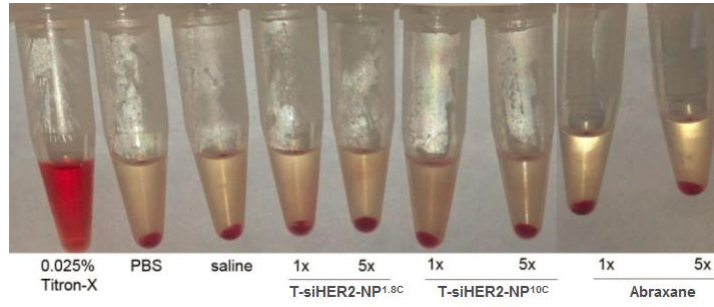
4.2.3 Blood compatibility

It is important that nanoparticle constructs intended for use systemically in vivo do not cause hemolysis, thrombogenesis, and platelet aggregation. We assessed these endpoints for T-siHER2-NP^{1.8C} and T-siHER2-NP^{10C} and compared to those for the FDA-approved nanoparticle products: Abraxane and Feraheme. Nanoconstructs were tested at 1X and 5X of the intended human blood level.

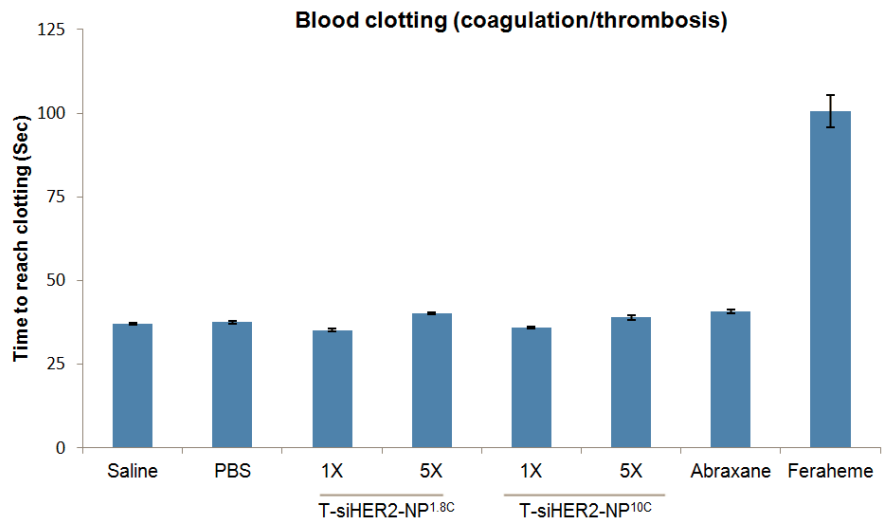
Cationic polymers (e.g., PEI) have a tendency to cause blood cell lysis. However, I hypothesized that a PEG layer on the nanoconstructs should shield PEI from direct contact with the cell membrane. As predicted, **Figure 4.4A** shows that our nanoconstructs did not cause hemolysis of red blood cells at either 1X or 5X the dose level, while complete blood lysis was achieved with 0.025% Triton-X (the positive control).

Furthermore, we performed a blood coagulation (clotting) test with the nanoconstructs (**Figure 4.4B**). It can be seen that the nanoconstructs did not affect the coagulation time of platelet-poor plasma (all took about 37 s), while Feraheme prolonged the coagulation time. This agrees with Feraheme's common side effects related to abnormal clotting (easy bruising and swelling) [231] (**Figure 4.4B**). Lastly, we evaluated siHER2-nanoconstructs for their ability to cause platelet aggregation (adverse effect and death in animals and humans). As shown in **Figure 4.4C**, the siHER2-nanoconstructs, similar to Abraxane, at 1X and 5X did not trigger platelet aggregation, while a collagen-related peptide used as a positive control triggered aggregation immediately.

A



B



C

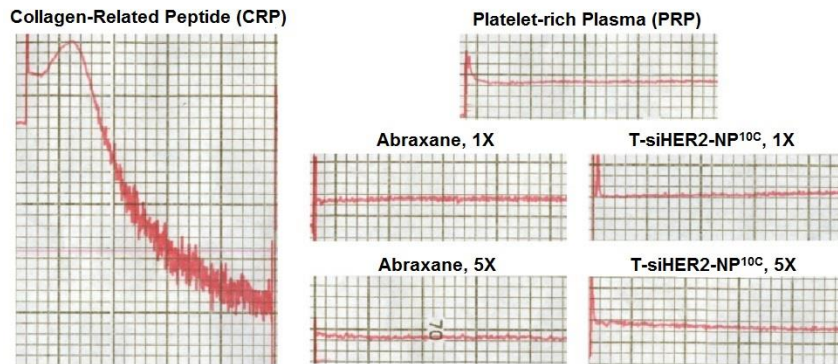


Figure 4.4: Blood compatibility of siRNA-nanoconstructs. **(A)** Hemolysis assay: siRNA-nanoconstructs were incubated with red blood cells (1×10^9 cells/mL) for 4 h at 37°C. At the end of incubation, red blood cells were pelleted down and supernatant was analyzed for lysed hemoglobin (Triton-X as positive control). **(B)** Coagulation time: siRNA-nanoconstructs were incubated in platelet-poor plasma (PPP) for 30 minutes at 37 °C. Clotting time was measured upon addition of APTT-xl reagent and CaCl_2 . **(C)** Evaluation on platelet aggregation of materials incubated in platelet-rich plasma (PRP); collagen related peptides (CRPs) served as a positive control.

4.2.4 Immune response

Induction of an adverse immune response is one of the major causes of failure of drug candidates during preclinical and clinical studies. Nanoconstructs may elicit an inflammatory response in immune cells via toll-like receptor activation. We evaluated the effect of T-siHER2-NP^{1.8C} and T-siHER2-NP^{10C} on immune response by treating peripheral blood mononuclear cells (PBMCs) isolated from human blood with these nanoconstructs. The cytokines evaluated include IL-1 β , IL-6, IFN- α , and TNF- α because their production is associated with Toll-like receptor activation on the surface of the cell membrane and on the endosomes [232]. PBMCs have been reported to respond to siRNA transfection with a sequence-specific TLR 7/8-dependent induction of IFN- α and TNF- α [233, 234]. The TLR7/8 agonist R848 was used as a direct positive control, since TLR7 and TLR8 are located within the endosomes [235] where nanoconstructs and siRNAs are expected to reside. The responses to our nanoconstructs were compared to those obtained for the FDA-approved nanoparticle-based drugs Abraxane and Feraheme. **Figure 4.5** shows that neither T-siHER2-NP^{1.8C} nor T-siHER2-NP^{10C} increased the levels of IL-6 and TNF- α at either the 1X or 5X level,

while Abraxane significantly increased both cytokines at the 5X level. Both nanoconstructs increased the levels of IFN- α and IL-1 β somewhat but not to the extent observed in Abraxane for IL-1 β and Feraheme for IFN- α . The immune response was not significantly different for nanoconstructs with or without siRNAs, suggesting that the response was not siRNA-specific. Lastly, the PBMC immunological response to T-siHER2-NP^{10C} was not worse than T-siHER2-NP^{1.8C}. This may be because the higher PEG content of T-siHER2-NP^{10C} compensates for its higher charge or higher-MW PEI (**Table 2.2**). The nanoconstructs were also tested for the presence of lipopolysaccharides or LPS, produced by gram-negative bacterial contamination, since this might also trigger an adverse immune response. About 35% of clinically relevant nanoparticles have been found to carry this contaminant [236]. **Figure 4.6** shows that T-siHER2-NP^{1.8C} and T-siHER2-NP^{10C} were not contaminated.

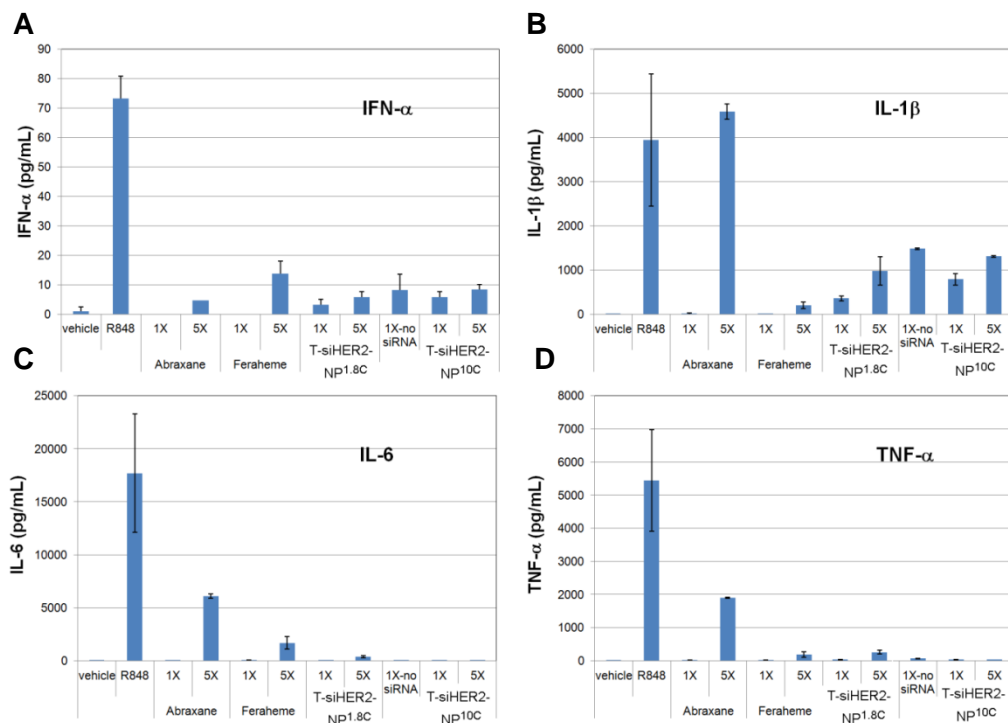


Figure 4.5: Cytokine induction in PBMCs. Levels of (A) IFN- α , (B) IL-1 β , (C) IL-6 and (D) TNF- α upon 24-h exposure with various nanoconstructs, T-siHER2-NP^{1.8C}, T-NP^{10C} (no-siRNA), T-siHER2-NP^{10C}, Abraxane, and Feraheme. 1X = estimated human blood levels of the materials (i.e., 94 μ g/mL for Abraxane, 102 μ g/mL for Feraheme, and 70 μ g/mL for the two nanoparticles), 5X = five-fold of such levels, Vehicle = PBS, R848 = TLR7/8 agonist at 10 μ M.

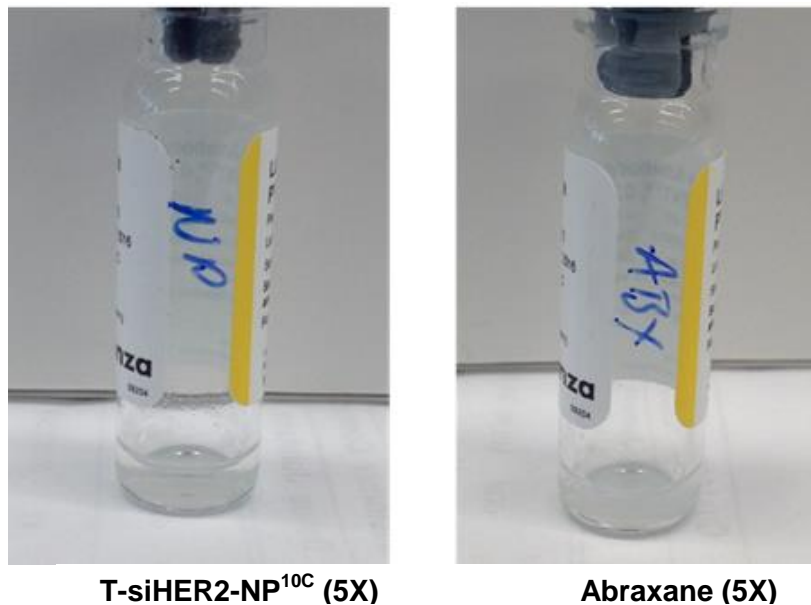


Figure 4.6: Images from the LAL gel-clot assay on the nanoconstructs (T-siHER2-NP^{10C}), benchmarked with Abraxane; both at 5X concentration (similar to Figure 4.4). Both are negative for endotoxin according to the manufacturer's protocol: "A negative test is characterized by the absence of solid clot after inversion. The lysate may show an increase in turbidity or viscosity. This is considered a negative result."

4.2.5 Serum biochemistry profiles after long-term treatment with nanoconstructs

Serum was collected from mice that underwent multiple injections in the efficacy study (section 3.2.5 and **Figure 3.8C**) upon sacrifice. Serum biomarkers for kidney functions (Blood urea nitrogen (BUN) and creatinine(CRE)) and for

liver functions (Alanine transaminase (ALT), Aspartate transaminase (AST), and total bilirubin (TBIL)) were measured and tabulated in **Table 4.1**. The normal ranges for these markers were obtained from Charles River specification sheet for SCID/hairless female mice. It can be seen that there is a small elevation of markers for liver function but not kidney function. However, the values still fall within the normal range.

Table 4.1: Serum biochemistry profiles.

Treatment	BUN (mg/dL)	CRE (mg/dL)	ALT (U/L)	AST (U/L)	TBIL (mg/dL)
T-siHER2-NP ^{10C}	24.9 ± 3.4	0.3 ± 0.1	40 ± 13	155 ± 59	0.4 ± 0.3
T-siSCR-NP ^{10C}	28.6 ± 3.3	0.3 ± 0.1	37 ± 8	138 ± 24	0.3 ± 0.2
Untreated	21.2 ± 2.7	0.2 ± 0.0	21 ± 3	117 ± 28	0.5 ± 0.3
Normal range (SCID/hairless) (Charles River Inc.)	17-35	0.2-0.5	29-76	62-319	0.2-0.8

This finding was substantiated by histology of the kidney and liver collected from mice treated with multiple doses of T-siHER2-NP^{10C} versus the untreated mice (9 doses, twice weekly, 1.25 mg siRNA/kg). Mice were sacrificed 31 days after the first treatment. Gross macroscopic observations upon necropsy showed conserved, normal anatomical features in the kidneys of the treated animals (e.g. characteristics of color, shape, and size). As shown in **Figure 4.7**, glomeruli were intact, and tubular structure and interstitium were conserved. More importantly, areas of necrosis or inflammatory cell infiltration were not observed.

Similar gross observations of the liver at necropsy also showed no overt changes upon nanoconstruct administration. There was no observed morphological difference between nanoconstruct and untreated groups (**Figure 4.7**). Both control and treated animals showed a prominent central vein, sinusoidal spaces and preserved cytoplasm/nuclei. There was also no evidence of necrosis or inflammatory cell infiltration.

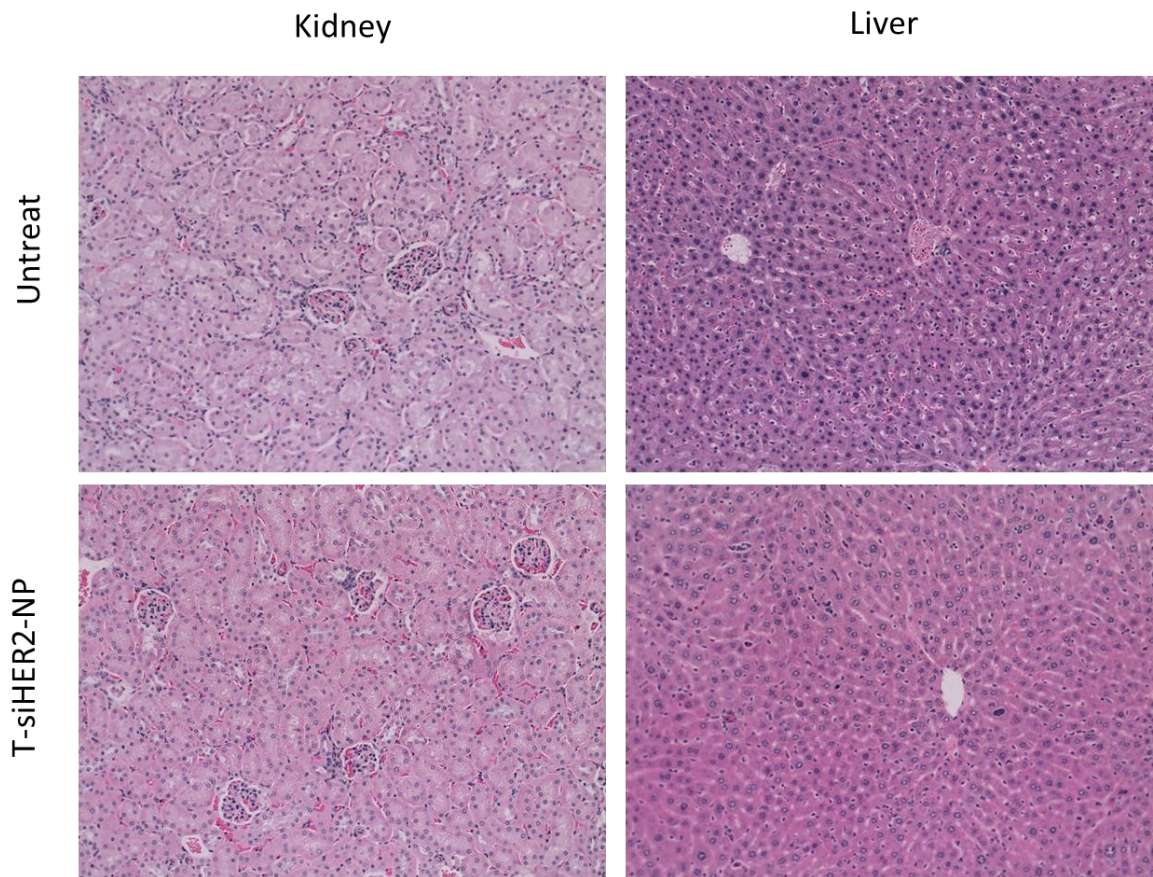


Figure 4.7: Histology of kidney and liver sections. Kidney and liver were harvested upon sacrifice, sectioned and stained with H&E. Representative images from light microscopy are shown.

4.2.6 Body weights of mice after administration of multiple doses of siRNA-nanoconstructs

We also monitored the body weights of the mice that underwent multiple injections (9 doses, twice weekly, 1.25 mg siRNA/kg) twice weekly. **Figure 4.8** suggests that treatment did not affect the body weights of mice after multiple dose administration. There was no significant difference between the treatment group and the saline control.

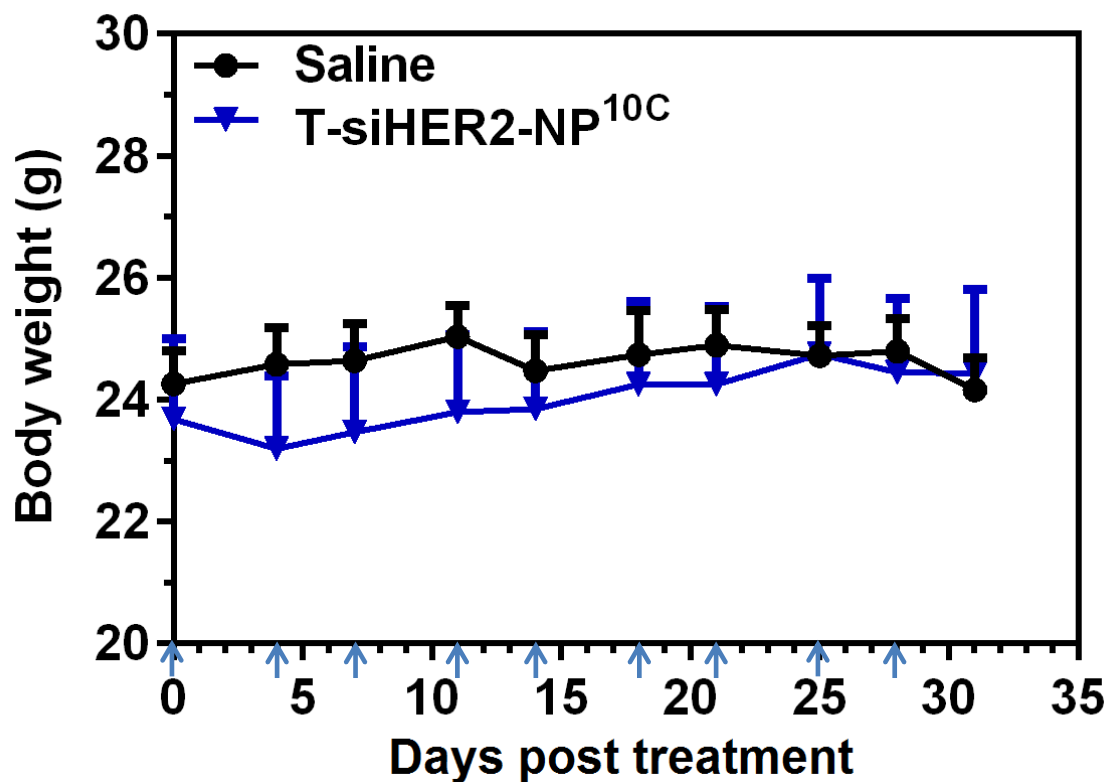


Figure 4.8: Body weights of mice receiving multiple doses of T-siHER2-NP^{10C} or saline. SiRNA dose is 1.25 mg/kg. Arrows indicate injection. All data are presented as means \pm SEM (n = 5/group).

4.3 Conclusions

This chapter covers the safety profile of the nanoconstructs. It can be seen that the lead candidate, T-siHER2-NP^{10C} (S-47 core), has a favorable safety profile. First, cytotoxicity in cell lines was evaluated by both cell viability and cell membrane leakage. Nanoconstructs did not appear to be toxic to the non-targeted HER2⁻ cells; nor did they trigger ROS production. The blood compatibility was encouraging, suggesting its use for systemic administration. In particular, nanoconstructs did not appear to cause hemolysis, prolong coagulation time, or cause platelet aggregation, and they did not appear to trigger significant immune response. All of the cytokine responses are on par with the FDA-approved nanoparticle-based drugs. Lastly, nanoconstructs did not cause a significant damage to clearance organs, a common concern for nanoparticle application. Both serum biomarker profile and histologic analysis are encouraging. More detailed dose-dependent studies and in vivo immune response in mice without tumors will be performed in future studies.

5. Chapter 5: Optimization for large-scale synthesis of nanoconstructs: reproducibility and scalability

One of the caveats regarding clinical application of nanoparticles is the feasibility for reproducibly scaling up development. This chapter describes the protocol for scale-up synthesis and the resultant materials. In preparation for scale-up synthesis, which can be cost-prohibitive, the regular-scale synthesis of nanoconstructs was first optimized to minimize the amount of excess reagents previously used in the initial proof-of-concept studies. This is to lower the cost of the synthesis. The synthesis was then scaled up by proportionally increasing the volume of reagents while maintaining same concentrations, temperature, and mixing speed. The scaled-up materials were compared with regular-scale materials in terms of size, charge, composition, and efficacy in delivering siRNA. In addition, different batches of synthesized nanoconstructs were compared and evaluated for reproducibility of the scale-up process.

5.1 Materials and Methods

5.1.1 Large-scale synthesis of nanoconstructs

“S-47” MSNPs were synthesized in a similar manner to section 2.1.2 for the standard small-scale (125 mL) synthesis. For the large-scale (2.5 L) synthesis, all reagents were increased by 20 times. CTAC (0.15 M) and TEA (7 mL) were mixed in water (2.5 L) at 95 °C. Then, TEOS (60 mL) was added and the mixture was stirred for one hour. Afterwards, the pellets were recovered from

suspension by centrifugation, washed with a copious amount of ethanol, and dried overnight. The particles were then re-suspended and refluxed in acidic methanol (HCl (0.6 M) in methanol) overnight to remove CTAC and TEA. Bare MSNPs were then washed with ethanol and dried in a desiccator.

Likewise, for 100-mg synthesis of nanoconstructs (T-NP^{10C}), the layer-by-layer modification was performed by scaling up all of the reagents used in 10-mg synthesis (section 2.1.2) by 10 times. The exception is discussed in section 5.2.1 where the excess amount of unreacted reagents is minimized

5.1.2 Characterization of nanoconstructs

Nanoconstructs were characterized for primary/dry size with TEM (Phillips/FEI CM120/Biotwin TEM) and hydrodynamic size with Zetasizer (ZS-90/Malvern). The composition of nanoconstructs, including silica yield, PEG, PEI, antibody, and siRNA loadings per silica, was measured in the same manner as described in section 2.1.3.

5.1.3 Efficacy evaluation of nanoconstructs

Multiple batches of nanoconstructs (T-siRNA-NP^{10C}) were evaluated for their ability to effectively deliver siRNAs in two systems. T-siLUC-NP^{10C} was tested for the ability to knock down luciferase gene, as described in section 3.1.3. Further, T-siHER2-NP^{10C} was tested for efficacy upon delivery of siHER2 by monitoring cell death in the HER2⁺ cell line, BT474, as described in section 3.1.5.

5.2 Results and Discussion

5.2.1 Optimizing synthesis condition for scale-up synthesis

The material synthesis for proof-of-concept studies has been performed by using a considerable amount of PEG and trastuzumab. However, for large-scale synthesis, this is cost-prohibitive. This section reviews the strategy to minimize the excess amount of reagents used.

PEG attachment

The Mal-PEG-NHS is used to attach PEG on the nanoparticles (via the NHS group) and provides a site for antibody conjugation (via the Mal group). The original version required 5-fold by weight of Mal-PEG-NHS per MSNPs. The Mal-PEG-NHS costs \$500 per gram. To reduce costs, I optimized the process to limit the spontaneous hydrolysis of the NHS ester groups on PEG. This was done by two approaches: (1) adding PEG to the nanoconstruct suspension directly under well-mixed conditions or (2) dissolving PEG in solvents such as DMF instead of PBS. Both limit hydrolysis of the NHS in aqueous solution and thus enhance its reaction capacity. The reaction time also decreased from overnight to two hours.

The amount of PEG required was reduced by 5-fold (from 5:1 weight ratio of PEG per MSNP to 1:1 weight ratio) while maintaining similar PEG loading. More importantly, it was still able to protect the nanoconstructs from aggregation upon binding with siRNA. The DMF method had approximately 70% of the yield compared with the original approach, while adding PEG directly to the suspension preserved the high yield without the concern of DMF toxicity. Therefore, adding PEG (as powder) directly to the suspension was the preferred

method for subsequent synthesis. With this new method and 5-fold less PEG used, the PEG content reduced from 18% to 15% by weight, but this did not affect the properties of the nanoconstructs. **Figure 5.1** confirms that the nanoconstructs did not aggregate upon siRNA loading (see section 2.2.7, **Figure 2.9**). Also, the nanoconstructs still protected siHER2 (**Figure 5.2**) effectively in the same manner as the original version of nanoconstructs (**Figure 2.8**).

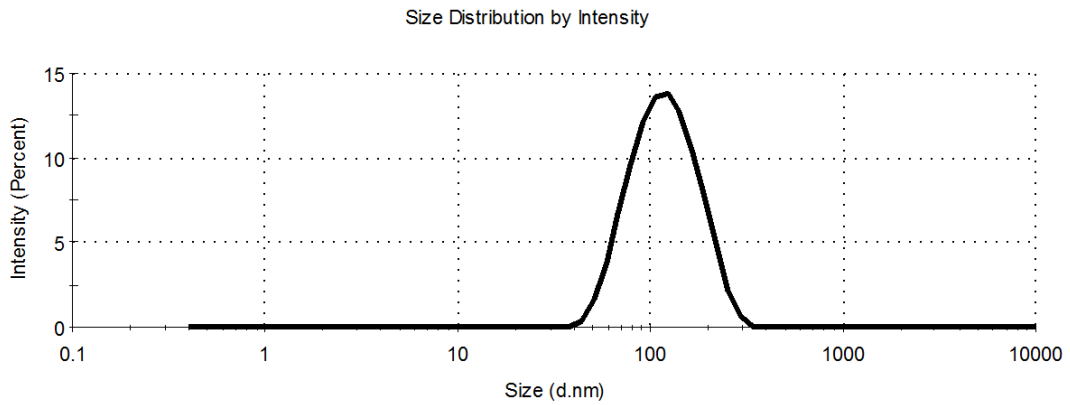


Figure 5.1: Hydrodynamic size distribution of T-siHER2-NP^{10C} synthesized by a newly optimized method.

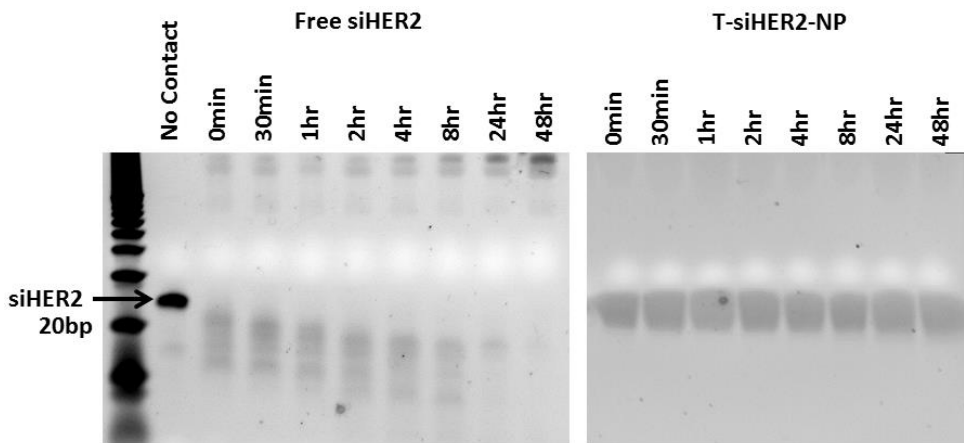


Figure 5.2: Stability of free siHER2 and siHER2 on T-NP (called T-siHER2-NP^{10C}) in human serum. Free siHER2 was degraded over time as shown by the reduction of size on the gel (band moving toward the bottom of gel), while siHER2 on T-siHER2-NP remained stable at the expected size of ~20 bp.

Antibody loading

Due to the high cost of trastuzumab (3,340 USD/440 mg), I also optimized the trastuzumab loading conditions to minimize the amount of trastuzumab required while maintaining acceptable efficacy criteria. **Figure 5.3** shows the efficacy in BT474 after being treated with siHER2 delivered by different nanoconstructs that were prepared by varying the weight ratio of milligrams of trastuzumab per milligrams of MSNP in the loading solution. Good silencing efficacy was achieved even when reducing the amount of trastuzumab by 10-fold of the original materials. The optimal material required only 10:1 (by weight) of mg MSNP per mg of trastuzumab in the loading step. This translates to 3% trastuzumab loading on nanoconstructs vs. 6% trastuzumab loading of the original material.

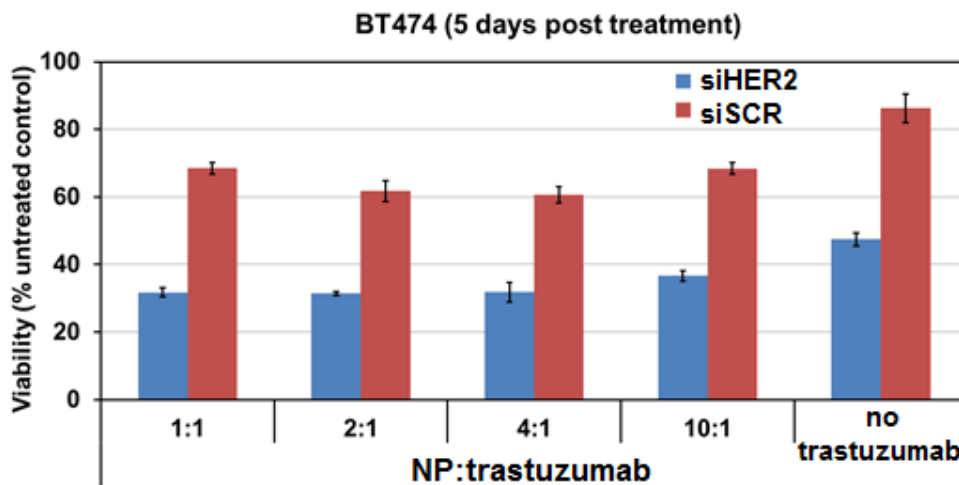


Figure 5.3: Impact of trastuzumab loading on efficacy of nanoconstructs. BT474 (HER2⁺) cells were treated with various nanoconstructs prepared by varying the weight ratio of the MSNPs over trastuzumab in the loading solution.

I further substantiated this finding with the cellular uptake by flow cytometry, performed in the same manner as described in **section 3.2.2**. siRNA-nanoconstructs containing 3% trastuzumab appear to be the most optimal, having the same degree of cellular uptake as the nanoconstructs containing higher amounts (e.g., 4%) of trastuzumab (**Figure 5.4**).

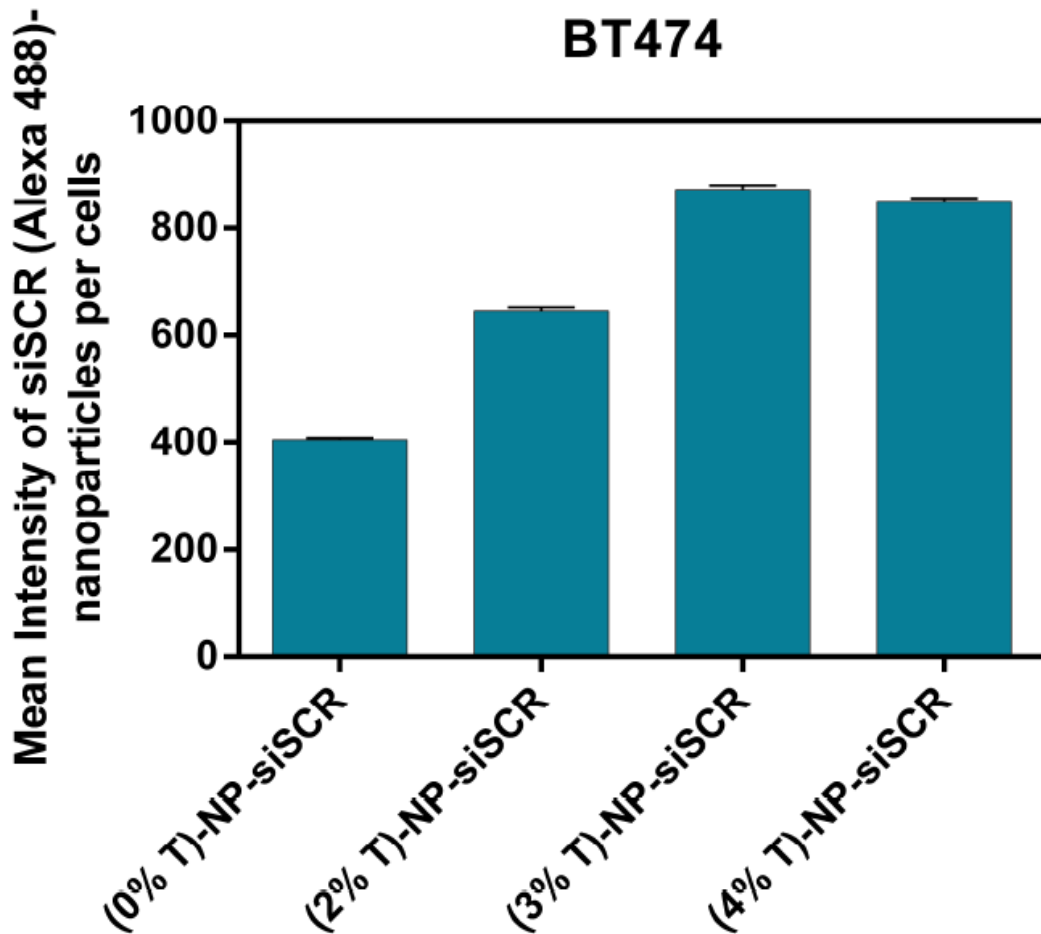


Figure 5.4: Effect of trastuzumab (T) loading on cellular uptake of siRNA-nanoconstructs. Data are reported as mean intensity (per cell) of Alexa 488-tagged scrambled siRNA (siSCR)-nanoparticles (NP^{10C}), and conjugated with varied percentage of trastuzumab (T).

The new method of material synthesis still yields similar nanoconstruct composition to the original method. The size profile and efficacy of nanoconstructs are also shown to be identical to those of nanoconstructs synthesized by the original method, as discussed later in section 5.2.3. Altogether, this optimization results in approximately \$5,000 in savings per gram of nanoconstruct (i.e., around \$3000 for trastuzumab and \$2,000 for Mal-PEG-NHS).

5.2.2 Reproducibility and scalability of mesoporous silica nanoparticle synthesis

As mentioned previously, nanoparticles are notorious for having issues with reproducibility and scalability. The sol-gel synthesis utilized for MSNPs offers a straightforward approach for scale-up production. The MSNP production was scaled up by increasing by 20 times the amounts of the typical required synthesis reagents, with no other modifications. **Figure 5.5** illustrates the synthesis set-up for the 125-mL scale and the 2.5-L scaled-up version, which yielded MSNPs of 300 mg and 6000 mg, respectively. Both versions of materials also had identical size profiles (**Figure 5.6**). In particular, the MSNP sizes in water (hydrodynamic size) at the end of synthesis for 125-mL scale and 2.5-L scale were 60.31 and 60.41 nm, respectively. TEM showed the same morphology for both MSNPs and the same average size, 45 nm. Hydrodynamic size is usually larger than TEM primary (dry) size due to the hydrated layer on nanoparticles when in solution.

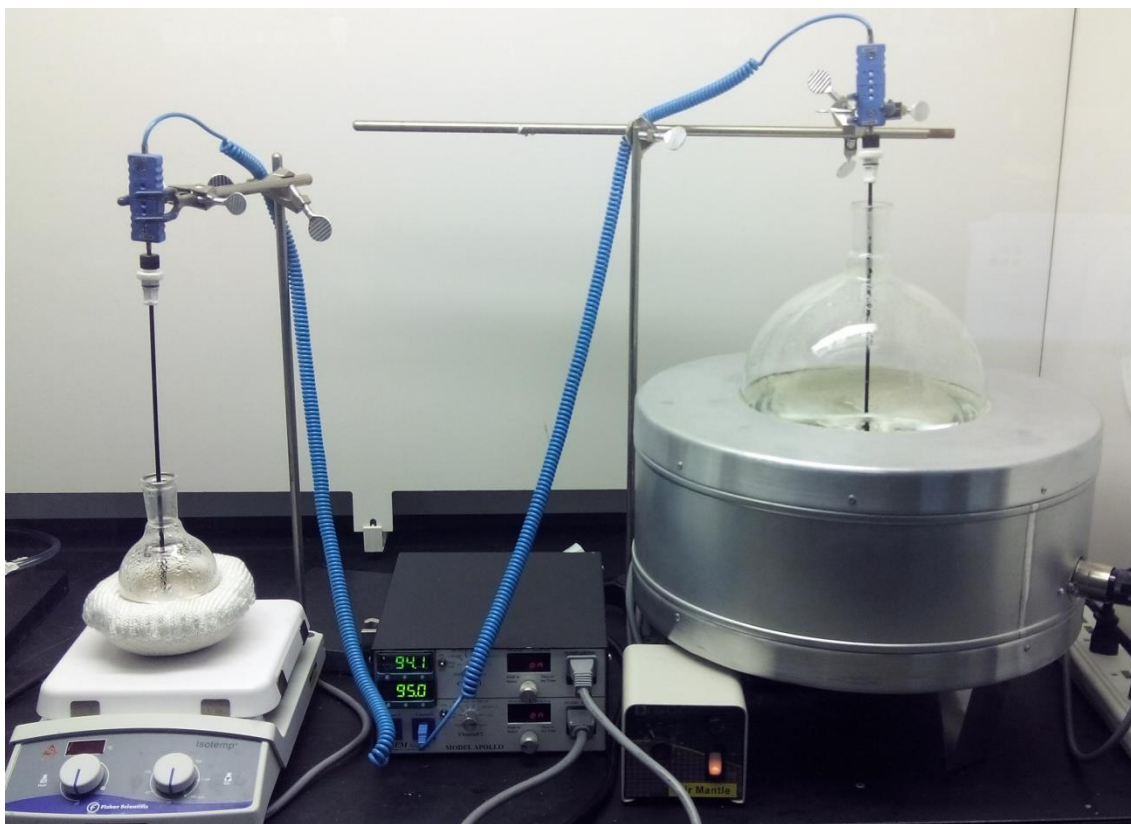


Figure 5.5: Mesoporous silica nanoparticle sol-gel synthesis. Regular scale synthesis (125-mL scale, left), scaled-up synthesis (2.5-L scale, right).

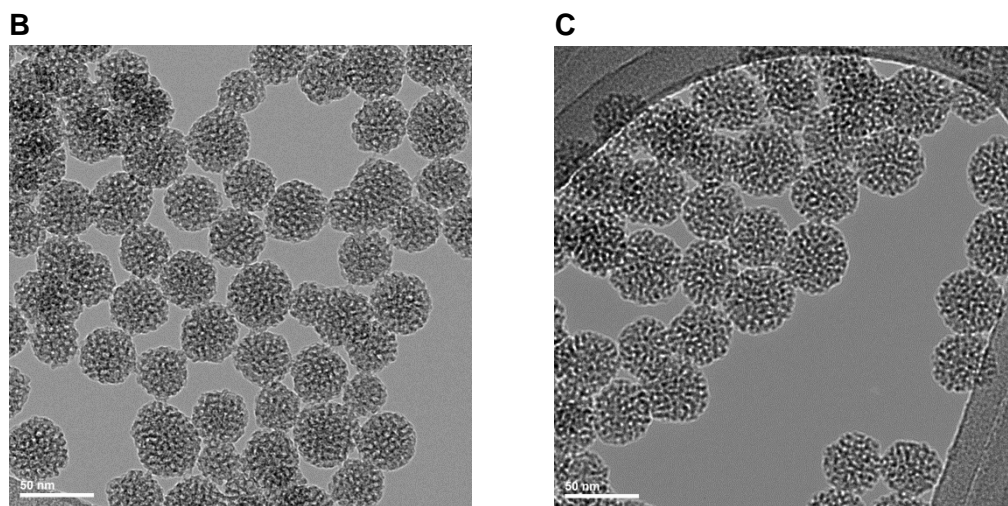
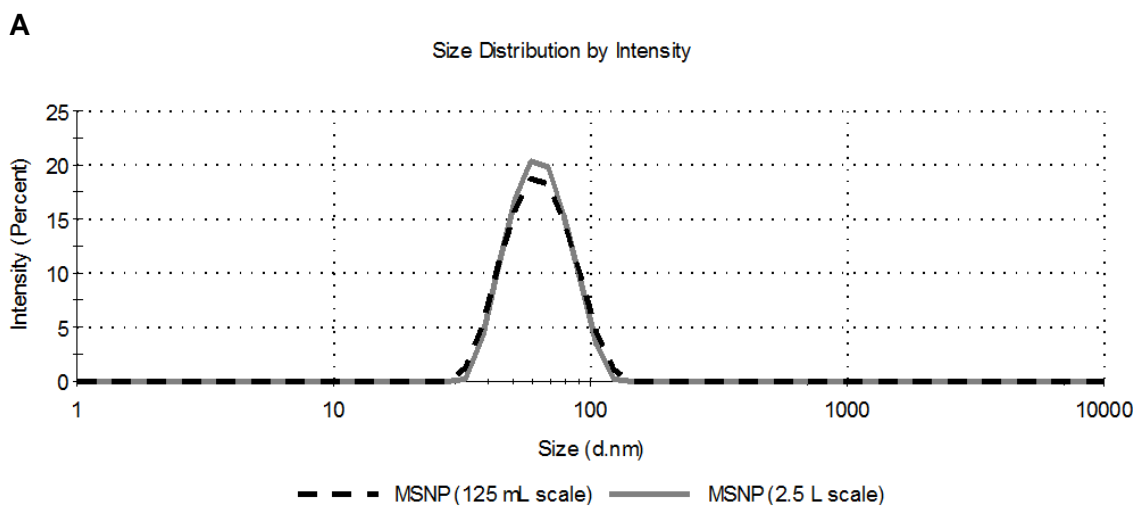


Figure 5.6: Size profile of mesoporous silica nanoparticles synthesized by 125-mL scale vs. 2.5-L scale. (A) hydrodynamic size of MSNPs. Both scales yielded nanoparticles with hydrodynamic size of 60 nm, PDI 0.06. **(B)** TEM images of MSNPs synthesized at 125-mL scale. **(C)** TEM images of MSNPs synthesized at 2.5-L scale.

5.2.3 Reproducibility and scalability of nanoconstruct synthesis (polymer coatings)

Batch-to-batch reproducibility is challenging to achieve when there are multiple components in the nanoconstruct, especially in a one-pot synthesis approach. Herein, layer-by-layer surface modification afforded scalability and reproducibility. It also facilitated impurity removal by washing after each of the loading steps.

The in vitro scale nanoconstruct synthesis yielded 5-10 mg per batch. Requirements for rodent animal studies necessitated a large-scale production of 60-100 mg batches (for 16 mice and 4 doses each). Size and silencing efficacy of 4 batches of materials are summarized in **Table 5.1** in comparison with the small batch (“Batch S”). I evaluated the efficacy of nanoconstructs by two analyses: first, the efficacy of luciferase gene silencing of T-siLUC-NP^{10C} using LUC-expressing cells (231-H2N-Luc) and second, cell viability of HER2⁺ cells (BT474) upon knocking down HER2 with T-siHER2-NP^{10C}. Cells were treated with T-siRNA-NP^{10C} for 24 h prior to media change. Luciferase activity and protein concentration were analyzed at 48 h post-treatment, while cell viability was measured at 5 days post-treatment. The cell viability was reported as a percentage of cell viability of the scrambled siRNA counterpart (T-siSCR-NP^{10C}) and the untreated control. Trastuzumab loaded on nanoconstructs also imparted therapeutic effects, explaining the reduction in cell viability with nanoconstructs loaded with siSCR (as previously described in Chapter 3). For the luciferase

silencing studies, 30 nM of siLUC was used, whereas 60 nM of siHER2 was used in the cell viability studies.

Table 5.1: Size profile and the siRNA delivery efficacy of four larger batches (60-100 mg, Batches 1-4) of nanoconstructs T-NP^{10C} vs. those of a small batch (10 mg, Batch S)

Materials	Hydrodynamic size by DLS (in PBS) (nm)	% Luc silencing efficacy (vs. siSCR) 231-H2N-Luc	% Cell viability (vs. siSCR) BT474	% Cell viability (vs. untreat) BT474
Batch 1	117 ± 0.5	80.5 ± 2.8	52.5 ± 2.7	82.1 ± 1.0
Batch 2	115 ± 7.1	76.1 ± 2.4	52.5 ± 2.9	72.8 ± 1.1
Batch 3	116 ± 4.0	75.6 ± 3.9	55.6 ± 2.0	71.7 ± 1.1
Batch 4	117 ± 4.0	81.9 ± 1.8	49.0 ± 2.6	79.0 ± 0.3
Average	116	78	52	76
S.D.	1.0	3.2	2.7	5.0
% RSD	0.8	4.0	5.2	6.5
<i>Batch S</i>	<i>117 ± 0.5</i>	<i>76.0 ± 7.8</i>	<i>52.2 ± 3.4</i>	<i>79.6 ± 1.0</i>

5.3 Conclusions

I found that it was possible to minimize the amount of starting reagents to lower the cost of the scale-up synthesis while still preserving material properties and performance. Both mesoporous silica nanoparticle synthesis (sol-gel synthesis) and surface modification (layer-by-layer coating) were scalable and reproducible. The size profiles and efficacy of nanoconstructs synthesized on different days displayed high reproducibility. Likewise, nanoconstructs synthesized from large-scale (2.5 L) synthesis behaved similarly to those synthesized from smaller-scale (125 mL) synthesis. To date, the largest yields obtained from mesoporous silica nanoparticles and subsequent surface-

functionalized nanoconstructs are 6000 mg and 300 mg, respectively. 300 mg nanoconstructs are sufficient for ~240 mouse doses. I fully anticipate that the nanoconstruct can be scaled up further as necessary because no major modifications were made to the current synthesis protocol besides proportionally scaling up the amount of reagents used, suggesting that large-scale manufacturing of this material is feasible.

6. Chapter 6: Other potential cargos (different oligonucleotides and chemotherapeutics)

In some refractory HER2⁺ breast cancers, HER2 knockdown might not be sufficient to achieve satisfactory therapeutic response. A parallel effort in our lab has confirmed that cancers engineered to acquire resistance to current HER2-targeted therapies (trastuzumab and lapatinib) by long-term in vitro treatment with such compounds still respond effectively to siHER2 (data not shown). But tumors in patients can be very heterogeneous, and therefore cancer cells will likely not rely on HER2 the same way across the cell population. I postulated that this could be one reason we could not eradicate tumors completely with the current formulation in the highly heterogeneous HCC1954 refractory tumors (T-siHER2-NP^{10C}, **Figure 3.8**). In such cases, alternative gene targets would be a more feasible approach. In light of this, I loaded different oligonucleotides (siRNAs and miRNAs) and chemotherapeutic drugs on nanoconstructs and evaluated their efficacy in killing cells in a small panel of cell lines. Trastuzumab-nanoconstructs were used to deliver these cargos to refractory HER2⁺ cells in a targeted manner. This chapter provides proof of concept for the versatility of the developed nanoconstruct.

Two oligonucleotides were tested in place of siHER2. The first was siPLK1 (siRNA against polo-like kinase 1 (PLK1) mRNA) [125]. PLK1 is a key protein in promoting proliferation in cells and is overexpressed in many cancer types [237,

238]. BI-2536 was the first PLK1 inhibitor to enter clinical trials [239]. As it is a potent anti-mitotic agent, mechanism-related side effects occurred in cells with high proliferation rates such as hematopoietic precursor cells. Consequently, dose-limiting toxicities were grade 4 thrombocytopenia (low count of platelets) and neutropenia (low count of neutrophils) [240]. I hypothesized that targeted delivery of siPLK1 with nanoconstructs would provide a more effective treatment, while limiting the toxicity commonly associated with PLK1 inhibitors.

The other oligonucleotide was miR-342-5p, an miRNA mimic that is downregulated in HER2⁺ breast cancer [241]. Leivonen et al. screened 810 human miRNAs and identified miR-342-5p as one of the most effective inhibitors of HER2 signaling and cell growth [241]. The MicMa and METABRIC databases also show that low levels of miR-342-5p correlate with poorer survival rates. These findings suggest it functions as a tumor suppressor. miR-342-5p is predicted to target EGFR, AKT2, CAMK and protein kinase C isoforms. Further, it was reported that miR-342-5p specifically inhibited HER2⁺ cell growth (JIMT-1 and KPL-4) and had no effect on HER2⁻ cells (MCF-7) [241].

The current first-line treatment for HER2⁺ metastatic breast cancer is a combination of trastuzumab and taxanes (paclitaxel or docetaxel) (see Chapter 1), supporting the idea of delivering HER2-targeted agents and paclitaxel simultaneously. As the developed nanoconstructs are capable of loading additional cargos, I loaded paclitaxel on the T-siHER2-NP^{10C}. I predicted that the simultaneous delivery of paclitaxel and trastuzumab to cells would enhance the collective therapeutic effects on HER2⁺ breast cancer. I also predicted that the

enhanced tumor targetability of nanoconstructs would decrease the side effects of paclitaxel in humans.

6.1 Materials and Methods

6.1.1 Materials

Paclitaxel (research grade) was obtained from LC Laboratories (MA). siPLK1 and miR-342-5p were obtained from GE Dharmacon (CO).

6.1.2 Loading additional cargos on the nanoconstruct

Paclitaxel was loaded during the PEI cross-linking step of the nanoconstruct (see section 2.1.2). Paclitaxel (3 mg) was dissolved in ethanol and loaded on the nanoconstruct (10 mg) for 40 minutes (the same duration as a PEI cross-linking step). The final volume of the mixture was 1 mL. siPLK1 and miR-342-5p were loaded in the exact same manner as siHER2 (see section 2.1.2).

6.1.3 Quantification of drug loading on the nanoconstruct

Nanoconstructs were first dissolved in 0.05 M KOH so that paclitaxel was released in the solution. Then the solution was diluted two times with acetonitrile. The paclitaxel concentration was determined by HPLC (Agilent 1260, Agilent Technologies (CA)) following the manufacturer's published application note [242].

6.1.4 Efficacy evaluation

Testing the efficacy of nanoconstructs in eliciting cell death was performed in the same manner as in section 3.1.5. Nanoconstructs were also tested for their ability to knock down the luciferase gene, as described in section 3.1.3.

6.2 Results and discussion

6.2.1 Delivery of other oligonucleotides

I treated HCC1954 (HER2⁺) and MCF-10a (HER2⁻, non-tumorigenic) with siPLK1 or miR-342-5p, delivered by DharmaFECT (**Figure 6.1A**) or T-NP^{10C} (**Figure 6.1B**). The siRNA dose was fixed at 30 nM. It should be noted that the efficacious dose of siHER2 (i.e., a dose that elicits at least 50% reduction in cell viability) on nanoconstructs is 60 nM. I measured cell viability at 5 days post-treatment. Both siPLK1 and miR-342-5p outperformed siHER2, as 30 nM is sufficient to elicit cell death. By contrast, I found that while miR-342-5p (delivered with DharmaFECT) appeared to affect the cell growth of HCC1954 (HER2⁺) as expected, it also affected the cell growth of MCF-10a (HER2⁻, non-tumorigenic) (**Figure 6.1A**). Knocking down PLK1 also affected non-tumorigenic cells (**Figure 6.1A**). This was expected, as PLK1 is one of the key regulators of cell division.

When these oligonucleotides were delivered with the HER2-targeted nanoconstructs (T-NP^{10C}), treatment specificity was achieved (**Figure 6.1B**). The treatment affected the viability of HER2⁺ cells (HCC1954) while sparing HER2⁻ non-tumorigenic breast cells (MCF-10a). This was owing to the limited uptake of the nanoconstruct (with HER2-antibody as targeting agent) to the non-HER2-amplified cells.

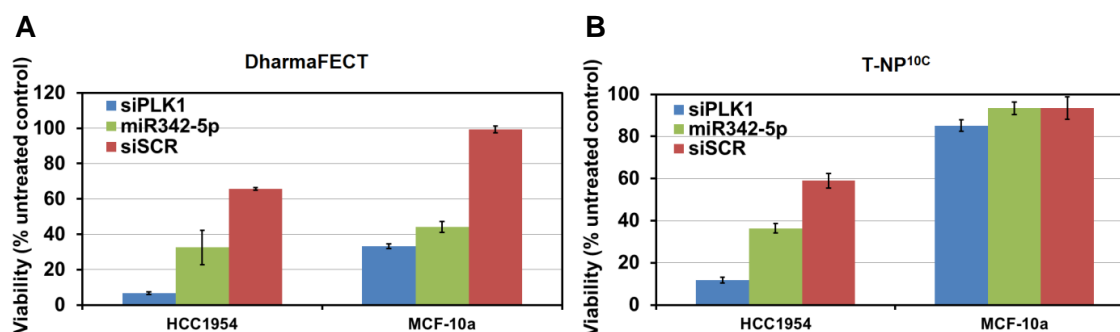


Figure 6.1: Delivery of other oligonucleotides to cells. Cell viability of HCC1954 and MCF-10a at 5 days post-treatment with oligonucleotides delivered with **(A)** DharmaFECT, and **(B)** T-NP^{10C} (with overnight media change). Nanoconstruct dose is 21 $\mu\text{g}/\text{ml}$. Oligonucleotide dose is 30 nM.

6.2.2 Co-delivery of paclitaxel and siHER2 to HER2⁺ breast cancer

I loaded nanoconstructs with paclitaxel at 4 wt.% and siRNA at 2 wt.% (i.e., NP/siRNA 50). JIMT-1 cells were treated with nanoconstructs (21 $\mu\text{g}/\text{mL}$) at an equivalent paclitaxel dose of 0.84 $\mu\text{g}/\text{mL}$ and siRNA dose of 30 nM. JIMT-1 was selected for the study since it was previously shown to be resistant to trastuzumab [37]. Nanoconstructs loaded with trastuzumab or paclitaxel showed some efficacy (~40% reduction in viability) in JIMT-1 (**Figure 6.2**). Upon co-delivery of trastuzumab and paclitaxel, nanoconstructs showed remarkably enhanced cytotoxic effects in JIMT-1 (~80% reduction in viability), such that the effect of further incorporation of siHER2 (~85% reduction in viability) is not apparent.

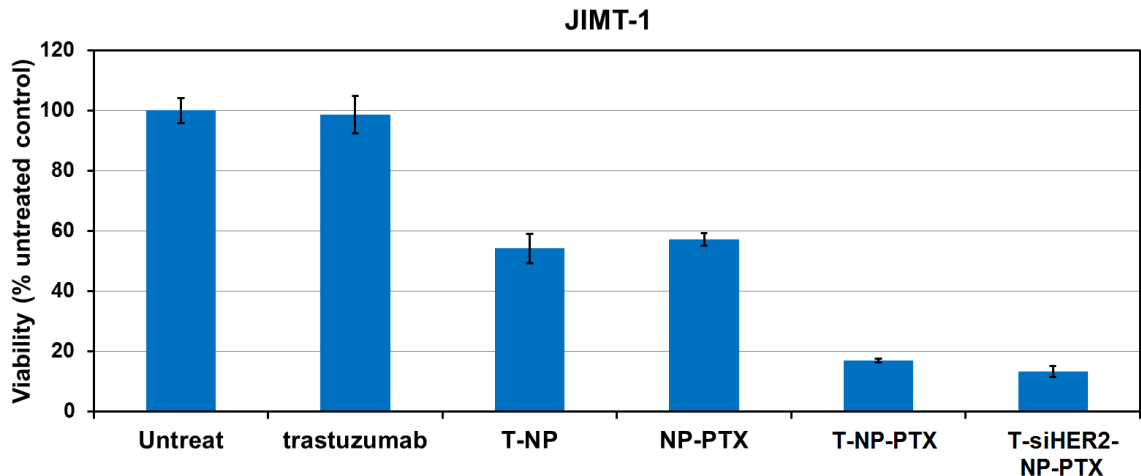


Figure 6.2: Co-delivery of paclitaxel and siRNA to JIMT-1. Cell viability after treatment with trastuzumab, nanoconstructs loaded with trastuzumab (T-NP) or paclitaxel (NP-PTX), nanoconstructs loaded with both trastuzumab and paclitaxel (T-NP-PTX), and nanoconstructs loaded with trastuzumab, paclitaxel and siHER2 (T-siHER2-NP-PTX). The trastuzumab dose is 30 $\mu\text{g/ml}$. The nanoconstruct dose is 21 $\mu\text{g/ml}$. SiRNA dose is 30 nM. Viability was measured 5 days post-treatment (with overnight media change).

The effect of siRNAs was not apparent in terms of cell viability (**Figure 6.2**), so I tested whether this paclitaxel-loaded nanoconstruct could still deliver siRNAs and elicit gene knockdown effectively. This was performed by evaluating luciferase gene knockdown upon treatment with the siLUC delivered with nanoconstructs (with or without paclitaxel). The paclitaxel-loaded nanoconstructs (T-NP-PTX) delivered siLUC and knocked down luciferase gene expression effectively, similar to nanoconstructs without paclitaxel (**Figure 6.3**). In other words, loading paclitaxel on the nanoconstruct did not affect its ability to deliver siRNA. It is worth noting that luciferase knockdown was monitored at 48 h post-treatment, at which point not all cells had died (unlike in **Figure 6.2**). It was thus still possible to capture the knockdown events by siRNA.

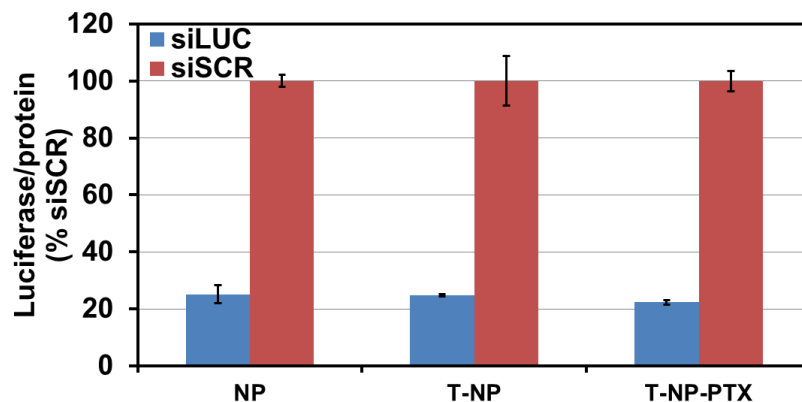


Figure 6.3: Luciferase silencing efficacy of nanoconstructs. Silencing of luciferase expression in MDA-MB-231-H2N-luc (high HER2, high luciferase) upon treatment with siLUC on nanoconstruct at NP/siRNA 50. The nanoconstruct dose is 21 $\mu\text{g/ml}$. SiRNA dose is 30 nM. Luciferase expression was measured 48 h post-transfection (with overnight media change).

6.3 Conclusions

This chapter covers the proof-of-concept studies showing that nanoconstructs can be loaded with additional cargos beyond siHER2, including other nucleotides and chemotherapeutic drugs--specifically in this case miR-342-5p and siPLK1. Whether this effect can be translated to an in vivo application requires additional studies. I also successfully loaded paclitaxel on the siHER2-nanoconstructs (T-siHER2-NP-PTX). The effects of paclitaxel outweighed the effects of siRNA in eliciting cell death in HER2⁺ breast cancer cells. Thus, siRNA did not appear to provide additional advantages. But luciferase gene knockdown confirmed that T-NP-PTX is still capable of delivering siRNAs and causing gene knockdown. Luciferase gene knockdown was performed at a short time point (48

h), so some cells were still alive and the knockdown events could be captured. This could be beneficial in an in vivo setting, where delivering chemotherapeutic drugs alone might not be sufficient in eradicating tumors. Co-delivery of siRNAs and paclitaxel will be tested in an animal model in due course.

This chapter also shows that the nanoconstruct has good versatility, especially in a personalized medicine setting, where different targeted genes can be identified and respective appropriate oligonucleotides can be determined for individual patients upon diagnosis. Oligonucleotides are loaded last on the nanoconstruct by 30-minute mixing, which vastly simplifies this personalized mode of application.

7. Chapter 7: Summary, conclusions, and future directions.

7.1 Summary

Chapter 1 reviewed the biology of HER2 protein and its importance in HER2⁺ breast cancer. Current treatment options for HER2⁺ metastatic breast cancer were described. HER2⁺ breast cancer has benefited significantly from the advent of HER2-targeted therapies. Trastuzumab is a monoclonal antibody against HER2 protein and serves as a prime example for targeted therapy. Pertuzumab is another monoclonal antibody that binds to HER2 extracellular domain but at a different site than trastuzumab. The combination of pertuzumab and trastuzumab appears to improve patient outcomes due to the more complete blockade of HER2 pathways. Consequently, the current first-line treatment is a combination of taxanes, trastuzumab, and pertuzumab. In spite of these improvements, however, patients receiving these HER2-targeted therapies tend to eventually develop resistance. Other HER2-targeted agents, including T-DM1, lapatinib, and neratinib, have been developed to address this shortfall, but none have replaced the current first-line treatment as of yet. In addition, strategies targeting alternative pathways other than HER2 are under investigation, and several are ongoing in clinical trials.

Non-coding oligonucleotides have garnered extensive interest as new candidates for targeted therapies to replace conventional small molecule inhibitors and monoclonal antibodies. These conventional compounds can target

only accessible (so-called druggable) targets, while oligonucleotides can interfere with the expression of any gene in cells. This creates possibilities to hit those “undruggable” targets that may be key players in cancer function and culprits in drug resistance. Among these oligonucleotides, small-interfering RNA (siRNA) is frequently utilized for gene silencing due to its robust and well-established mechanism of RNA interference. However, the hurdle of translating this technology to cancer treatment lies in the development of an effective delivery system. Naked siRNAs are readily cleared and not bioavailable upon systemic administration, and thus inefficient at reaching cells within the target organ.

Nanoparticle platforms have been researched to address this challenge. In chapter 1, several classes of nanoparticles under development for siRNA development were described. To date, there are no siRNA-therapeutics on the market. The first nanoparticle-based siRNA therapeutic to reach a cancer clinical trial was the cyclodextrin polymeric nanoparticles. However, their development was halted at Phase I. Other siRNA therapeutics that advanced to clinical trials are mainly lipid-based, but the applications are confined primarily to liver cancer or other cancers with liver involvement because they are naturally deposited in this organ. Targeted delivery of siRNAs to other solid tumor remains an unmet need.

In this dissertation project, I developed a functional nanoconstruct for siRNA delivery. This nanoconstruct is a hybrid of polymer and mesoporous silica nanoparticles (MSNPs). This strategy exploits both the chemical functionalities of polymers and the defined and controllable structure of MSNPs.

Chapter 2 discussed the design, synthesis, and characterization of the nanoconstructs. The nanoconstruct consists of a rigid MSNP functionalized with PEI, PEG, HER2-targeted antibody (trastuzumab), and siRNA. **MSNPs** with different sizes were synthesized and screened for the best size profile after coating with all of the components. MSNP was selected because of its low toxicity, large surface area, and ease of controlling synthesis. **PEI** is a functional polymer for siRNA delivery. It functions by loading negatively charged siRNAs and triggering siRNA endosomal escape by the proton sponge effect. **Cross-linking** was performed on PEI to increase the number of secondary and tertiary amines and, in turn, increase the buffering capacity. PEG was used as a stabilizer to protect siRNAs from nuclease degradation and enhance blood compatibility. **PEG** also helps to avoid nanoparticle aggregation, non-specific protein binding, and adverse immune responses. These properties help prolong the blood circulation of the nanoconstructs. **Trastuzumab** serves as a targeting antibody for HER2-overexpressed cancer cells. **SiRNAs** were loaded last via electrostatic interactions with the PEI layer.

Multiple iterations of the nanoconstructs were optimized for size and charge. I characterized the composition of the nanoconstructs by thermogravimetric analysis to quantify polymer coating, BCA analysis to quantify trastuzumab loading, and fluorescence detection to confirm siRNA loading. The 47-nm mesoporous silica nanoparticle (S-47) modified with cross-linked 10-kDa PEI, 5-kDa PEG, and trastuzumab (T-NP^{10C}) appears to have the best size

profile and best efficacy (shown in Chapter 3). S-47 MSNP core was thus used in the rest of the chapter and dissertation.

Chapter 2 also detailed cross-linking on the PEI layer to increase the buffering capacity of lower-molecular-weight PEI, since low-MW PEI is known to have a better safety profile. Also, T-NP^{10C} appears to protect siRNAs from serum enzyme degradation. The amount of intact siRNAs on T-NP^{10C} was fully protected (0% degradation) for at least 24 hours, while naked siRNAs degraded by 50% in less than an hour. Lastly, the function of the PEG layer was illustrated. Without PEG, nanoconstructs aggregated upon siRNA loading and failed to protect siRNAs from serum enzyme degradation.

Chapter 3 described the in vitro and in vivo efficacy evaluation of the siRNA-nanoconstructs. I screened a library of nanoconstructs for the ability to deliver siLUC (siRNA against luciferase mRNA) and knock down luciferase expression. The trend was in agreement with the buffering capacity data described in Chapter 2. The nanoconstructs also showed high preferential uptake to HER2⁺ cells, compared with HER2⁻ cells. Alternatively, replacing trastuzumab with a negative control antibody (CD20) significantly reduced cell uptake in these same cell lines. T-NP^{10C}, based on S-47 core, appeared to work best in all tests and was thus used in the rest of the dissertation, unless otherwise specified.

T-NP^{10C} also showed significant HER2 knockdown activity (i.e. over 80% reduction vs. scrambled siRNA counterpart) in three HER2⁺ cell lines tested following siHER2 (siRNA against HER2 mRNA) delivery. Also, this knockdown

induced apoptotic events (measured by cleaved caspase-3) and overall cell death. Cell viability across cell lines showed that the treatment (T-siHER2-NP^{10C}) can elicit cell death in HER2⁺ cells while sparing HER2⁻ cells. This treatment, despite also targeting HER2 pathway, was found to decrease the viability of HER2⁺ breast cancer that is resistant to trastuzumab (a current gold-standard HER2-targeted therapy). This suggests that inhibiting production of HER2 at the mRNA level can provide a more effective treatment than merely inhibiting the function of HER2 protein by conventional monoclonal antibody. More importantly, the in vitro efficacy translated well to in vivo efficacy in a mouse model of orthotopic HER2⁺ breast cancer (HCC1954, which is considered multiple-drug resistant). Systemic administration of T-siHER2-NP^{10C} was shown to cause 60% HER2 protein knockdown in tumors after one dose (1.25 mg siRNA/kg) and resulted in significant tumor growth inhibition after five doses of T-siHER2-NP^{10C} (1.25 mg siRNA/kg).

Chapter 4 established the in vitro and in vivo safety and toxicity profile of the siRNA-nanoconstructs. The studies used for evaluation followed the guidelines and published protocols by the Nanotechnology Characterization Laboratory (NCL). T-siHER2-NP^{10C} neither causes cell death in non-targeted HER2⁻ cells nor induced ROS production. Blood compatibility was found to be favorable. Specifically, we found that nanoconstructs did not appear to cause hemolysis, affect coagulation time, or cause platelet aggregation. FDA-approved nanoparticle-based drugs (Abraxane and Feraheme) were used as benchmarks in these studies. Furthermore, we evaluated nanoconstructs for their potential to

trigger an immune response. This was performed with peripheral blood mononuclear cells (PBMCs) isolated from human blood. The cytokines evaluated included IL-1 β , IL-6, IFN- α , and TNF- α due to their association with Toll-like receptors on the surface of the cell membrane and within endosomes. Nanoconstructs did not increase the levels of IL-6 and TNF- α . While the nanoconstructs elevated the levels of IFN- α and IL-1 β , the observed increases were lower than the levels induced by Feraheme and Abraxane.

Lastly, serum from mice that underwent multiple injections in the efficacy study was analyzed for serum biochemistry profiles (including kidney and liver functions). Kidneys and livers were also harvested and stained with H&E. Gross morphology suggested no organ damage in the treatment groups. These findings provide evidence that multiple doses of T-siHER2-NP^{10C} did not damage the kidney or liver.

Chapter 5 describes the large-scale synthesis of the nanoconstructs. In this chapter, I optimized the synthesis to reduce the amount of two reagents (PEG and trastuzumab) used in the initial loading solution while maintaining the performance of the material. This is to reduce the cost of the synthesis (especially at large scale) and minimize the amount of remaining unreacted reagents after each synthesis. Specifically, this optimization saves around \$5000 for each synthesized gram of nanoconstruct. After the synthesis was optimized, the synthesis was scaled up by 20-fold. The yield is around 6000 mg, which is sufficient for approximately 17 human doses. This was achieved by merely scaling up all of the reagents proportionally. No other major modification was

made. This scaled-up material performed as effectively as the regular-scale material. Accordingly, the nanoconstruct synthesis is both reproducible and scalable.

Chapter 6 explored additional therapeutic targets to be delivered with or in place of siHER2. First, other oligonucleotides (siRNA and miRNA) were loaded on nanoconstructs in place of siHER2. siPLK1 (siRNA against PLK1 mRNA) on nanoconstructs elicited cell death in HER2⁺ cell lines, while sparing HER2⁻ non-tumorigenic cells, due to targeted delivery. The same observation was also found with miR-342-5p, which is of great interest considering that studies have correlated decreased expression with better patient survival.

Nanoconstructs could also be employed to deliver both paclitaxel and siHER2 simultaneously, mirroring a current first-line treatment of HER2⁺ metastatic breast cancer. In other words, anti-HER2 nanoconstructs function in place of trastuzumab and pertuzumab. Combining paclitaxel and siHER2 on the nanoconstruct may be a more effective approach, as the cargos will be delivered simultaneously to tumors in a targeted manner. Future in vivo studies are needed to confirm the feasibility of this development.

Taken together, these studies validate the remarkable versatility of the nanoconstructs, which can be used to load and deliver different types of oligonucleotides. This can be achieved because the loading of oligonucleotides on the nanoconstructs relies on electrostatic interaction; hence the loading

strategy is amenable to most classes of oligonucleotides and not dependent on their specific nucleotide sequences.

7.2 Conclusions and Future directions

In this dissertation project, I designed mesoporous silica-based nanoconstructs for targeted siRNA delivery to HER2⁺ breast cancer. Efficacy, safety, and toxicity studies with the nanoconstructs were performed and evaluated in vitro and in vivo. The lead nanoconstruct could deliver siRNAs and elicit gene knockdown in tumors. Furthermore, the synthesis of nanoconstructs was reproducible and scalable. This anti-HER2 construct may be a more effective method than current first-line treatments in patients because siHER2, which knocks down HER2 at the mRNA level, is more effective than HER2 antibodies, which merely block the activities but do not stop new HER2 production. Further, the current first-line treatment, which includes the combination of trastuzumab, pertuzumab and taxanes (docetaxel and paclitaxel), can be cost-prohibitive. Although docetaxel and paclitaxel are more affordable now (~\$10-20 per vial) because of their generic versions, trastuzumab and pertuzumab cost approximately \$3300 and \$4000 per dose, respectively. Considering that they are recommended as a combination treatment, the incurred cost equates to around \$7300 per each cycle (once every three weeks until diseases progress). Administration of anti-HER2 nanoconstructs as a single HER2-targeted therapy (with or without taxanes) should be a more effective and affordable strategy.

Furthermore, the developed nanoconstruct is a versatile platform, as it can be loaded with different types of cargos beyond siHER2, such as chemotherapeutic drugs and other oligonucleotides. Animal studies are planned to evaluate the delivery of these alternative cargos.

Although our treatment (T-siHER2-NP^{10C}) can deliver siRNAs to tumors and inhibit tumor growth, the tumors were not completely eradicated. To address this, ongoing efforts include (1) evaluation of alternative therapeutic targets, (2) understanding tumor heterogeneity in terms of cancer populations with different protein expression profiles and their siRNA response, (3) understanding the tumor microenvironment (e.g., degree of vascular leakiness and tumor stroma) that may affect siRNA response, and (4) evaluation of the combination therapy (e.g., siRNA cocktails, combinations of siRNAs and chemotherapeutic drugs) to achieve synergistic therapeutic effects. More extensive toxicity evaluations--such as acute and chronic toxicities, and the maximum tolerated dose from dose escalation studies-- will also be required to pursue IND-enabling studies of this platform.

Lastly, this developed nanoconstruct has the potential to be extended to other cancer types. The nanoconstruct can be conjugated with different targeting agents, such as monoclonal antibodies, single-chain variable fragments, aptamers, and targeting peptides. Also, this nanoconstruct can be loaded with a vast selection of cargos, such as drugs and oligonucleotides. Oligonucleotides are loaded last on the nanoconstruct by 30-minute mixing before administration, facilitating personalized therapy where important gene targets can be identified

upon diagnosis, and appropriate oligonucleotides can be prescribed accordingly. The nanoparticle platform can also be developed as a diagnostic probe. Specifically, fluorescent dyes or metal probes (e.g., lanthanides) can be loaded on the MSNP construct. Antibody-nanoconstructs can thus be used to stain the proteins of interest in tissue specimens or cells. The advantage of nanoconstructs over conventional probe-conjugated antibodies is the enhanced sensitivity: one nanoconstruct can be loaded with a large number of probes, which, in turn, gives a higher signal per antibody.

References

1. Croce, C.M., *Oncogenes and Cancer*. New England Journal of Medicine, 2008. **358**(5): p. 502-511.
2. Hanahan, D. and Robert A. Weinberg, *Hallmarks of Cancer: The Next Generation*. Cell, 2011. **144**(5): p. 646-674.
3. ACS, *Cancer Facts & Figures 2015*. 2015, American Cancer Society: Atlanta.
4. Siegel, R.L., K.D. Miller, and A. Jemal, *Cancer statistics, 2015*. CA: A Cancer Journal for Clinicians, 2015. **65**(1): p. 5-29.
5. Prat, A. and C.M. Perou, *Deconstructing the molecular portraits of breast cancer*. Molecular Oncology, 2011. **5**(1): p. 5-23.
6. *Comprehensive molecular portraits of human breast tumours*. Nature, 2012. **490**(7418): p. 61-70.
7. Parker, J.S., et al., *Supervised Risk Predictor of Breast Cancer Based on Intrinsic Subtypes*. Journal of Clinical Oncology, 2009. **27**(8): p. 1160-1167.
8. Prat, A., et al., *Phenotypic and molecular characterization of the claudin-low intrinsic subtype of breast cancer*. Breast Cancer Res, 2010. **12**(5): p. R68.
9. Nassar, A., et al., *Correlation of HER2 overexpression with gene amplification and its relation to chromosome 17 aneuploidy: a 5-year experience with invasive ductal and lobular carcinomas*. International Journal of Clinical and Experimental Pathology, 2014. **7**(9): p. 6254-6261.

10. Burstein, H.J., *The Distinctive Nature of HER2-Positive Breast Cancers*. New England Journal of Medicine, 2005. **353**(16): p. 1652-1654.
11. Rexer, B.N. and C.L. Arteaga, *Intrinsic and acquired resistance to HER2-targeted therapies in HER2 gene-amplified breast cancer: mechanisms and clinical implications*. Crit Rev Oncog, 2012. **17**(1): p. 1-16.
12. Alvarez, R.H., et al., *Handbook of HER2-Targeted Agents in Breast Cancer*. 2013, London, UK: Springer Healthcare Communications.
13. Spector, N.L. and K.L. Blackwell, *Understanding the Mechanisms Behind Trastuzumab Therapy for Human Epidermal Growth Factor Receptor 2-Positive Breast Cancer*. Journal of Clinical Oncology, 2009. **27**(34): p. 5838-5847.
14. Vu, T. and F.X. Claret, *Trastuzumab: updated mechanisms of action and resistance in breast cancer*. Front Oncol, 2012. **2**: p. 62.
15. Yarden, Y., *Biology of HER2 and Its Importance in Breast Cancer*. Oncology, 2001. **61**(suppl 2)(Suppl. 2): p. 1-13.
16. Tzahar, E., et al., *Bivalence of EGF-like ligands drives the ErbB signaling network*. Embo j, 1997. **16**(16): p. 4938-50.
17. Castiglioni, F., et al., *Role of exon-16-deleted HER2 in breast carcinomas*. Endocr Relat Cancer, 2006. **13**(1): p. 221-32.
18. Alajati, A., et al., *Mammary tumor formation and metastasis evoked by a HER2 splice variant*. Cancer Res, 2013. **73**(17): p. 5320-7.
19. Rubin, I. and Y. Yarden, *The basic biology of HER2*. Ann Oncol, 2001. **12** Suppl 1: p. S3-8.

20. Prat, A., et al., *Molecular features and survival outcomes of the intrinsic subtypes within HER2-positive breast cancer*. J Natl Cancer Inst, 2014. **106**(8).
21. Yarden, Y. and G. Pines, *The ERBB network: at last, cancer therapy meets systems biology*. Nat Rev Cancer, 2012. **12**(8): p. 553-563.
22. Gill, S. and D. Sargent, *End Points for Adjuvant Therapy Trials: Has the Time Come to Accept Disease-Free Survival as a Surrogate End Point for Overall Survival?* The Oncologist, 2006. **11**(6): p. 624-629.
23. Ahmed, S., A. Sami, and J. Xiang, *HER2-directed therapy: current treatment options for HER2-positive breast cancer*. Breast Cancer, 2015. **22**(2): p. 101-116.
24. Ewer, M.S., et al., *Reversibility of Trastuzumab-Related Cardiotoxicity: New Insights Based on Clinical Course and Response to Medical Treatment*. Journal of Clinical Oncology, 2005. **23**(31): p. 7820-7826.
25. Jones, A.L., et al., *Management of cardiac health in trastuzumab-treated patients with breast cancer: updated United Kingdom National Cancer Research Institute recommendations for monitoring*. Br J Cancer, 2009. **100**(5): p. 684-92.
26. Dubska, L., L. Andera, and M.A. Sheard, *HER2 signaling downregulation by trastuzumab and suppression of the PI3K/Akt pathway: an unexpected effect on TRAIL-induced apoptosis*. FEBS Lett, 2005. **579**(19): p. 4149-58.

27. Hynes, N.E. and J.H. Dey, *PI3K inhibition overcomes trastuzumab resistance: blockade of ErbB2/ErbB3 is not always enough*. *Cancer Cell*, 2009. **15**(5): p. 353-5.
28. Baselga, J., et al., *Mechanism of action of trastuzumab and scientific update*. *Semin Oncol*, 2001. **28**(5 Suppl 16): p. 4-11.
29. Esteva, F.J., et al., *PTEN, PIK3CA, p-AKT, and p-p70S6K status: association with trastuzumab response and survival in patients with HER2-positive metastatic breast cancer*. *Am J Pathol*, 2010. **177**(4): p. 1647-56.
30. Fornier, M.N., et al., *Serum HER2 extracellular domain in metastatic breast cancer patients treated with weekly trastuzumab and paclitaxel: association with HER2 status by immunohistochemistry and fluorescence in situ hybridization and with response rate*. *Annals of Oncology*, 2005. **16**(2): p. 234-239.
31. Zhou, J., et al., *Predictive value of serum HER2 ECD in patients with HER2-positive advanced gastric cancer treated with trastuzumab plus chemotherapy*. *J Gastroenterol*, 2015.
32. Petit, A.M., et al., *Neutralizing antibodies against epidermal growth factor and ErbB-2/neu receptor tyrosine kinases down-regulate vascular endothelial growth factor production by tumor cells in vitro and in vivo: angiogenic implications for signal transduction therapy of solid tumors*. *Am J Pathol*, 1997. **151**(6): p. 1523-30.

33. Lange, T., et al., *Trastuzumab has anti-metastatic and anti-angiogenic activity in a spontaneous metastasis xenograft model of esophageal adenocarcinoma*. *Cancer Lett*, 2011. **308**(1): p. 54-61.
34. Boone, J.J., et al., *Involvement of the HER2 pathway in repair of DNA damage produced by chemotherapeutic agents*. *Mol Cancer Ther*, 2009. **8**(11): p. 3015-23.
35. Valabrega, G., F. Montemurro, and M. Aglietta, *Trastuzumab: mechanism of action, resistance and future perspectives in HER2-overexpressing breast cancer*. *Ann Oncol*, 2007. **18**(6): p. 977-84.
36. Kute, T., et al., *Understanding key assay parameters that affect measurements of trastuzumab-mediated ADCC against Her2 positive breast cancer cells*. *Oncoimmunology*, 2012. **1**(6): p. 810-821.
37. Barok, M., et al., *Trastuzumab causes antibody-dependent cellular cytotoxicity-mediated growth inhibition of submacroscopic JIMT-1 breast cancer xenografts despite intrinsic drug resistance*. *Molecular Cancer Therapeutics*, 2007. **6**(7): p. 2065-2072.
38. Gennari, R., et al., *Pilot study of the mechanism of action of preoperative trastuzumab in patients with primary operable breast tumors overexpressing HER2*. *Clin Cancer Res*, 2004. **10**(17): p. 5650-5.
39. Musolino, A., et al., *Immunoglobulin G fragment C receptor polymorphisms and clinical efficacy of trastuzumab-based therapy in patients with HER-2/neu-positive metastatic breast cancer*. *J Clin Oncol*, 2008. **26**(11): p. 1789-96.

40. Vogel, C.L., et al., *Efficacy and safety of trastuzumab as a single agent in first-line treatment of HER2-overexpressing metastatic breast cancer*. J Clin Oncol, 2002. **20**(3): p. 719-26.
41. Slamon, D.J., et al., *Use of Chemotherapy plus a Monoclonal Antibody against HER2 for Metastatic Breast Cancer That Overexpresses HER2*. New England Journal of Medicine, 2001. **344**(11): p. 783-792.
42. Nahta, R. and F.J. Esteva, *HER2 therapy: molecular mechanisms of trastuzumab resistance*. Breast Cancer Res, 2006. **8**(6): p. 215.
43. Pohlmann, P.R., I.A. Mayer, and R. Mernaugh, *Resistance to Trastuzumab in Breast Cancer*. Clin Cancer Res, 2009. **15**(24): p. 7479-7491.
44. Singh, J.C., K. Jhaveri, and F.J. Esteva, *HER2-positive advanced breast cancer: optimizing patient outcomes and opportunities for drug development*. Br J Cancer, 2014. **111**(10): p. 1888-1898.
45. Capelan, M., et al., *Pertuzumab: new hope for patients with HER2-positive breast cancer*. Annals of Oncology, 2012.
46. Baselga, J., et al., *Pertuzumab plus trastuzumab plus docetaxel for metastatic breast cancer*. N Engl J Med, 2012. **366**(2): p. 109-19.
47. Barok, M., H. Joensuu, and J. Isola, *Trastuzumab emtansine: mechanisms of action and drug resistance*. Breast Cancer Res, 2014. **16**(2): p. 209.

48. Lewis Phillips, G.D., et al., *Targeting HER2-Positive Breast Cancer with Trastuzumab-DM1, an Antibody–Cytotoxic Drug Conjugate*. *Cancer Research*, 2008. **68**(22): p. 9280-9290.
49. Hurvitz, S.A., et al., *Phase II randomized study of trastuzumab emtansine versus trastuzumab plus docetaxel in patients with human epidermal growth factor receptor 2-positive metastatic breast cancer*. *J Clin Oncol*, 2013. **31**(9): p. 1157-63.
50. Roche, *Roche provides update on Phase III MARIANNE study in people with previously untreated advanced HER2-positive breast cancer*. 2014, Roche: Basel, Switzerland.
51. Blackwell, K.L., et al., *Overall survival benefit with lapatinib in combination with trastuzumab for patients with human epidermal growth factor receptor 2-positive metastatic breast cancer: final results from the EGF104900 Study*. *J Clin Oncol*, 2012. **30**(21): p. 2585-92.
52. Blackwell, K.L., et al., *Randomized Study of Lapatinib Alone or in Combination With Trastuzumab in Women With ErbB2-Positive, Trastuzumab-Refractory Metastatic Breast Cancer*. *Journal of Clinical Oncology*, 2010. **28**(7): p. 1124-1130.
53. Gelmon, K.A., et al., *Lapatinib or Trastuzumab Plus Taxane Therapy for Human Epidermal Growth Factor Receptor 2–Positive Advanced Breast Cancer: Final Results of NCIC CTG MA.31*. *Journal of Clinical Oncology*, 2015.

54. Verma, S., et al., *Trastuzumab emtansine for HER2-positive advanced breast cancer*. N Engl J Med, 2012. **367**(19): p. 1783-91.
55. Saura, C., et al., *Safety and Efficacy of Neratinib in Combination With Capecitabine in Patients With Metastatic Human Epidermal Growth Factor Receptor 2–Positive Breast Cancer*. Journal of Clinical Oncology, 2014.
56. Goss, P.E., et al. *A phase III trial of adjuvant neratinib (NER) after trastuzumab (TRAS) in women with early stage HER2+ breast cancer (BC)*. in *2011 ASCO Annual Meeting*. 2011. J Clin Oncol.
57. Puma, *Puma Biotechnology Announces Positive Top Line Results from Phase III PB272 Trial in Adjuvant Breast Cancer (ExteNET Trial)*. 2014: Los Angeles, CA.
58. Arteaga, C.L., et al., *Treatment of HER2-positive breast cancer: current status and future perspectives*. Nat Rev Clin Oncol, 2012. **9**(1): p. 16-32.
59. Gajria, D. and S. Chandarlapaty, *HER2-amplified breast cancer: mechanisms of trastuzumab resistance and novel targeted therapies*. Expert Rev Anticancer Ther, 2011. **11**(2): p. 263-75.
60. Tsang, R.Y. and R.S. Finn, *Beyond trastuzumab: novel therapeutic strategies in HER2-positive metastatic breast cancer*. British Journal of Cancer, 2012. **106**(1): p. 6-13.
61. Rexer, B.N., et al., *Direct inhibition of PI3K in combination with dual HER2 inhibitors is required for optimal antitumor activity in HER2+ breast cancer cells*. Breast Cancer Res, 2014. **16**(1): p. R9.

62. Modi, S., et al., *HSP90 inhibition is effective in breast cancer: a phase II trial of tanespimycin (17-AAG) plus trastuzumab in patients with HER2-positive metastatic breast cancer progressing on trastuzumab*. Clin Cancer Res, 2011. **17**(15): p. 5132-9.
63. Le, X.F., et al., *Specific blockade of VEGF and HER2 pathways results in greater growth inhibition of breast cancer xenografts that overexpress HER2*. Cell Cycle, 2008. **7**(23): p. 3747-58.
64. Montero, A., et al., *Bevacizumab in the Treatment of Metastatic Breast Cancer: Friend or Foe?* Current Oncology Reports, 2012. **14**(1): p. 1-11.
65. Singel, S.M., et al., *A targeted RNAi screen of the breast cancer genome identifies KIF14 and TLN1 as genes that modulate docetaxel chemosensitivity in triple-negative breast cancer*. Clin Cancer Res, 2013. **19**(8): p. 2061-70.
66. Bauer, J.A., et al., *RNA interference (RNAi) screening approach identifies agents that enhance paclitaxel activity in breast cancer cells*. Breast Cancer Res, 2010. **12**(3): p. R41.
67. Ashworth, A. and R. Bernards, *Using Functional Genetics to Understand Breast Cancer Biology*. Cold Spring Harbor Perspectives in Biology, 2010. **2**(7).
68. Burnett, J.C. and J.J. Rossi, *RNA-based Therapeutics- Current Progress and Future Prospects*. Chemistry & biology, 2012. **19**(1): p. 60-71.

69. Gomes-da-Silva, L.C., S. Simoes, and J.N. Moreira, *Challenging the future of siRNA therapeutics against cancer: the crucial role of nanotechnology*. Cell Mol Life Sci, 2014. **71**(8): p. 1417-38.
70. Patzel, V., I. Dietrich, and S.H. Kaufmann, *RNA Silencing in the struggle against disease*. Ann N Y Acad Sci, 2006. **1082**: p. 44-6.
71. Dong, H., et al., *MicroRNA: Function, Detection, and Bioanalysis*. Chemical Reviews, 2013. **113**(8): p. 6207-6233.
72. Skinner, H.D., et al., *A validated miRNA profile predicts response to therapy in esophageal adenocarcinoma*. Cancer, 2014. **120**(23): p. 3635-41.
73. Hayes, J., P.P. Peruzzi, and S. Lawler, *MicroRNAs in cancer: biomarkers, functions and therapy*. Trends Mol Med, 2014. **20**(8): p. 460-9.
74. Hansen, T.F., et al., *Changes in circulating microRNA-126 during treatment with chemotherapy and bevacizumab predicts treatment response in patients with metastatic colorectal cancer*. Br J Cancer, 2015. **112**(4): p. 624-629.
75. Zhang, B., et al., *microRNAs as oncogenes and tumor suppressors*. Developmental Biology, 2007. **302**(1): p. 1-12.
76. Bouchie, A., *First microRNA mimic enters clinic*. Nat Biotech, 2013. **31**(7): p. 577-577.
77. Daige, C.L., et al., *Systemic delivery of a miR34a mimic as a potential therapeutic for liver cancer*. Mol Cancer Ther, 2014. **13**(10): p. 2352-60.

78. Moreno, P.M. and A.P. Pego, *Therapeutic antisense oligonucleotides against cancer: hurdling to the clinic*. Front Chem, 2014. **2**: p. 87.
79. Herbst, R.S. and S.R. Frankel, *Oblimersen Sodium (Genasense bcl-2 Antisense Oligonucleotide): A Rational Therapeutic to Enhance Apoptosis in Therapy of Lung Cancer*. Clinical Cancer Research, 2004. **10**(12): p. 4245s-4248s.
80. Uckun, F.M., et al., *Cellular expression of antiapoptotic BCL-2 oncoprotein in newly diagnosed childhood acute lymphoblastic leukemia: a Children's Cancer Group Study*. Blood, 1997. **89**(10): p. 3769-77.
81. Frantz, S., *Lessons learnt from Genasense's failure*. Nat Rev Drug Discov, 2004. **3**(7): p. 542-542.
82. Stein, C.A., *The Genasense 'learning curve'*. Nat Biotech, 2007. **25**(9): p. 972-973.
83. Zellweger, T., et al., *Antitumor activity of antisense clusterin oligonucleotides is improved in vitro and in vivo by incorporation of 2'-O-(2-methoxy)ethyl chemistry*. J Pharmacol Exp Ther, 2001. **298**(3): p. 934-40.
84. Zielinski, R. and K.N. Chi, *Custirsen (OGX-011): a second-generation antisense inhibitor of clusterin in development for the treatment of prostate cancer*. Future Oncol, 2012. **8**(10): p. 1239-51.
85. Inman, S., *Custirsen Combination Misses Goal in Phase III mCRPC Trial*, in *OncLive*. 2014: Plainsboro, NJ.

86. Hong, D., et al., *Abstract LB-227: Preclinical pharmacology and clinical efficacy of AZD9150 (ISIS-STAT3Rx), a potent next-generation antisense oligonucleotide inhibitor of STAT3*. *Cancer Research*, 2014. **74**(19 Supplement): p. LB-227.
87. Chiarle, R., et al., *Stat3 is required for ALK-mediated lymphomagenesis and provides a possible therapeutic target*. *Nat Med*, 2005. **11**(6): p. 623-9.
88. Ko, Y.J., et al., *Androgen receptor down-regulation in prostate cancer with phosphorodiamidate morpholino antisense oligomers*. *J Urol*, 2004. **172**(3): p. 1140-4.
89. Yamamoto, Y., et al., *Generation 2.5 Antisense Oligonucleotides Targeting the Androgen Receptor and its Splice Variants Suppress Enzalutamide Resistant Prostate Cancer Cell Growth*. *Clinical Cancer Research*, 2015.
90. Weng, D.E., et al., *A phase I clinical trial of a ribozyme-based angiogenesis inhibitor targeting vascular endothelial growth factor receptor-1 for patients with refractory solid tumors*. *Molecular Cancer Therapeutics*, 2005. **4**(6): p. 948-955.
91. Morrow, P.K., et al., *An open-label, phase 2 trial of RPI.4610 (Angiozyme) in the treatment of metastatic breast cancer*. *Cancer*, 2012. **118**(17): p. 4098-104.

92. Rayburn, E.R. and R. Zhang, *Antisense, RNAi, and gene silencing strategies for therapy: mission possible or impossible?* Drug Discov Today, 2008. **13**(11-12): p. 513-21.
93. Sundaram, P., et al., *Therapeutic RNA aptamers in clinical trials.* Eur J Pharm Sci, 2013. **48**(1-2): p. 259-71.
94. Laber, D.A., et al., *Extended phase I study of AS1411 in renal and non-small cell lung cancers in 2006 ASCO Annual Meeting.* 2006, Journal of Clinical Oncology. p. 13098.
95. Rosenberg, J.E., et al., *A phase II trial of AS1411 (a novel nucleolin-targeted DNA aptamer) in metastatic renal cell carcinoma.* Invest New Drugs, 2014. **32**(1): p. 178-87.
96. Hoellenriegel, J., et al., *The Spiegelmer NOX-A12, a novel CXCL12 inhibitor, interferes with chronic lymphocytic leukemia cell motility and causes chemosensitization.* Vol. 123. 2014. 1032-1039.
97. Roccaro, Aldo M., et al., *SDF-1 Inhibition Targets the Bone Marrow Niche for Cancer Therapy.* Cell Reports. **9**(1): p. 118-128.
98. Steurer, M., et al., *Results from a Phase IIa Study of the Anti-CXCL12 Spiegelmer® Olaptosed Pegol (NOX-A12) in Combination with Bendamustine/Rituximab in Patients with Chronic Lymphocytic Leukemia,* in *ASH 2014.* 2014: San Francisco, CA.
99. Fischer, K., et al., *Bendamustine combined with rituximab in patients with relapsed and/or refractory chronic lymphocytic leukemia: a multicenter*

- phase II trial of the German Chronic Lymphocytic Leukemia Study Group.*
J Clin Oncol, 2011. **29**(26): p. 3559-66.
100. Li, J., et al., *Aptamer imaging with Cu-64 labeled AS1411: preliminary assessment in lung cancer.* Nucl Med Biol, 2014. **41**(2): p. 179-85.
101. Li, J., et al., *Evaluation of 64Cu-DOTA-AS1411 as a PET tracer for lung cancer imaging.* Journal of Nuclear Medicine, 2009. **50**(supplement 2): p. 1915.
102. Lares, M.R., J.J. Rossi, and D.L. Ouellet, *RNAi and small interfering RNAs in human disease therapeutic applications.* Trends in Biotechnology, 2010. **28**(11): p. 570-579.
103. Zorde Khvalevsky, E., et al., *Mutant KRAS is a druggable target for pancreatic cancer.* Proceedings of the National Academy of Sciences, 2013. **110**(51): p. 20723-20728.
104. Golan, T., et al. *A phase I trial of a local delivery of siRNA against k-ras in combination with chemotherapy for locally advanced pancreatic adenocarcinoma.* in *2013 ASCO Annual Meeting.* 2013. J Clin Oncol
105. Ku, S.H., et al., *Tumor-Targeting Multifunctional Nanoparticles for siRNA Delivery: Recent Advances in Cancer Therapy.* Advanced Healthcare Materials, 2014. **3**(8): p. 1182-1193.
106. Hickerson, R.P., et al., *Stability Study of Unmodified siRNA and Relevance to Clinical Use.* Oligonucleotides, 2008. **18**(4): p. 345-354.

107. Sinn, P.L., S.L. Sauter, and P.B. McCray, Jr., *Gene therapy progress and prospects: development of improved lentiviral and retroviral vectors-- design, biosafety, and production*. *Gene Ther*, 2005. **12**(14): p. 1089-98.
108. Nel, A.E., et al., *Understanding biophysicochemical interactions at the nano-bio interface*. *Nat Mater*, 2009. **8**(7): p. 543-557.
109. Jokerst, J.V., et al., *Nanoparticle PEGylation for imaging and therapy*. *Nanomedicine (Lond)*, 2011. **6**(4): p. 715-28.
110. Otsuka, H., Y. Nagasaki, and K. Kataoka, *PEGylated nanoparticles for biological and pharmaceutical applications*. *Advanced Drug Delivery Reviews*, 2003. **55**(3): p. 403-419.
111. Bengel, H.H., et al., *Biodistribution of an ultrasmall superparamagnetic iron oxide colloid, BMS 180549, by different routes of administration*. *Magn Reson Imaging*, 1994. **12**(3): p. 433-42.
112. Pain, D., et al., *Increased circulatory half-life of liposomes after conjunction with dextran*. *Journal of Biosciences*, 1984. **6**(6): p. 811-816.
113. Dai, F., et al., *Folic acid-conjugated glucose and dextran coated iron oxide nanoparticles as MRI contrast agents for diagnosis and treatment response of rheumatoid arthritis*. *Journal of Materials Chemistry B*, 2014. **2**(16): p. 2240-2247.
114. Zhang, T., et al., *Application of sialic acid/polysialic acid in the drug delivery systems*. *Asian Journal of Pharmaceutical Sciences*, 2014. **9**(2): p. 75-81.

115. Knudsen, K.B., et al., *In vivo toxicity of cationic micelles and liposomes*. *Nanomedicine: Nanotechnology, Biology and Medicine*, 2015. **11**(2): p. 467-477.
116. Lv, H., et al., *Toxicity of cationic lipids and cationic polymers in gene delivery*. *J Control Release*, 2006. **114**(1): p. 100-9.
117. Fischer, D., et al., *In vitro cytotoxicity testing of polycations: influence of polymer structure on cell viability and hemolysis*. *Biomaterials*, 2003. **24**(7): p. 1121-31.
118. Chen, H.-T., et al., *Cytotoxicity, Hemolysis, and Acute in Vivo Toxicity of Dendrimers Based on Melamine, Candidate Vehicles for Drug Delivery*. *Journal of the American Chemical Society*, 2004. **126**(32): p. 10044-10048.
119. O'Mahony, A.M., et al., *Cationic and PEGylated Amphiphilic Cyclodextrins: Co-Formulation Opportunities for Neuronal Sirna Delivery*. *PLoS ONE*, 2013. **8**(6): p. e66413.
120. Nelson, C.E., et al., *Balancing Cationic and Hydrophobic Content of PEGylated siRNA Polyplexes Enhances Endosome Escape, Stability, Blood Circulation Time, and Bioactivity in Vivo*. *ACS Nano*, 2013. **7**(10): p. 8870-8880.
121. Maeda, H., et al., *Tumor vascular permeability and the EPR effect in macromolecular therapeutics: a review*. *J Control Release*, 2000. **65**(1-2): p. 271-84.

122. Yu, B., et al., *Receptor-targeted nanocarriers for therapeutic delivery to cancer*. *Molecular Membrane Biology*, 2010. **27**(7): p. 286-298.
123. Li, S.-D., et al., *Tumor-targeted Delivery of siRNA by Self-assembled Nanoparticles*. *Mol Ther*, 2007. **16**(1): p. 163-169.
124. Wang, K., et al., *Specific aptamer-conjugated mesoporous silica-carbon nanoparticles for HER2-targeted chemo-photothermal combined therapy*. *Acta Biomater*, 2015. **16**: p. 196-205.
125. Yao, Y.D., et al., *Targeted delivery of PLK1-siRNA by ScFv suppresses Her2+ breast cancer growth and metastasis*. *Sci Transl Med*, 2012. **4**(130): p. 130ra48.
126. Wartlick, H., et al., *Highly Specific HER2-mediated Cellular Uptake of Antibody-modified Nanoparticles in Tumour Cells*. *Journal of Drug Targeting*, 2004. **12**(7): p. 461-471.
127. Zwicke, G.L., G.A. Mansoori, and C.J. Jeffery, *Utilizing the folate receptor for active targeting of cancer nanotherapeutics*. *Nano Rev*, 2012.
128. Kularatne, S.A. and P.S. Low, *Targeting of nanoparticles: folate receptor*. *Methods Mol Biol*, 2010. **624**: p. 249-65.
129. Hogemann-Savellano, D., et al., *The transferrin receptor: a potential molecular imaging marker for human cancer*. *Neoplasia*, 2003. **5**(6): p. 495-506.
130. Qian, Z.M., et al., *Targeted Drug Delivery via the Transferrin Receptor-Mediated Endocytosis Pathway*. *Pharmacological Reviews*, 2002. **54**(4): p. 561-587.

131. Dominska, M. and D.M. Dykxhoorn, *Breaking down the barriers: siRNA delivery and endosome escape*. Journal of Cell Science, 2010. **123**(8): p. 1183-1189.
132. Whitehead, K.A., R. Langer, and D.G. Anderson, *Knocking down barriers: advances in siRNA delivery*. Nat Rev Drug Discov, 2009. **8**(2): p. 129-138.
133. Gomes-da-Silva, L.C., et al., *Lipid-based nanoparticles for siRNA delivery in cancer therapy: paradigms and challenges*. Acc Chem Res, 2012. **45**(7): p. 1163-71.
134. Draz, M.S., et al., *Nanoparticle-mediated systemic delivery of siRNA for treatment of cancers and viral infections*. Theranostics, 2014. **4**(9): p. 872-92.
135. Taetz, S., et al., *Hyaluronic acid-modified DOTAP/DOPE liposomes for the targeted delivery of anti-telomerase siRNA to CD44-expressing lung cancer cells*. Oligonucleotides, 2009. **19**(2): p. 103-16.
136. Hattori, Y., et al., *siRNA delivery to lung-metastasized tumor by systemic injection with cationic liposomes*. J Liposome Res, 2014: p. 1-8.
137. Tagalakis, A.D., et al., *Receptor-targeted liposome-peptide nanocomplexes for siRNA delivery*. Biomaterials, 2011. **32**(26): p. 6302-15.
138. Wang, X., et al., *Enhanced hepatic delivery of siRNA and microRNA using oleic acid based lipid nanoparticle formulations*. Journal of controlled release : official journal of the Controlled Release Society, 2013. **172**(3): p. 690-698.

139. Landen, C.N., Jr., et al., *Therapeutic EphA2 gene targeting in vivo using neutral liposomal small interfering RNA delivery*. *Cancer Res*, 2005. **65**(15): p. 6910-8.
140. Xu, Y. and F.C. Szoka, *Mechanism of DNA Release from Cationic Liposome/DNA Complexes Used in Cell Transfection*. *Biochemistry*, 1996. **35**(18): p. 5616-5623.
141. Lorenzer, C., et al., *Going beyond the liver: Progress and challenges of targeted delivery of siRNA therapeutics*. *J Control Release*, 2015. **203**: p. 1-15.
142. Akinc, A., et al., *Development of Lipidoid-siRNA Formulations for Systemic Delivery to the Liver*. *Mol Ther*, 2009. **17**(5): p. 872-879.
143. Liu, F. and D. Liu, *Serum independent liposome uptake by mouse liver*. *Biochimica et Biophysica Acta (BBA) - Biomembranes*, 1996. **1278**(1): p. 5-11.
144. Davis, M.E., *The first targeted delivery of siRNA in humans via a self-assembling, cyclodextrin polymer-based nanoparticle: from concept to clinic*. *Mol Pharm*, 2009. **6**(3): p. 659-68.
145. Beyerle, A., et al., *Toxicity Pathway Focused Gene Expression Profiling of PEI-Based Polymers for Pulmonary Applications*. *Molecular Pharmaceutics*, 2010. **7**(3): p. 727-737.
146. von Gersdorff, K., et al., *The Internalization Route Resulting in Successful Gene Expression Depends on both Cell Line and Polyethylenimine Polyplex Type*. *Mol Ther*, 2006. **14**(5): p. 745-753.

147. Liu, X., et al., *Efficient delivery of sticky siRNA and potent gene silencing in a prostate cancer model using a generation 5 triethanolamine-core PAMAM dendrimer*. *Mol Pharm*, 2012. **9**(3): p. 470-81.
148. Taratula, O., et al., *Surface-engineered targeted PPI dendrimer for efficient intracellular and intratumoral siRNA delivery*. *J Control Release*, 2009. **140**(3): p. 284-93.
149. Tan, S.J., et al., *Engineering Nanocarriers for siRNA Delivery*. *Small*, 2011. **7**(7): p. 841-56.
150. Hong, C.A. and Y.S. Nam, *Functional nanostructures for effective delivery of small interfering RNA therapeutics*. *Theranostics*, 2014. **4**(12): p. 1211-32.
151. Lee, S.J., et al., *Tumor-homing poly-siRNA/glycol chitosan self-cross-linked nanoparticles for systemic siRNA delivery in cancer treatment*. *Angew Chem Int Ed Engl*, 2012. **51**(29): p. 7203-7.
152. Han, H.D., et al., *Targeted gene silencing using RGD-labeled chitosan nanoparticles*. *Clin Cancer Res*, 2010. **16**(15): p. 3910-22.
153. Mu, P., et al., *Systemic delivery of siRNA specific to tumor mediated by atelocollagen: Combined therapy using siRNA targeting Bcl-xL and cisplatin against prostate cancer*. *International Journal of Cancer*, 2009. **125**(12): p. 2978-2990.
154. Kim, J., S.W. Kim, and W.J. Kim, *PEI-g-PEG-RGD/small interference RNA polyplex-mediated silencing of vascular endothelial growth factor receptor*

- and its potential as an anti-angiogenic tumor therapeutic strategy. Oligonucleotides*, 2011. **21**(2): p. 101-7.
155. Isaac, O.-J., et al., *Engineered nonviral nanocarriers for intracellular gene delivery applications. Biomedical Materials*, 2012. **7**(5): p. 054106.
156. Chung, T.H., et al., *The effect of surface charge on the uptake and biological function of mesoporous silica nanoparticles in 3T3-L1 cells and human mesenchymal stem cells. Biomaterials*, 2007. **28**(19): p. 2959-66.
157. Tarn, D., et al., *Mesoporous silica nanoparticle nanocarriers: biofunctionality and biocompatibility. Acc Chem Res*, 2013. **46**(3): p. 792-801.
158. Phillips, E., et al., *Clinical translation of an ultras-small inorganic optical-PET imaging nanoparticle probe. Science Translational Medicine*, 2014. **6**(260): p. 260ra149.
159. Shen, J., et al., *Cyclodextrin and Polyethylenimine Functionalized Mesoporous Silica Nanoparticles for Delivery of siRNA Cancer Therapeutics. Theranostics*, 2014. **4**(5): p. 487-97.
160. Lin, D., et al., *Intracellular cleavable poly(2-dimethylaminoethyl methacrylate) functionalized mesoporous silica nanoparticles for efficient siRNA delivery in vitro and in vivo. Nanoscale*, 2013. **5**(10): p. 4291-301.
161. Meng, H., et al., *Codelivery of an Optimal Drug/siRNA Combination Using Mesoporous Silica Nanoparticles To Overcome Drug Resistance in Breast Cancer in Vitro and in Vivo. ACS Nano*, 2013. **7**(2): p. 994-1005.

162. Wu, C., et al., *An RGD-modified MRI-visible polymeric vector for targeted siRNA delivery to hepatocellular carcinoma in nude mice*. PLoS One, 2013. **8**(6): p. e66416.
163. Li, J., et al., *Biodegradable Calcium Phosphate Nanoparticle with Lipid Coating for Systemic siRNA Delivery*. Journal of controlled release : official journal of the Controlled Release Society, 2010. **142**(3): p. 416-421.
164. Li, J., Y. Yang, and L. Huang, *Calcium Phosphate Nanoparticles with an Asymmetric Lipid Bilayer Coating for siRNA Delivery to the Tumor*. Journal of Controlled Release, 2012. **158**(1): p. 108-114.
165. Ma, D., *Enhancing endosomal escape for nanoparticle mediated siRNA delivery*. Nanoscale, 2014. **6**(12): p. 6415-6425.
166. Yang, Y., et al., *Nanoparticle Delivery of Pooled siRNA for Effective Treatment of Non-Small Cell Lung Cancer*. Molecular Pharmaceutics, 2012. **9**(8): p. 2280-2289.
167. Huang, X. and M.A. El-Sayed, *Gold nanoparticles: Optical properties and implementations in cancer diagnosis and photothermal therapy*. Journal of Advanced Research, 2010. **1**(1): p. 13-28.
168. Chen, C.H., Y.-J. Wu, and J.-J. Chen, *Gold Nanotheranostics: Photothermal Therapy and Imaging of Mucin 7 Conjugated Antibody Nanoparticles for Urothelial Cancer*. BioMed Research International, 2015. **2015**: p. 8.

169. Jensen, S.A., et al., *Spherical Nucleic Acid Nanoparticle Conjugates as an RNAi-Based Therapy for Glioblastoma*. *Science Translational Medicine*, 2013. **5**(209).
170. Liu, Y., et al., *Understanding the toxicity of carbon nanotubes*. *Acc Chem Res*, 2013. **46**(3): p. 702-13.
171. Lam, C.W., et al., *A review of carbon nanotube toxicity and assessment of potential occupational and environmental health risks*. *Crit Rev Toxicol*, 2006. **36**(3): p. 189-217.
172. Podesta, J.E., et al., *Antitumor Activity and Prolonged Survival by Carbon-Nanotube-Mediated Therapeutic siRNA Silencing in a Human Lung Xenograft Model*. *Small*, 2009. **5**(10): p. 1176-1185.
173. Siu, K.S., et al., *Non-covalently functionalized single-walled carbon nanotube for topical siRNA delivery into melanoma*. *Biomaterials*, 2014. **35**(10): p. 3435-42.
174. Gaan, S., et al., *Size, shape, composition, and electronic properties of InAs/GaAs quantum dots by scanning tunneling microscopy and spectroscopy*. *Journal of Applied Physics*, 2010. **108**(11): p. 114315.
175. Sabaeian, M. and A. Khaledi-Nasab, *Size-dependent intersubband optical properties of dome-shaped InAs/GaAs quantum dots with wetting layer*. *Appl Opt*, 2012. **51**(18): p. 4176-85.
176. Wang, Z., et al., *Rigid nanoparticle-based delivery of anti-cancer siRNA: challenges and opportunities*. *Biotechnol Adv*, 2014. **32**(4): p. 831-43.

177. Lin, G., et al., *In vivo toxicity assessment of non-cadmium quantum dots in BALB/c mice*. *Nanomedicine: Nanotechnology, Biology and Medicine*. **11**(2): p. 341-350.
178. Subramaniam, P., et al., *Generation of a library of non-toxic quantum dots for cellular imaging and siRNA delivery*. *Advanced materials (Deerfield Beach, Fla.)*, 2012. **24**(29): p. 4014-4019.
179. Molitoris, B.A., et al., *siRNA Targeted to p53 Attenuates Ischemic and Cisplatin-Induced Acute Kidney Injury*. *Journal of the American Society of Nephrology : JASN*, 2009. **20**(8): p. 1754-1764.
180. Zuckerman, J.E., et al., *Correlating animal and human phase Ia/Ib clinical data with CALAA-01, a targeted, polymer-based nanoparticle containing siRNA*. *Proceedings of the National Academy of Sciences*, 2014. **111**(31): p. 11449-11454.
181. Ozcan, G., et al., *Preclinical and clinical development of siRNA-based therapeutics*. *Adv Drug Deliv Rev*, 2015.
182. Davis, M.E., et al., *Evidence of RNAi in humans from systemically administered siRNA via targeted nanoparticles*. *Nature*, 2010. **464**(7291): p. 1067-1070.
183. Schultheis, B., et al., *First-in-Human Phase I Study of the Liposomal RNA Interference Therapeutic Atu027 in Patients With Advanced Solid Tumors*. *Journal of Clinical Oncology*, 2014. **32**(36): p. 4141-4148.

184. Tabernero, J., et al., *First-in-humans trial of an RNA interference therapeutic targeting VEGF and KSP in cancer patients with liver involvement*. *Cancer Discov*, 2013. **3**(4): p. 406-17.
185. Aleku, M., et al., *Atu027, a liposomal small interfering RNA formulation targeting protein kinase N3, inhibits cancer progression*. *Cancer Res*, 2008. **68**(23): p. 9788-98.
186. Strumberg, D., et al., *Phase I clinical development of Atu027, a siRNA formulation targeting PKN3 in patients with advanced solid tumors*. *Int J Clin Pharmacol Ther*, 2012. **50**(1): p. 76-8.
187. Judge, A.D., et al., *Confirming the RNAi-mediated mechanism of action of siRNA-based cancer therapeutics in mice*. *The Journal of Clinical Investigation*, 2009. **119**(3): p. 661-673.
188. Dudek, H., et al., *Knockdown of [beta]-catenin with Dicer-Substrate siRNAs Reduces Liver Tumor Burden In vivo*. *Mol Ther*, 2014. **22**(1): p. 92-101.
189. Inoue, S., et al., *Polymalic Acid-Based Nanobiopolymer Provides Efficient Systemic Breast Cancer Treatment by Inhibiting both HER2/neu Receptor Synthesis and Activity*. *Cancer research*, 2011. **71**(4): p. 1454-1464.
190. Ngamcherdtrakul, W., et al., *Cationic Polymer Modified Mesoporous Silica Nanoparticles for Targeted siRNA Delivery to HER2+ Breast Cancer*. *Advanced Functional Materials*, 2015. **25**(18): p. 2646-2659.
191. Meng, H., et al., *Use of Size and a Copolymer Design Feature To Improve the Biodistribution and the Enhanced Permeability and Retention Effect of*

- Doxorubicin-Loaded Mesoporous Silica Nanoparticles in a Murine Xenograft Tumor Model.* ACS Nano, 2011. **5**(5): p. 4131-4144.
192. Huang, I.P., et al., *Enhanced chemotherapy of cancer using pH-sensitive mesoporous silica nanoparticles to antagonize P-glycoprotein-mediated drug resistance.* Mol Cancer Ther, 2011. **10**(5): p. 761-9.
193. Zhang, Q., et al., *Biocompatible, Uniform, and Redispersible Mesoporous Silica Nanoparticles for Cancer-Targeted Drug Delivery In Vivo.* Advanced Functional Materials, 2014. **24**(17): p. 2450-2461.
194. Lu, J., et al., *Mesoporous Silica Nanoparticles for Cancer Therapy: Energy-Dependent Cellular Uptake and Delivery of Paclitaxel to Cancer Cells.* Nanobiotechnology, 2007. **3**(2): p. 89-95.
195. Pan, L., et al., *Nuclear-Targeted Drug Delivery of TAT Peptide-Conjugated Monodisperse Mesoporous Silica Nanoparticles.* Journal of the American Chemical Society, 2012. **134**(13): p. 5722-5725.
196. Slowing, I.I., et al., *Mesoporous Silica Nanoparticles for Drug Delivery and Biosensing Applications.* Advanced Functional Materials, 2007. **17**(8): p. 1225-1236.
197. Lodha, A., et al., *Synthesis of mesoporous silica nanoparticles and drug loading of poorly water soluble drug cyclosporin A.* Journal of Pharmacy & Bioallied Sciences, 2012. **4**(Suppl 1): p. S92-S94.
198. Yousefpour, P., et al., *Targeted delivery of doxorubicin-utilizing chitosan nanoparticles surface-functionalized with anti-Her2 trastuzumab.* Int J Nanomedicine, 2011. **6**: p. 1977-90.

199. Koopaei, M.N., et al., *Docetaxel immunonanocarriers as targeted delivery systems for HER 2-positive tumor cells: preparation, characterization, and cytotoxicity studies*. Int J Nanomedicine, 2011. **6**: p. 1903-12.
200. Ketola, T.M., et al., *Independent versus cooperative binding in polyethylenimine-DNA and Poly(L-lysine)-DNA polyplexes*. J Phys Chem B, 2013. **117**(36): p. 10405-13.
201. Aravindan, L., et al., *A comparison of thiolated and disulfide-crosslinked polyethylenimine for nonviral gene delivery*. Macromol Biosci, 2013. **13**(9): p. 1163-73.
202. Wu, Y., et al., *The investigation of polymer-siRNA nanoparticle for gene therapy of gastric cancer in vitro*. International Journal of Nanomedicine, 2010. **5**: p. 129-136.
203. Akinc, A., et al., *Exploring polyethylenimine-mediated DNA transfection and the proton sponge hypothesis*. J Gene Med, 2005. **7**(5): p. 657-63.
204. Eliyahu, H., Y. Barenholz, and A.J. Domb, *Polymers for DNA delivery*. Molecules, 2005. **10**(1): p. 34-64.
205. Gref, R., et al., *'Stealth' corona-core nanoparticles surface modified by polyethylene glycol (PEG): influences of the corona (PEG chain length and surface density) and of the core composition on phagocytic uptake and plasma protein adsorption*. Colloids and Surfaces B: Biointerfaces, 2000. **18**(3-4): p. 301-313.
206. Mantei, A., et al., *siRNA stabilization prolongs gene knockdown in primary T lymphocytes*. Eur J Immunol, 2008. **38**(9): p. 2616-25.

207. Dykxhoorn, D.M., D. Palliser, and J. Lieberman, *The silent treatment: siRNAs as small molecule drugs*. *Gene Ther*, 2006. **13**(6): p. 541-52.
208. Bartlett, D.W., et al., *Impact of tumor-specific targeting on the biodistribution and efficacy of siRNA nanoparticles measured by multimodality in vivo imaging*. *Proceedings of the National Academy of Sciences*, 2007. **104**(39): p. 15549-15554.
209. Zhang, Z., et al., *Synthesis of poly(ethylene glycol) (PEG)-grafted colloidal silica particles with improved stability in aqueous solvents*. *J Colloid Interface Sci*, 2007. **310**(2): p. 446-55.
210. Gref, R., et al., *'Stealth' corona-core nanoparticles surface modified by polyethylene glycol (PEG): influences of the corona (PEG chain length and surface density) and of the core composition on phagocytic uptake and plasma protein adsorption*. *Colloids Surf B Biointerfaces*, 2000. **18**(3-4): p. 301-313.
211. Mao, S., et al., *Influence of polyethylene glycol chain length on the physicochemical and biological properties of poly(ethylene imine)-graft-poly(ethylene glycol) block copolymer/SiRNA polyplexes*. *Bioconjug Chem*, 2006. **17**(5): p. 1209-18.
212. Murphy, C.G. and S. Modi, *HER2 breast cancer therapies: a review*. *Biologics*, 2009. **3**: p. 289-301.
213. Wang, Y.-C., et al., *Different mechanisms for resistance to trastuzumab versus lapatinib in HER2- positive breast cancers -- role of estrogen*

- receptor and HER2 reactivation*. Breast Cancer Research, 2011. **13**(6): p. R121.
214. Ritter, C.A., et al., *Human Breast Cancer Cells Selected for Resistance to Trastuzumab In vivo Overexpress Epidermal Growth Factor Receptor and ErbB Ligands and Remain Dependent on the ErbB Receptor Network*. Clinical Cancer Research, 2007. **13**(16): p. 4909-4919.
215. Cooke, T., et al., *HER2 as a prognostic and predictive marker for breast cancer*. Ann Oncol, 2001. **12 Suppl 1**: p. S23-8.
216. du Manoir, J.M., et al., *Strategies for Delaying or Treating In vivo Acquired Resistance to Trastuzumab in Human Breast Cancer Xenografts*. Clinical Cancer Research, 2006. **12**(3): p. 904-916.
217. Zhang, H., et al., *Differential Expression of Syndecan-1 Mediates Cationic Nanoparticle Toxicity in Undifferentiated versus Differentiated Normal Human Bronchial Epithelial Cells*. ACS Nano, 2011. **5**(4): p. 2756-2769.
218. Weigel, P.H. and J.A. Oka, *Temperature dependence of endocytosis mediated by the asialoglycoprotein receptor in isolated rat hepatocytes. Evidence for two potentially rate-limiting steps*. Journal of Biological Chemistry, 1981. **256**(6): p. 2615-2617.
219. Lee, R.J. and P.S. Low, *Delivery of liposomes into cultured KB cells via folate receptor-mediated endocytosis*. J Biol Chem, 1994. **269**(5): p. 3198-204.
220. Shim, M.S., et al., *Dynamics of nucleic acid/cationic polymer complexation and disassembly under biologically simulated conditions using in situ*

- atomic force microscopy*. Microscopy Research and Technique, 2010. **73**(9): p. 845-856.
221. Christianson, H.C. and M. Belting, *Heparan sulfate proteoglycan as a cell-surface endocytosis receptor*. Matrix Biology, 2014. **35**(0): p. 51-55.
222. Hess, G.T., et al., *Cellular binding, motion, and internalization of synthetic gene delivery polymers*. Biochimica et Biophysica Acta (BBA) - Molecular Cell Research, 2007. **1773**(10): p. 1583-1588.
223. Nikitovic, D., et al., *The Motile Breast Cancer Phenotype Roles of Proteoglycans/Glycosaminoglycans*. BioMed Research International, 2014. **2014**: p. 13.
224. Nahta, R., *Molecular Mechanisms of Trastuzumab-Based Treatment in HER2-Overexpressing Breast Cancer*. ISRN Oncol, 2012. **2012**: p. 428062.
225. Sorkin, A. and M. von Zastrow, *Signal transduction and endocytosis: close encounters of many kinds*. Nat Rev Mol Cell Biol, 2002. **3**(8): p. 600-614.
226. Beyer, I., et al., *Coadministration of epithelial junction opener JO-1 improves the efficacy and safety of chemotherapeutic drugs*. Clin Cancer Res, 2012. **18**(12): p. 3340-51.
227. Beyer, I., et al., *Controlled extracellular matrix degradation in breast cancer tumors improves therapy by trastuzumab*. Mol Ther, 2011. **19**(3): p. 479-89.

228. Henjes, F., et al., *Strong EGFR signaling in cell line models of ERBB2-amplified breast cancer attenuates response towards ERBB2-targeting drugs*. *Oncogenesis*, 2012. **1**: p. e16.
229. Slowing, I.I., et al., *Mesoporous Silica Nanoparticles for Reducing Hemolytic Activity Towards Mammalian Red Blood Cells*. *Small*, 2009. **5**(1): p. 57-62.
230. Hinson, J.A., D.W. Roberts, and L.P. James, *Mechanisms of Acetaminophen-Induced Liver Necrosis*. *Handbook of experimental pharmacology*, 2010(196): p. 369-405.
231. Schwenk, M.H., *Ferumoxitol: a new intravenous iron preparation for the treatment of iron deficiency anemia in patients with chronic kidney disease*. *Pharmacotherapy*, 2010. **30**(1): p. 70-9.
232. Takeda, K. and S. Akira, *Toll-like receptors in innate immunity*. *International Immunology*, 2005. **17**(1): p. 1-14.
233. Broering, R., et al., *Chemical modifications on siRNAs avoid Toll-like-receptor-mediated activation of the hepatic immune system in vivo and in vitro*. *International Immunology*, 2014. **26**(1): p. 35-46.
234. Zamanian-Daryoush, M., et al., *Determinants of cytokine induction by small interfering RNA in human peripheral blood mononuclear cells*. *J Interferon Cytokine Res*, 2008. **28**(4): p. 221-33.
235. Chaturvedi, A. and S.K. Pierce, *How location governs toll-like receptor signaling*. *Traffic*, 2009. **10**(6): p. 621-8.

236. Crist, R.M., et al., *Common pitfalls in nanotechnology: lessons learned from NCI's Nanotechnology Characterization Laboratory*. Integr Biol (Camb), 2013. **5**(1): p. 66-73.
237. Wierer, M., et al., *PLK1 signaling in breast cancer cells cooperates with estrogen receptor-dependent gene transcription*. Cell Rep, 2013. **3**(6): p. 2021-32.
238. Strebhardt, K. and A. Ullrich, *Targeting polo-like kinase 1 for cancer therapy*. Nat Rev Cancer, 2006. **6**(4): p. 321-330.
239. Frost, A., et al., *Phase I study of the Plk1 inhibitor BI 2536 administered intravenously on three consecutive days in advanced solid tumours*. Current Oncology, 2012. **19**(1).
240. Vose, J.M., et al., *The Plk1 inhibitor BI 2536 in patients with refractory or relapsed non-Hodgkin lymphoma: a phase I, open-label, single dose-escalation study*. Leuk Lymphoma, 2013. **54**(4): p. 708-13.
241. Leivonen, S.K., et al., *High-throughput screens identify microRNAs essential for HER2 positive breast cancer cell growth*. Mol Oncol, 2014. **8**(1): p. 93-104.
242. Huber, U. and A.O. Onigbind, *Analysis of Taxol by HPLC: Application 2002*, Agilent Technologies.